Martin Fossen

Aggregation, Interfacial Properties and Structural Characteristics of Asphaltene Solubility Fractions

Thesis for the degree of doctor philosophiae

Trondheim, August 2007

Norwegian University of
Science and Technology
Faculty of Natural Sciences and Technology
Department of Chemical Engineering

NTNU
Innovation and Creativity

NTNU
Norwegian University of Science and Technology

Thesis for the degree of doctor philosophiae

Faculty of Natural Sciences and Technology
Department of Chemical Engineering

ISBN 978-82-471-3456-6 (printed ver.)
ISBN 978-82-471-3473-3 (electronic ver.)
ISSN 1503-8181

Theses at NTNU, 2007:158

Printed by Tapir Uttrykk

PREFACE

This thesis is submitted in partial fulfilment of the PhD degree at the Norwegian University of Science and Technology (NTNU). The work has been performed at the Ugelstad Laboratory at the Department of Chemical Engineering.

I received my BSc in Chemical Engineering in June 2000 at Telemark University College. In 2004, at the Ugelstad Laboratory (Department of Chemical Engineering, NTNU, Trondheim), I received my MSc in the field of surface, colloid and polymer chemistry on the subject of developing polarity indices for polar macromolecules in crude oil.

The present study has been done within the scope of the Joint Industrial Program (JIP) on Particle Stabilized Emulsions/Heavy Crude Oils financed by the industry. In addition Statoil ASA has contributed both financially and with a co-supervisor to my project. The thesis consists of 6 papers or manuscripts, motivated with an introduction to the field of crude oil processing, asphaltenes and separation technology followed by a description of the experimental methods used.

ACKNOWLEDGEMENTS

I would like to thank Professor Johan Sjöblom for the opportunity to do my PhD at the Ugelstad Laboratory, for excellent supervision and the extraordinary good research facilities and means available at the Ugelstad Laboratory. Thanks also for all the social events.

Thanks to Harald Kallevik for his great contribution as my supervisor.

Thanks to the JIP1 consortium consisting of Statoil ASA, Norsk Hydro, British Petroleum, Shell Global Solutions, Total, Mærsk Oil and Gas - Qatar, Champion Technologies, Chevron Texaco (now Chevron), ENI Technology, Petrobras, Vetco Aibel (changed to Vetco Gray) and Aker Kværner (Subsea and Process Systems) for the interest and discussions.

Thanks to Joakim Jakobsson for working on the rig during three summers, Richard Arntzen who initiated the project on the rig, Christian Melbye Bjørn for all the work used in the construction and continuously repair of the CEC, Morten Hana for your constant belief in us, Astrid Salvesen (glassworker) and Jan Ole Sundli (Electrical engineer), Kenneth D. Knudsen (SANS measurements), Jostein Krane (introduction to, and help with the NMR).

Thanks to past and present students and researchers at the Ugelstad Laboratory for good times and constructive discussions. Thanks to the staff at the Department of Chemical Engineering especially Jan Morten Roel, Lisbeth Roel and Arne Fossum.

My office mates through these years, Ann-Mari Dahl Hanneseth, Anne Silset, Sondre Volden and Torbjørn Vrålstad, thank you.

Thanks Helene Magnusson, Wilhelm Glomm and Sondre Volden for proofreading.

Thanks to my family (Mamma, Pappa, Elisabet, Beate og Runar). I am forever grateful to my parents for teaching me the love of outdoor activities!

Vibeke, thank you for showing up at the right moment in my life!

ABSTRACT

Crude oil is the primary source for energy in the world and serves as the raw material for many daily products. Two topics, important in the daily processing of crude oils, are treated in this thesis. Water-in-oil emulsions must be broken to obtain the desired quality of the crude oil delivered to the refineries with respect to water and salt content and asphaltenes are of concern at all stages of the recovery, transportation and processing of crude oils. The work has been of experimental nature and the results are reported in journal papers and manuscripts.

A lab-scale continuous separation rig was constructed and later equipped with a compact electro coalescer. The results show that water cut and pressure drop affect the droplet size distribution of water-in-oil emulsions. Moreover, two demulsifiers were tested on crude oil emulsions under high electric fields. The study indicated that it is not trivial which type of demulsifier to choose when an electric field is applied in combination with chemical destabilization.

Hansen solubility parameters for solvents and binary mixtures were correlated to infrared and near infrared spectra by partial least squares regression. Regression coefficients and errors of validation indicated that the regressions and predictions were good. The models were used to predict solubility parameters for crude oils and SARA fractions and the values obtained were in range of what has been reported in the literature.

Asphaltenes were separated into several solubility fractions directly from the crude oil by stepwise addition and precipitation by *n*-pentane. The solubility fractions had very different properties with regard to aggregation onset and interfacial activity which to a certain degree were explained by the differences found in the average size and molecular structures of the fractions. It was shown that the less soluble fractions consisted of molecules with larger average molecular weight, higher aromaticity and more polar aromatic cores. For the more soluble fractions results indicated that the substituted alkyl side chains on the aromatic cores were more branched and contained more of the hydroxylic and carboxylic groups, which again could explain the higher interfacial activity. Experiments also suggested that neither the least nor the most soluble of the asphaltenes under investigation were the ones with the highest interfacial activity, but a middle fraction. The findings suggest the need for looking into solubility fractions of asphaltene in further research and compare with the asphaltenes found in deposits or obtained from pressure drop experiments.

LIST OF PAPERS

Paper I

Solubility Parameters Based on IR and NIR Spectra

I. Correlation to Polar Solutes and Binary Mixtures

Martin Fossen, Pål Viggo Hemmingsen, Andreas Hannisdal, Harald Kallevik and Johan Sjöblom

Journal of Dispersion Science and Technology, 227-241, 26, 2005

Paper II

Asphaltenes Precipitated by a Two-Step Precipitation Procedure

1. Interfacial Tension and Solvent Properties

Martin Fossen, Harald Kallevik, Kenneth D. Knudsen, and Johan Sjöblom

Energy&Fuels, 1030 – 1037, 21(2), 2007

Paper III

Asphaltenes Precipitated by a Two-Step Precipitation Procedure

2. Physical and Chemical Characteristics

Martin Fossen, Marcos D. Lobato, Harald Kallevik, Kenneth D. Knudsen and Johan Sjöblom

In preparation, to be submitted to Energy&Fuels

Paper IV

A New Procedure for Direct Precipitation and Fractionation of Asphaltenes From Crude Oil

Martin Fossen, Harald Kallevik, Joakim Jakobsson and Johan Sjöblom

Journal of Dispersion Science and Technology, 193-197, 28, 2007

Paper V

A Laboratory-Scale Vertical Gravity Separator for Emulsion Characterization

Martin Fossen, Richard Arntzen, Pål Viggo Hemmingsen, Joakim Jakobsson and Johan Sjöblom

Journal of Dispersion Science and Technology, 453-461, 27, 2006

Paper VI

Electrostatic Coalescence under Flowing Conditions: A Study of the Effect of a High Electric AC Field on the Efficiency of Two Demulsifiers

Martin Fossen, Christian Melby Bjørn, Morten Hana, Johan Sjöblom

In preparation

ADDITIONAL PUBLICATIONS

Solubility Parameters based on IR and NIR spectra

II. Correlation to Aromatic Solvents and Model Compounds and Prediction on Asphaltene Solubility Fractions

Martin Fossen, Erland L. Nordgård, Harald Kallevik and Johan Sjöblom

In preparation

Influence of Interfacial Tension on Seeded Calcium Carbonate Scale Precipitation: Effect of Adsorbed Asphaltenes

Torbjørn Vrålstad, Martin Fossen, Johan Sjöblom and Preben Randhol

Journal of Dispersion Science and Technology 2007, in press

CONTENTS

1 INTRODUCTION TO CRUDE OIL

Oil and natural gas are important parts of our everyday life. They are the main source of energy for transportation, heating and cooling, and generation of electricity. In addition millions of products are prepared from oil and gas, including plastics, clothing and cosmetics.[1, 2] As a matter of fact, very few things you use in the daily life cannot be traced back to crude oil (Figure 1-1).

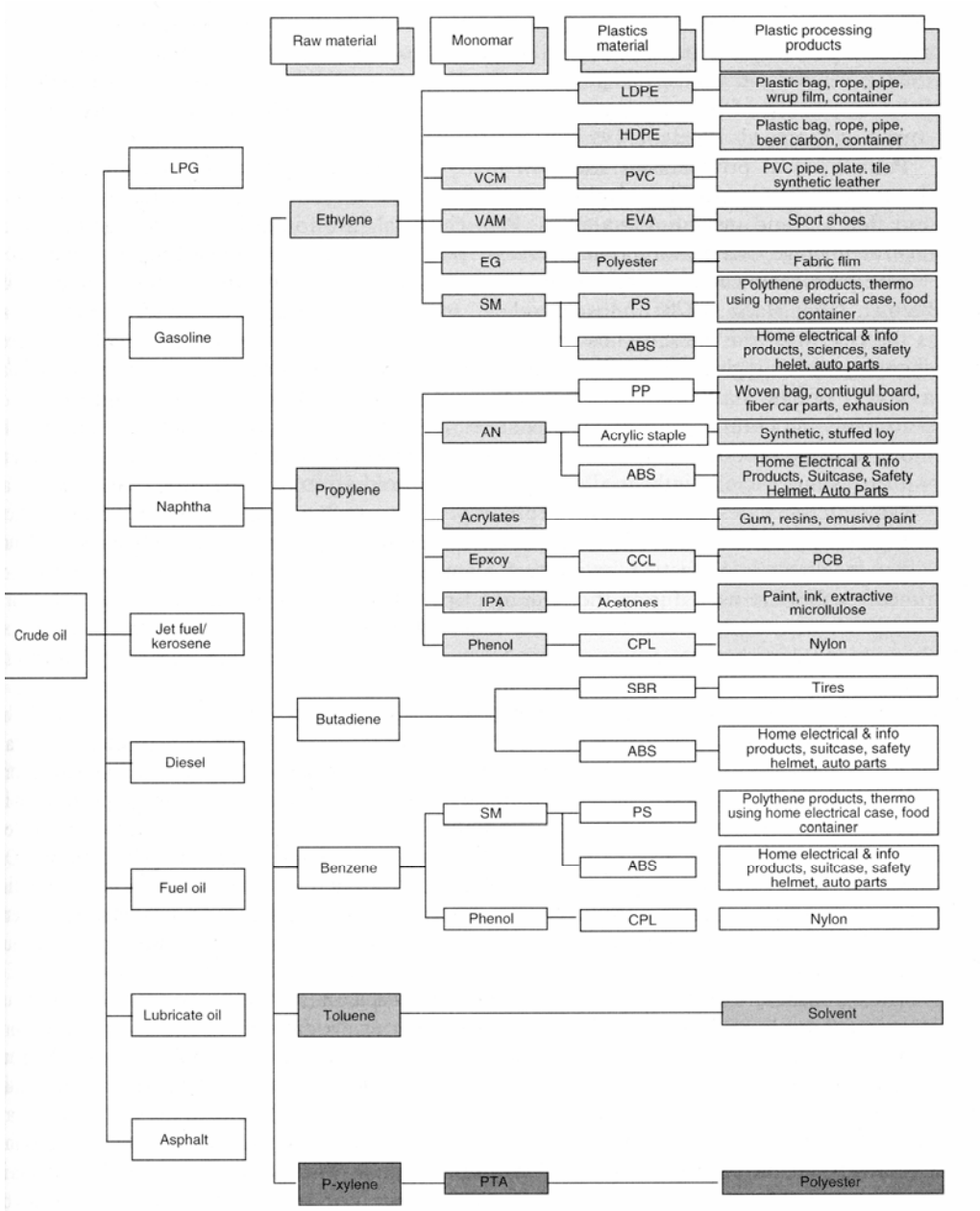

Figure 1-1[1] Crude oil and gas are the raw material for numerous products that are used daily such asfabric, plastic bags, paint, medicine etc.

Whether it is plastic, rubber, fabric, shampoo, or medicine, it is likely that some of the base chemicals originate from petroleum. Also the tires on your car and the very asphalt roads are products of crude oil. Crude oil is also currently the primary energy source in the world and seem to continue to have a dominant role for at least two more decades.[1] Throughout this work both petroleum and crude oil, which are equivalent terms[1] will be used.

However, the quality of the crude oil is decreasing and the heavy oils will be more and more prominent, leading to the need for more advanced recovery and refining methods. Crude oils are often divided into conventional and unconventional crude oils. Conventional oils are light oils with a high API gravity and low viscosity (see section 2.1), while unconventional crude oils are the opposite and may be so viscous that they can hardly be treated as liquids at room temperatures. In addition the crude oil will not last forever, although there will be produced fossil fuels for decades the peak of production will, sooner or later, be reached (Figure 1-2).[3]

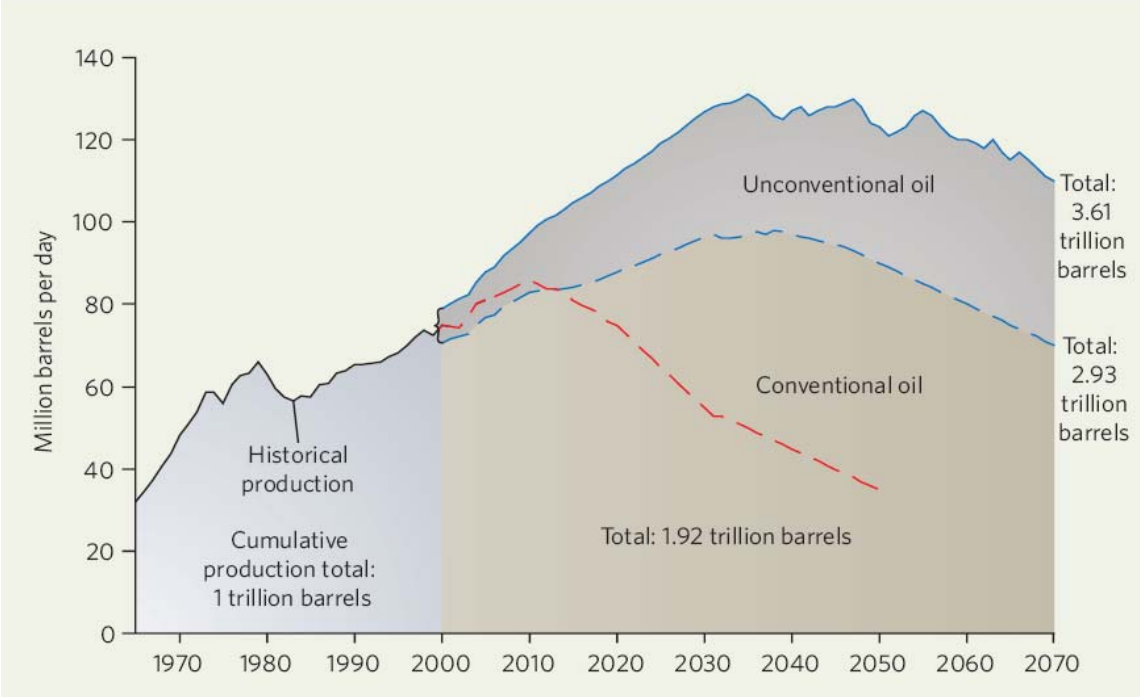

Figure 1-2. Many believe that we already have or very soon will reach the peak of production (red line). The more optimistic oil analysts believe that the production will increase for many years to come depending on if one counts on conventional oils only (stippled blue line), or include unconventional oils also (whole blue line).[4]

As the crude oil prices increase, the investment costs will be reduced compared to the profit so that fields earlier seen as non-profitable may be profitable due to the reduced availability of conventional crude oil and thus the point where production decreases can be delayed.

1.1 Petroleum

Petroleum occurs in sedimentary rock deposits throughout the world. By definition, petroleum (or crude oil) is a mixture of gaseous, liquid, and solid hydrocarbon compounds.[1] Petroleum also contains small quantities of nitrogen-, oxygen-, and sulfur containing compounds as well as trace amounts of metallic constituents. Petroleum is classified as a hydrocarbon resource along with coal and oil shale kerogen.[1] Fossil energy resources may be divided into two classes (1) naturally occurring hydrocarbons (petroleum, natural gas, and natural waxes), and (2) hydrocarbon sources (oil shale and coal) which may be used to generate hydrocarbons by the application of conversion processes. The latter may also be called *organic sediments* (Figure 1-3).[1]

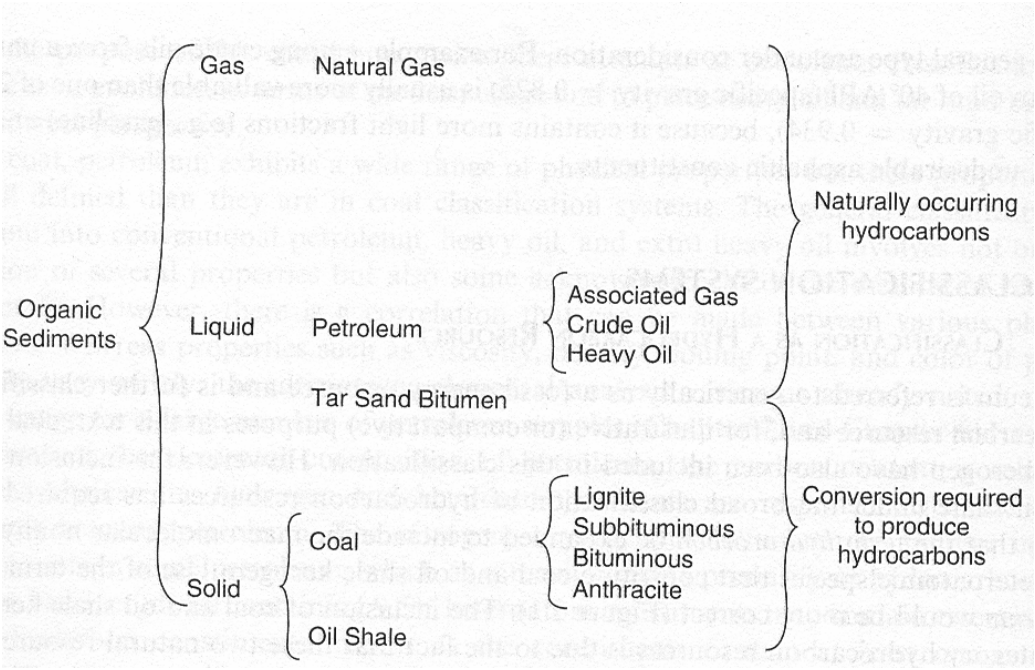

Figure 1-3. Organic sediments are generated into solids, liquids and gas wich are resources for energy and materials.[1]

1.2 Origin of petroleum

Although there have been attempts to formulate theories where inorganic substances serve as the origin for petroleum (abiogenic origin), there is now generally accepted that petroleum arises from the decay of organic matter in the earth (biogenic origin).[1] Hydrocarbons synthesized by living organisms account for less than 20 % of the petroleum. The remainder of the hydrocarbons in petroleum is produced by maturation processes generally referred to as diagenesis, catagenesis and metagenesis. Dia-, cata-, and metagenesis is the alteration of

organic matter during the formation of petroleum that may involve temperatures up to 50°C, between 50 and 200°C and above 200°C respectively. These three processes are a combination of bacteriological action and low-temperature reactions that convert the source material into petroleum.[1] During these processes, migration of the liquid products from the source sediment to the reservoir rock may also occur. Three conditions must be present for oil reservoirs to form: a rich source rock, a migration conduit, and a trap that forms the reservoir. The reactions that form petroleum are dependent on pressure and they are also very temperature sensitive. Reactions that produce oil commence at about 130 °C, and those that continue the breakdown to natural gas commence at about 180 °C. The range of 130-150 °C is generally considered the oil window.[1] The typical depth of the oil window would be 4-5000 meter. Transformation of sedimentary material to petroleum probably began soon after deposition, with bacteria playing a role in the initial stages, and clay particles serving as catalysts. Heat within the strata may have provided energy for the reactions and temperatures are increasing more or less directly with increasing depth.[1] Petroleum may therefore have been formed at temperatures not exceeding about 100 °C to 120 °C, with the generation of petroleum hydrocarbons beginning as low as 65 °C.[1]

1.3 Generation of petroleum

Generation of petroleum is associated with the deposition of organic detritus, and so, the composition of petroleum is greatly influenced not only by the nature of the precursors that eventually form petroleum but also by the relative amount of the precursors.[1] This means that the petroleum composition is dependent on the local flora and fauna which may explain some of the variation in petroleum around the world. In addition, the age of the field and the depth of the well influence the characteristics of the petroleum.[1] For the accumulation of hydrocarbons to occur, there needs to be a reservoir rock in which to store the fluid, and a source rock in which the oil and gas are formed. Reservoir rocks must be porous to hold onto the fluid and fluid-transmitting, i.e. permeable. Petroleum migrates to a pool or field, displacing the water, in which the oil or gas occupies pore space in the rock. Such pools may be large, extending laterally many square kilometres and up to several hundred meters vertically.[1] Since the oil and gas have migrated to the field, this was not the location where it was generated, as explained by the fact that petroleum generally is found in relatively coarse-grained porous and permeable rock that contain little or no insoluble organic matter.[1] Petroleum constituents may migrate through one or more formations that have permeability

and porosity similar to those of the ultimate reservoir rock. It is the occurrence of an impermeable, or a very low permeability, barrier that causes the formation of oil and gas accumulations (Figure 1-4). Flow within the networks of capillaries and pores must take place in the presence of the aqueous pore fluid, either with the flow, by displacement or by diffusion. In addition the fluid system may be single (oil and gas dissolved in water) or multiphase (separate water and hydrocarbon phases).[1] Due to the relatively low API gravity (defined in section 2.1) of gas and petroleum compared to saline water, petroleum accumulation is usually found in structural heights where reservoir rocks of suitable porosity and permeability are covered by a dense, relatively impermeable cap rock like evaporite or shale.[1]

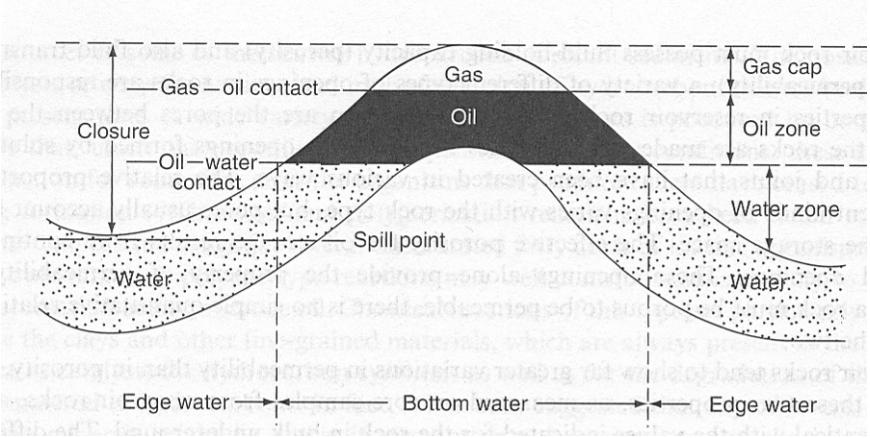

Figure 1-4. The oil and gas are found in so called reservoir rock, sealed by a non-penetrable cap. The lightest compounds (gas) is on top, while oil, and water if present, is found further down in the formation leading to gas, oil and water zones.[1]

This is known as a structural petroleum cap (Figure 1-4), where reservoir rock is sealed by a cap rock in the position of a geological height, such as an *anticline* (saddle shaped). Other types of traps like sand lenses, reefs and pinch-outs are also known.[1]

1.4 In situ transformation of petroleum

During its migration and when it has reached its trap and accumulates in the field, the petroleum will still be susceptible to alteration. Chemical alteration is thermal maturation and microbial degradation of the reservoir oils. Physical alteration may be the loss of low boiling compounds by diffusion or the addition of new constituents to the oil by migration of these constituents from a source outside the reservoir.[1] Moreover, it is likely that these processes

are interrelated and that they occur simultaneously. It is recognized that an increase in the temperature of a reservoir gradually increases the content of compounds containing 15 carbon atoms at the expense of heavier (C_{15+}) liquids, which themselves become increasingly paraffin in nature.[1] The overall result is lighter oil with lower sulfur content and higher paraffin content. Sulfur is presumably incorporated into the hydrocarbons by thermal reactions with elemental sulfur and hydrogen sulphide and these reactions may continue in the reservoir.[1]

1.5 Deasphalting in the reservoir

Deasphalting in the reservoir occurs as a natural process among the heavier crude oils whenever considerable amounts of the lower molecular weight hydrocarbons are generated in substantial quantities. Reasons for deasphalting may be generation of low molecular weight hydrocarbons by thermal alteration of the oil or as gas incursion from secondary migration.[1] Adsorption onto clay surfaces can play a major role in the fixation of asphaltenes during deasphalting.[5] In addition crude oils can be deasphaltenated by admixture with or dissolution in to the oil of large amounts of light hydrocarbons.[1, 5]

1.6 Occurrence of petroleum

The peaks of petroleum discoveries were in the end of the 1940`s and end of the 1960`s. Since then the amount of new resources discovered is 10 percent of the amount of new discoveries made in the top years (Figure 1-5).[4]

.

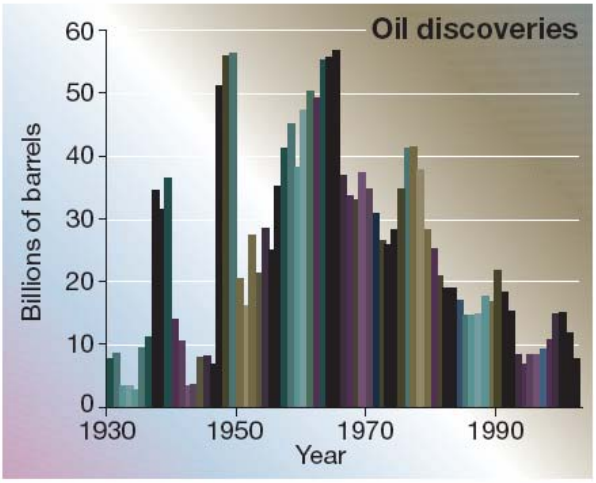

Figure 1-5. Amount of oil discovered each year was at maximum in the 1960´s. Since then the amount of new resources discovered has decreased gradually (except for some years in the late 1970´s).[4]

The majority of the crude oil reserves identified to date are located in a relatively small number of very large fields, known as giants. Three hundred of the largest oil fields contain almost 75% of the available crude oil.[1] Although most of the world's nations produce at least minor amounts of oil, the primary concentrations are in Saudi Arabia, Russia, the United States (chiefly Texas, California, Louisiana, Alaska, Oklahoma, and Kansas), Iran, China, Norway, Mexico, Venezuela, Iraq, Great Britain, the United Arab Emirates, Nigeria, and Kuwait.[1] The largest reserves are in the Middle East. Most of the crude oil currently recovered is produced from underground reservoirs. However, surface seepage of crude oil and natural gas is common in many regions, and it was surface seepage of oil that led to the first use of the high boiling material (bitumen) in the area known as the Fertile Crescent in the Middle East.[1]

1.7 Recovery, transportation and refining

1.7.1 Recovery

Recovery is the production of oil from a reservoir. There is a great difference in the production of conventional crude oil and the recovery of bitumen from tar sand deposits.[1] Only recovery of the conventional crude oil will be treated in this text. Oil wells are drilled, using a drilling rig after which the flow of oil into the well commences.[1] Different methods are used in order to increase the flow of oil from the reservoir to the well. Acid is pumped down the well for limestone reservoir rock in order to dissolve channels. For sandstone reservoir rock, fluid containing proppants (sand, walnut shells, aluminium pellets) is pumped down the well to induce small fractures in the sandstone that allow oil to flow into the well.[1] Once the oil starts flowing, the oil rig is removed and production equipment is set up to extract the oil from the well. Recovery of the crude oil can be divided into three (succeeding) phases called the primary recovery, secondary recovery and enhanced oil recovery (EOR).[1]

1.7.2 Primary recovery

Primary recovery is when the underground pressure by itself is sufficient to force the oil from the reservoir into the well. The crude oil will then move out of the reservoir into the well by one or a combination of the following processes; dissolved gas drive, gas cap drive and water

drive.[1] Dissolved gas in the oil goes out of the solution when the pressure is reduced. The dissolved gas drive is the least efficient leading to a total eventual recovery of less than 20 %.[1] Gas cap drive usually recovers 40-50% of the total recoverable oil. In primary recovery the most efficient propulsive force in driving oil into the well is natural water drive. Here the pressure of the water forces the lighter recoverable oil out of the reservoir and into the producing wells.[1]

1.7.3 Secondary recovery

Secondary recovery is sooner or later inevitable in order to produce more oil from a well. Over the lifetime of the well the pressure will fall until the there is insufficient pressure to force the oil to the surface. Secondary recovery methods may consist of pumping aid, either from the surface or submerged.[1] Increasing the pressure by water or gas injection is another method. Together, primary and secondary recovery allows 25% to 35% of the reservoir's oil to be recovered.[1]

1.7.4 Enhanced oil recovery (EOR)

Enhanced oil recovery (EOR) is the production of the oil that cannot be recovered from a petroleum reservoir by primary and secondary recovery methods. EOR processes use thermal, chemical, or fluid phase behaviour effects to reduce or eliminate the capillary forces that trap oil within pores, to thin the oil or otherwise improve its mobility or to alter the mobility of the displacing fluids.[1] EOR methods are designed to increase the production by reducing the viscosity of the crude oil. EOR is started when secondary oil recovery methods are no longer enough to sustain production. EOR includes polymer flooding with water by injection to improve horizontal and vertical sweep efficiency.[1] In contrast to polymer flooding, surfactant flooding is complex and requires a lot of laboratory work and knowledge about the reservoir conditions. Alkaline flooding is only used in reservoirs containing specific types of high acid-number crude oils. Carbon dioxide flooding has also proved efficient for displacing many crude oils, thus permitting recovery of most of the oil from the reservoir rock that is contacted.[1] Thermal EOR methods use steam injection methods (water) to heat the oil in the reservoir. Also in situ combustion, where some of the oil is burned to heat the surrounding oil is used, is normally used for reservoirs containing low-gravity oils.[1]

Technologies such as alkaline flooding, microemulsion (micellar/emulsion) flooding, polymer augmented water flooding, and carbon dioxide-miscible/immiscible flooding do not require or cause any change to the oil. Steaming technologies may lead to changes in the composition of the oil, but do not change the oil as such. In situ combustion, on the other hand, leads to thermal decomposition of parts of the oil. The fluid recovered from the well will contain not only oil, but gases such as H_2S, nitrogen, carbon dioxide, salt water, sand and precipitated salt, calcium naphtenates and precipitated asphaltenes. This multiphase system has to be transported to the refinery, but before this the gas, water and sand have to be separated out of the oil before further transportation to the refinery can continue.[1]

1.7.5 Transportation

Transportation of petroleum from the producing fields to the refinery usually takes place using pipelines. Often, several satellite fields from sub sea completions are tied to the same production facility saving the oil companies the investment cost for expensive offshore facilities (Figure 1-6).[6]

Figure 1-6. The Statoil operated Åsgard ´field´, showing sub sea well templates linked by multiphase flow lines and risers to the Åsgard B floating production platform (left) and the Åsgard A floating production, storage and offloading ship. [7]

Flow assurance of the multiphase system is of great importance, both from an economic and an environmental point of view. The tiebacks are usually 5 to 10 km long, but can be much longer.[6] This gives possibilities for changes in temperature, pressure and composition during

the transportation. Furthermore the crude oil must be treated at the refinery prior to distillation and cracking. Most often the crude oil and water has formed an emulsion which needs to be broken so that the water can be separated from the oil phase.[8] Traditionally gravity separators were used, while more recently the additional use of strong electric fields, forcing the water droplets to coalesce, has become industrial practice. The topics emulsions and gravity separators and electrical coalescence will be treated later (section 4).

1.7.6 Refining

Refining of the crude oil is the end of the beginning. The refining starts with the crude oil and gas and the goal is twofold: production of fuels for energy consumption and production of raw materials for the chemical industry especially.[1] The refining starts with a distillation of the crude oil into fractions based on boiling points. From there, several chemical and physical processes are needed to get the desired products and products qualities (Figure 1-7).[9]

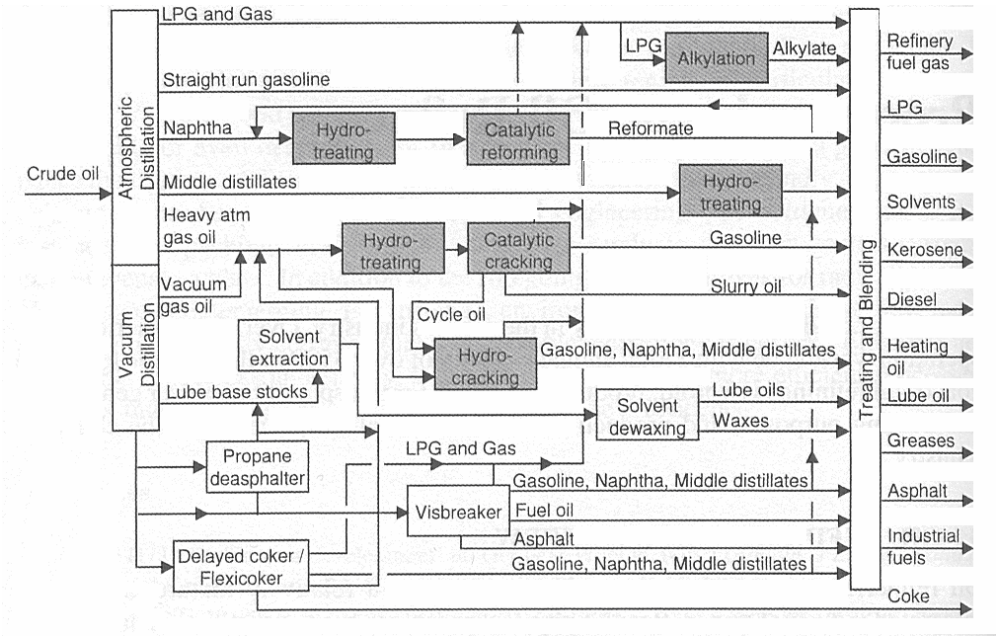

Figure 1-7. Flow scheme of a complex modern oil refinery. Crude oil is first heated and enters an atmospheric distillation column (left). Distillation fractionates the crude oil based on boiling point and heavy compounds which do not evaporate are distilled under vacuum. After distillation, the fractions are further treated and blended to various raw materials and products (right).[9]

Many challenges are present in the processes of refining crude oil. Asphaltenes may be a problem upstream by precipitation in the well, but they are probably as large a challenge in the refining process downstream the distillation column. Asphaltenes may coke on walls and

poison catalysts and large amount of heat is often needed in treating asphaltenes.[1, 8, 9] More on the refining of petroleum generally and problems related to asphaltenes specifically can be found in Speight[1] and Moulijn et. al.[9] and Nomura et. al.[8]

2 CRUDE OIL CONSTITUENTS

Crude oils are a continuum of tens of thousands of different hydrocarbon species. However, the proportions of the elements in crude oils vary over fairly narrow limits despite the wide variation found in properties from the lightest crude oils to highly asphaltenic crudes.[10] Carbon content is usually in the range 83 – 87% and the hydrogen content varies between 10 and 14 %. In addition small amounts of heteroatoms like nitrogen, sulphur, oxygen and metals (Fe, Ni, V, Mg etc.) are found in crude oils.[1]

Crude oil is considered as a black, viscous liquid. This is not always the case. As shown below there may be a large difference in colour nuances for various types of crude oils (Figure 2-1). The samples are obtained from different heights in a single column of oil.[11] The top sample is to the right and the bottom samples to the left and the differences in the samples are due to the differences in density of the constituents. Lighter samples are less dense while the darker samples contain more complex compounds with higher density. Furthermore the coloration is in part related to the constituent polycyclic aromatic hydrocarbons (PAHs). PAHs in crude oils are usually identified as the resins and the asphaltenes which are solubility classes in crude oils. In addition, two more solubility classes are defined in crude oils, namely the aromatics and saturates.

Figure 2-1. Crude oils are seen as black fluids for the most part, but this picture shows the separation of the crude oil due to gravity in the well. The dark oils (left) are higher in density and has higher concentrations of asphaltenes and other poly aromatic hydrocarbons (PAH).[11]

2.1 Heavy crude oils

Crude oils are often divided into conventional crude oils, heavy crude oils, and extra heavy crude oils. One common measure of the heaviness of petroleum is the API gravity which is related to the density and specific gravity (spgr at 15.6 °C) of the oil according to:[1]

°API= (141.5/spgr@15.6°C) - 131.5 2-1

It is shown (Equation 2-1 and Figure 2-2) that light oils have a high °API while heavier oils have lower °API.

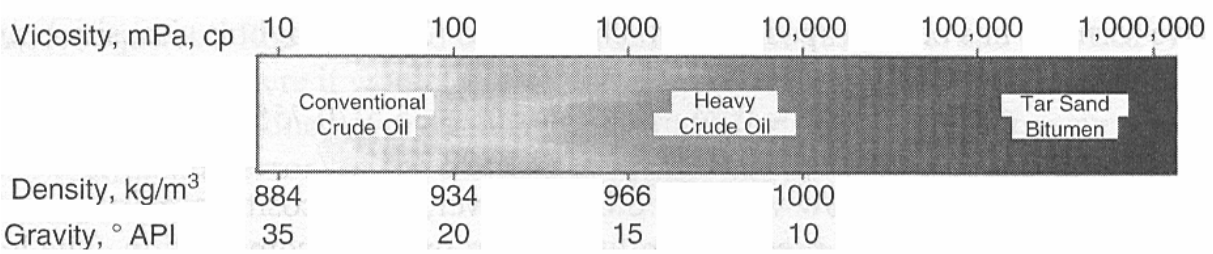

Figure 2-2 Classification of petroleum, heavy oil, and bitumen by API gravity and viscosity.[1]

Attempts have been made to correlate API gravity to both acid and base number of crude oils. Furthermore, with more success, the API gravity has been correlated to the refractive index.[12] It has also been shown that the API gravity to a certain degree can be correlated to the amount of aromatics and compounds containing nitrogen, oxygen and sulfur like asphaltenes and resins.[13]

2.2 SARA

Division of the crude oil into saturates, aromatics, resins and asphaltenes (SARA) is a subdivision based on solubility of various component classes in the crude oil. SARA consists of saturates which are non-polar iso and cyclo paraffin compounds including waxes. Aromatics is the fraction soluble in soluble in *n*-hexane[10] which is not part of the saturates. Resins are larger, more polar aromatic compounds which, at room temperature, are semi-solid and sticky. Asphaltenes are believed to be of the same type as the resins although of larger molecular weight and with a larger aromatic ring structure with a brittle powder like appearance. Asphaltenes and resins also contain naphtenic groups, alkyl side chains and heteroatoms like nitrogen, oxygen and sulfur.[1] Asphaltenes, which are the first fraction extracted in the SARA procedure (Figure 2-3), are precipitated by dilution of the crude oil with excess *n*-alkane, usually *n*-heptane or *n*-hexane (the ratio may be 30:1 or 40:1 *n*-alkane-to-crude oil). When the asphaltenes have been precipitated, the saturates, aromatics and resins are eluted with the proper solvents.[14] The saturate fraction is usually eluted using *n*-hexane or *n*-heptane. Aromatics may be eluted with the same solvents, but it may also be convenient

using toluene. Resins are eluted using a highly polar solvent like trichloromethane[10] or a mixture of polar solutes like 40:30:30 acetone:toluene:methylene dichloride.[15]

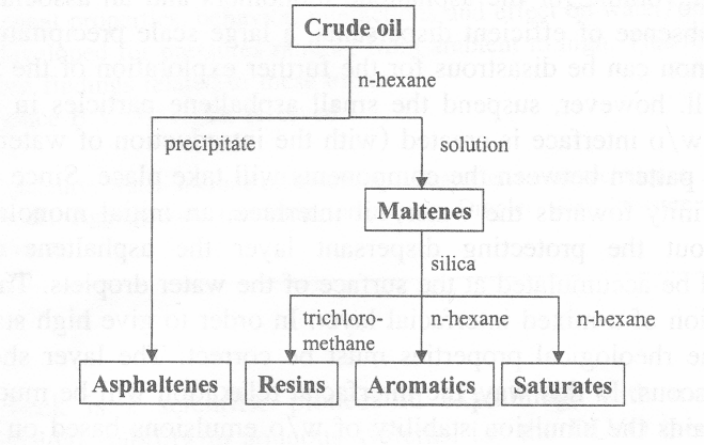

Figure 2-3. The fractionation of crude oil starts with the precipitation and filtration off of the asphaltenes using an *n*-alkane like *n*-hexane. The remaining crude oil is called the maltenes and may be further separated in a silica column to resins, aromatics and saturates using the solvents indicated.[10]

2.3 Asphaltenes – functionality versus structure

"Does the live oil have an asphaltene deposition problem?" "Drop the pressure on the live oil and see if asphaltenes precipitate".[16] That's what is called a phenomenological approach to uncover problems associated with oil chemistry, opposed to the approach of understanding the crude oil chemistry and the behaviour of crude oil components with regard to their chemical characteristics. Oliver Mullins describes the ultimate goal for petroleum science as developing a complete listing of every compound in a crude oil. He also stresses the need for understanding the structure-functionality relationships of the crude oil components, whether it is for the whole crude oil or for bulk fractions of the oil.[16] He often cites Francis Crick[17], one of the discoverers of the alpha-helix, "if you want to understand functionality, study structure". The structure and functionality of asphaltenes will be treated below and has also been a major part of the experimental work performed in this thesis.

2.3.1 Composition

The elemental composition of the asphaltenes is of great importance for starting to understand its structural traits. The most common elements building up crude oils and asphaltenes are the carbon, hydrogen, nitrogen, oxygen, and sulfur (CHNOS) atoms which vary over relatively

narrow ranges (Table 2-1).[1] In addition some metals of which nickel and vanadium are most prominent are also found in asphaltene bulk samples.[1]

Table 2-1. The composition and proportions (% weight) of the most abundant chemical elements found in petroleum. [1, 18]

Element	Content in crude oils %	Content in asphaltenes %
Carbon	83.0% to 87.0%	78% to 89.0%
Hydrogen	10.0% to 14.0%	6.5% to 11.9%
Nitrogen	0.1% to 2.0%	0.6 to 3.3%
Oxygen	0.05% to 6.0%	0.3% to 4.9%
Sulfur	0.05% to 6.0%	0.3% to 10.3%
Metals (Ni and V)	< 1000 ppm	

As shown (Table 2-1), the variation in the elemental composition is fairly low for crude oils and a little higher for asphaltenes. It is therefore surprising that both the light mobile crude oils and the very heavy asphaltic crude oils fit within the ranges shown. Furthermore, the hydrogen-to-carbon ratio is 1.15 ± 0.5% although a value outside of this range is sometimes found.[1] The elemental analysis can give an indication about the polarity of the asphaltene molecule but it does not reveal anything about size or structure with regard to aromaticity, the length of alkyl side chains, or the type of polar functional groups. Elemental analysis is important but reveals little about the asphaltene molecule, and therefore other experiments are mandatory in order to elucidate the structure of asphaltenes (and other crude oil components).

2.3.2 Molecular Weight

The debate over the size of the asphaltene molecule has lasted for a very long time, and it is still not settled.[19-21] Asphaltenes consist of tens of thousands of different molecules with a high degree of polydispersity both in size and structure. The molar mass of asphaltenes has been reported in the range of some hundreds up to several millions g/mol depending on the techniques used.[16, 22, 23] One of the reasons for the lack of agreement is the different and often inadequate techniques previously used (Figure 2-4). Early methods for determining the molecular weight of asphaltenes, included cryoscopic methods, viscosity measurements, ultracentrifugation, electron microscopy, film balance, small angle neutron scattering and

vapour pressure osmometry. Vapour pressure osmometry suggested that asphaltene MWs were dependent on both solvent and temperature.[24] What has been known for a long time is that asphaltenes form molecular aggregates, even in dilute solutions and that this association is influenced by solvent polarity, asphaltene concentration and the temperature.[25]

Table I. Various Methods for the Determination of Molecular Weight of Asphaltics

Method	Range	Investigator
Ebullioscopic	2,500–5,000	R. L. Griffin, W. C. Simpson, and T. K. Miles, ACS, Div. of Petroleum Chem., *Preprints*, **3**, No. 2, A13 (1958).
Cryoscopic, benzene	5,000–6,000	A. N. Sakhanov and N. A. Vassiliev, *C.A.*, **28**, 298 (1934).
		M. Katz, *Can. J. Research*, **10**, 435 (1934).
Cryoscopic, naphthalene	1,700	E. S. Hilman and B. Barnett, *Proc. Am. Soc. Testing Materials*, **37**, 558 (1937).
Cryoscopic, phenanthrene	2,500	M. L. Boyd and D. S. Montgomery, *Fuel*, **41**, 335 (1962).
Viscosity	900–4,000	K. A. Fischer and A. Schram, 5th World Petroleum Congress, New York, Sec. V, Paper 20 (1959).
		G. W. Eckert and B. Weetman, *Ind. Eng. Chem.* **39**, 1512 (1947).
Osmotic pressure	20,000–80,000	J. W. A. Labout and J. P. H. Pfeiffer, "Properties of Asphaltic Bitumen," Elsevier, p. 36, 1950.
		W. M. Zarrella and W. E. Hanson, Geological Soc. Am. meeting, Denver, 1960.
Ultracentrifuge	13,000–46,000 (r = 15.9–24.7 Å)	P. A. Witherspoon, Ill. State Geological Survey, R. I., No. 206 (1958).
		B. R. Ray, P. A. Witherspoon, and R. E. Grim, *J. Phys. Chem.*, **61**, 1296 (1957).
Ultracentrifuge	50,000–2,500,000	R. S. Winniford, *J. Inst. Petroleum*, **49**, 215 (1963).
Electron microscope	<100,000 (d<65 Å)	D. L. Katz and K. E. Beu, *Ind. Eng. Chem.*, **37**, 195 (1945).
Electron microscope	(d = 50–150 Å)	R. S. Winniford (loc. cit.)
	(d = 20–35 Å)	J. P. Dickie and T. F. Yen, ACS, Div. of Petroleum Chem., *Preprints*, **11**, No. 3, 39 (1966).
Film balance	80,000–140,000	J. P. H. Pfeiffer and R. N. J. Saal, *J. Phys. Chem.*, **44**, 139 (1940).
Small angle scattering	(R = 30–70 Å)	C. W. Dwiggins, Jr., *J. Phys. Chem.*, **69**, 3500 (1965).
	(d = 100–300 Å) (R ~ 50 Å)	J. P. Dickie, S. S. Pollack and T. F. Yen (unpublished data).

Figure 2-4 The table shows some of the older techniques for determining the molecular weight of asphaltenes. Note the large variation in the measured molecular weights ranging from less than 1,000 to more than 2, 500 000 g/mol. [22]

The molecular weights for asphaltenes have been determined to be very large in previous literature, depending on solvent and method. Yen[25] lists a table showing the variation of insoluble fractions obtained by soxhlet extraction of pentane precipitated asphaltenes (Figure 2-5).

Asphaltenes	Solvent [a] (wt%)	Molecular weight			
		C_6H_6	CH_2Br_2	C_5H_5N	$C_6H_5NO_2$ [b]
Untreated	100	4050	2730	2310	1610
Pentane-extracted	90	8450	6740		2820
Extract	10	845			
Heptane-extracted	72	8940	7120	4380	2980
Extract	28	2310			
Hexadecane-extracted [c]	58	12490	8800		3510
Extract	42	2530			
Methylethyl ketone-extracted	93	15650		5980	3060
Extract	7	983			
3-Pentanone-extracted	65	18000		12410	6380
Extract	35	1352			
Ether-extracted	93	11370	8730		2910
Extract	7	1822			
Ethyl acetate-extracted	95	12000	8260	4270	2880
Extract	5	728			

[a] Asphaltene concentration: 2.5% w/w; temperature: 37°C.
[b] Extrapolated values from data derived at 100, 115 and 130°C.
[c] Stirred at 85°C for 24 h; insolubles separated by filtration; solubles separated by removal of the solvent in vacuo.

Figure 2-5. Measured molecular weights (by VPO) vary depending on the solvent on which the asphaltenes were dissolved during the measurements. The figure shows molecular weights determined for various asphaltene fractions precipitated by various solvents from pentane pre precipitated asphaltenes.[25]

As seen (Figure 2-5) there is a huge variation in the different asphaltene fractions. Dependent on both the solvent and the non-solvent (precipitation agent) used, the MWs ranged from 728 g /mol for the ethyl acetate-extracted to 18,000 for the 3-pentanone-extracted asphaltenes. Furthermore the molecular weight determined for *n*-pentane asphaltenes using different dispersing solvents varied from 5,120 g/mol for benzene to 13,390 g/mol for pyridine as dispersing solvent. The MWs determined for solvents that prevent or reduce association was usually in the range of 2000 ± 500 g/mol.

Yen[26] introduced in 1974 the notion of the asphaltene molecule as a single unit sheet in complex particules, whose weight is around 1000 g/mol. This single unit sheet is built up by an aromatic condensed cycle system in the centre surrounded by some aliphatic naphthene radicals. The asphaltene particule consists of several parallel unit sheets held together by physicochemical forces. Bunger[27] suggested in 1979 that asphaltenes are monomeric in nature and possess average molecular weights in the range of 500-800 g/mol, broadly distributed with respect to aromaticity and heteroatom content. Others such as Speight and Moschopedis[28] and references cited in chapter 3 in Yen[25] accepted that the molecular weight is higher than 1000, but that monomeric units in asphaltene polymer molecules are quite small (400-500 g/mol) and connected through carbon-carbon or sulphide linkages. One of the early studies using electron impact (ionization) mass spectrometry on asphaltenes showed that the

largest molecules in the asphaltene sample analyzed were around 1400 g/mol and that the number molecular weight was less than 814 g/mol.[29]

The newest research with regard to the molecular size of asphaltenes has been driven by Oliver C. Mullins and Henning Groenzin. They have published articles and books the last decade or so, addressing the size and structure of the asphaltene molecules (chapter 2, reference [16], and references herein). The Time Resolved Fluorescence Depolarization (TRFD) technique has showed that the rotational diffusion constant of all asphaltene molecules is small, thus, the asphaltene molecules are small. Furthermore, TRFD results have indicated that there is one chromophore per asphaltene molecule and that the mean molecular weight of essentially all virgin crude oil asphaltenes is ~750 g/mol with a range of ~500 – 1000 g/mol.[16, 30, 31] This value is disputed by others who argues that the FD technique is not capable of detecting the full breadth of the molecular mass distribution and thus can not detect some of the heavier materials within the asphaltene samples.[19, 32]

In several studies where vapour pressure osmometry (VPO) and gel permeation chromatography (GPC) have been used, NMP (1-methyl-2-pyrrolidinone or *N*-methyl pyrrolidone) has been applied as a solvent for the asphaltenes, based on conclulsions that NMP is a better solvent for asphaltenes than tetra hydrofuran (THF).[19] This may have led to overestimations of the molecular weights of the asphaltenes measured since NMP aggregates and flocculates a significant part of the asphaltene fraction.[20, 33] Therefore, molecular weights in the million g/mol region obtained using GPC[34] is probably due to aggregated and flocculated asphaltenes.[21] Furthermore, both GPC and vapour pressure osmometry suffer from an unknown state of aggregation of asphaltenes[32, 35] which may be the major source of the discrepancies in the determination of molecular weights when compared with FD, and diffusion measurements[16, 21]. An even stronger proof of the possible overestimation of molecular weights for asphaltenes were obtained by using VPO on alkyl substituted hexabenzocoronenes. In that study it was shown that the model compound and asphaltenes showed concentration dependency on the apparent molecular weights.[36] Very high molecular weights, several tens of thousands and up to millions of g/mol, implies that it is very likely that the average weights of particles in various states of aggregation have been measured due to intermolecular and inter particle forces.[22]

2.3.3 Are asphaltenes monomeric or polymeric?

The discussion about the size and structural characteristics of asphaltenes is closely linked to the debate around the molecular weights. There is still not settled if asphaltene molecules are of the "polymeric", archipelago structure[23, 37] (Figure 2-6 a) or of the "monomeric", island[38] structure (Figure 2-6 b).

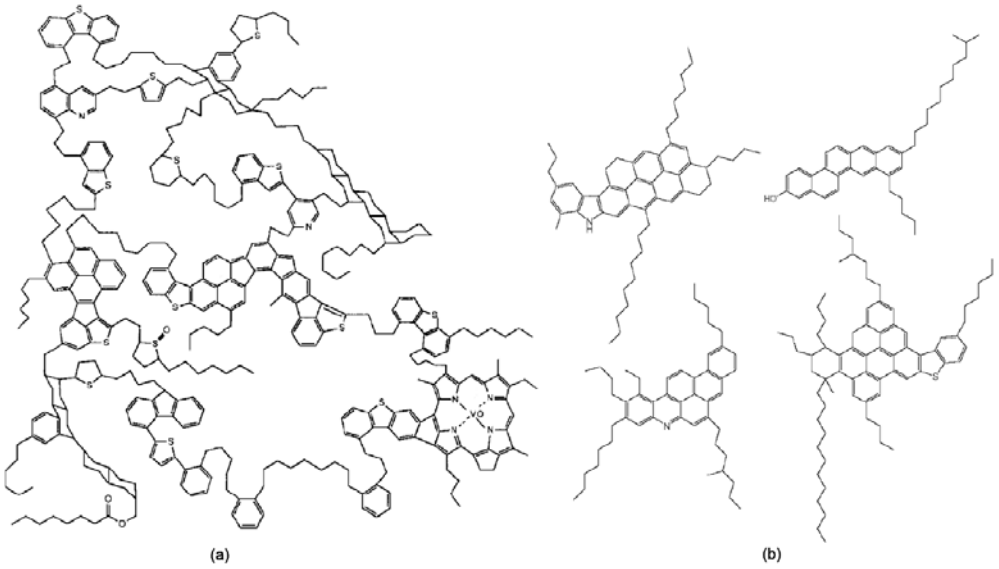

Figure 2-6. (a) A hypothetical asphaltene molecule according to Strausz[23] ('Archipelago model'). (b) Four hypothetical asphaltene molecules representing the island structure according to Mullins[38].

From structural characterizations (NMR and IR, see section 5) and elemental analysis a high average molecular weight determined for the asphaltene will give a molecule with a large structure (Figure 2-6 a), while low molecular weights will give a molecule with a smaller structure (Figure 2-6 b). The molecular weight determination will of course not affect the general structure obtained from the structural characterization methods leading to either an "island" or an "archipelago". As discussed in section 2.3.2, the molecular weight has been one of, if not the most disputed characteristic of asphaltenes and the enormous variations in the molecular weights determined may have resulted in erroneous assumptions of the structure of the asphaltene molecule. Furthermore, the so called polymeric asphaltene molecule as described in the literature does not constitute all the traits of a polymer. Although asphaltenes are polydisperse and may have aromatic cores which are cross linked, they do not constitute long repetitive structures of similar monomeric compounds.[22, 39]

Studies which are used to argue for the "polymeric" archipelago structures of asphaltenes are pyrolysis, oxidation and thermal degradation, and also small angle neutron scattering. It is suggested that only pyrolysis of asphaltene molecules with archipelago structures would yield products with a wide range of molecular weights while pericondensed (island) structures would yield products only in the gas, naphta, and residue fractions.[37]

Yen and coworkers[22, 39] suggested that asphaltenes are macromolecules but not in the traditional sense of large molecules where all the various chemical elements are held together by strong chemical forces. Still, in their structural asphaltene model, there are true large molecules involved. These molecules are condensed heterocyclic aromatic sheets with attached alkyl chains restricted to the plane of the sheet. Furthermore they perceived these sheets to be approximately 8.5-15 Å in diameter. They reported these molecules to be capable of associating with each other in their third dimension in the presence of non-polar or slightly polar solvents to form stacked clusters about 16-20 Å in height. Such clusters consist of about five sheets, a number which most likely will depend on the asphaltene type and the environment the asphaltene finds themselves in.[25]

The hierarchical structures proposed by Yen, which suggest that asphaltenes are indeed monomeric and not polymeric species, are supported and updated by the work of Mullins et al.[16] The dynamics of asphaltene solutions at low concentrations are explained by the additional constraints of the small molecular size of asphaltenes. For example dilute toluene solutions of asphaltenes start to form nano aggregates at approximately 150 mg/litre and maybe at even lower concentrations. Asphaltenes associate as nano aggregates and one molecule participates only in a single aggregate structure. The molecules are held together by van der Waals interactions of geometrically positioned ring systems whose size is restricted by steric hindrance due to alkyl side chains which may also contain OH or sulfur functional groups. At higher concentrations, the nano aggregates will cluster together and eventually form bigger aggregates that precipitate out of the solution.[16] The most important factors for the understanding and prediction of the properties of asphaltenes are to know the size of the asphaltene molecules and the chemical structure of the important fractions of the asphaltene solubility class. From that knowledge it may be possible improve predictions on the phase behaviour of the asphaltene solubility class(es) and design better asphaltene inhibitors.

2.3.4 Phase behaviour of asphaltenes

By definition the asphaltene fraction of the SARA is the fraction insoluble upon addition of an *n*-alkane and soluble in toluene. Asphaltene aggregation and precipitation problems are encountered both in the reservoir and during transportation and processing of petroleum (Figure 2-7).[40]

Figure 2-7 Asphaltene debris dug out from a separator.[7]

It is difficult to predict where and when in the production such problems might arise.[41] However, problems may be severe, can damage production equipment and personnel and lower production.[42] This again will affect the production capacity and profit for the companies. In order to try to inhibit or reduce asphaltene precipitation, solvents and chemical inhibitors are used. These often have negative impact on the environment and therefore it is of great importance to understand the phase behaviour and chemistry of asphaltenes in order to find the best measures to solve the problems. In order to understand the solvent, solubility and surface activity of compounds in crude oil emulsions, the structure-functionality relationships of the asphaltenes have to be elucidated.

What is special about crude oils and asphaltenes is that it is most often the light crude oils, containing small amounts of asphaltenes (less than one percent by weight) which are most susceptible to asphaltene problems (Ting et. al., chapter 12 ref [16]). The effect of pressure is most pronounced for light oils near the bubble point. Asphaltenes are stable at high pressure and at pressures well below the bubble point, but, in many cases, they are unstable at pressures somewhat above and below the bubble point.[16] Temperature changes may result in either asphaltene precipitation or solubilization. For instance, in the propane deasphalting process (part of the refinery processing of crude oils), asphaltenes become increasingly unstable with temperature increase. However, for *n*-alkane (*n*-C_{5+}) titrations, asphaltene

stability improves with increasing temperature.[16] The detection of bubble points and asphaltene aggregation onset pressures can be done by near infrared spectroscopy (NIR) where aggregation onset is seen as a baseline elevation of the NIR spectra due to light scattering.[41, 43] or by measuring the refractive index of the oil phase.[44, 45]

Heavy oils typically have relatively low proportions of volatile compounds with low molecular weights and quite high proportions of high molecular weight compounds.[16] The high molecular weight fraction of heavy oils are comprised of a mixed bag of compounds (not necessarily just paraffins or asphaltenes) with high melting points and high pour points that greatly contribute to the poor fluid properties of heavy oils and hence poor mobility. Pour point is the temperature at which the crude oil no longer can be poured from a container and is related to wax precipitation due to a lowering of the temperature. It is this poor mobility of the crude oil, as opposed to accumulations of paraffins or asphaltenes in formation rock pore throats or production strings, which is usually at the heart of the production problems.[46]

In summary, there is really no direct positive correlation between heavy oil and paraffin or asphaltene problems. The "heaviness" of heavy oil is primarily the result of a relatively high proportion of complex, high molecular weight, non-paraffinic compounds and a low proportion of volatile, low molecular weight compounds. Heavy oils typically contain very little paraffin and may or may not contain high levels of asphaltenes. Also, the problems associated with producing heavy oils are typically a result of the poor fluid properties and mobility of the oil as opposed to paraffin or asphaltene accumulations.[46]

There are several models for prediction of the phase equilibrium of crude oils and asphaltenes. The compositional models which addresses each compositional group in the crude oils separately, treats the heavy fractions of the crude oils as pseudo pure components. These models are poor predictors and require a minimum of experimental data under conditions similar to those of the reservoir.[42] Models considering asphaltenes and resins as polymers or chains of oligomers have led to major breakthroughs over the last few years. Another research direction consists in using flocculation measurements under ambient conditions to input data to models as a function of pressure. The various fluid phase equilibrium models and flocculation models for asphaltenes will not be treated further but can be found elsewhere in the literature.[42, 47-52]

2.3.5 Pressure and deposit asphaltenes versus laboratory obtained asphaltenes

Most often, research on crude oil and crude oil components is performed on dead oil samples. When oil is referred to as "dead" it means that it has been depressurized so that it no longer can be assumed to hold reservoir conditions. The reason for working with dead oils is basically that it is easier to handle since high pressure liquids and containers are for the few to operate, due to safety precautions and expensive equipment.[52] Dead oils can be re-pressurized and studied under the assumptions that the properties of the oils are reversible upon re-pressurization and at addition of lighter hydrocarbons and gases lost during depressurization. Nevertheless, studies show that there may be a large difference between live and dead oil in the properties of the crude oil as such and its separate components.[16, 53, 54] Klein and co-workers[53] studied two asphaltene samples collected from *n*-heptane precipitation and live oil depressurization experiments from the same well. By the use of Fourier transform ion cyclotron resonance mass spectrometry (FT-ICR-MS) with microelectrospray ionization, they found that the C_7 (heptane) asphaltenes contained lower relative abundance of the nitrogen containing species but had higher amount of rings plus double bonds compared to the pressure drop (P-drop) asphaltenes. Pressure drop asphaltenes were enriched in compounds containing sulfur (NS and NS_2) with fewer rings plus double bonds. The conclusion was that analysis of dead-oil samples may be very misleading because if the oil loses components upon pressure reduction, then only a subset of the asphaltene fraction remains in the dead oil.[53]

Although the P-drop asphaltenes may drop out of solution upon depressurization it does not mean they are "lost" (as long as they still are transported with the crude oil from the well) but that they will not behave as they do under reservoir conditions. Nevertheless, if already precipitated, they will be included in the asphaltene fraction upon precipitation and filtration. But if it is the P-drop fraction and not the C_7 asphaltenes that poses the problems related to asphaltene precipitation and other asphaltene related problems, then the focus should solely be on P-drop asphaltenes and their behaviour under real conditions. However, if it is found that it is possible to separate the P-drop fraction out of the dead oil by some precipitation procedure other than the normal 40:1 procedure, then one can continue to study asphaltenes and base predictions and phase equilibrium models on research derived from asphaltenes from dead or re-pressurized crude oils.

2.3.6 Main challenges in the further research on asphaltenes

One of the main challenges in the prediction of the behaviour of crude oils is to obtain reliable parameters for the crude oil components, and particularly with respect to the asphaltene fraction, to insert into phase equilibrium models. In order to achieve this, there is a need to know which part of the asphaltene fraction is causing most problems, and where these problems might arise. It may be that one fraction of the asphaltenes is mainly responsible for the problems related to precipitation and blocking of pores in the well, while other fractions are responsible for adsorption to surfaces, stabilizing of emulsions, coking and poisoning of catalysts.

The comments in this chapter will be on the precipitation of asphaltenes upstream the refinery where, the precipitation is most often due to pressure drop. Most work on asphaltenes have been on solvent precipitated asphaltenes. There should be more focus on the pressure drop and deposit asphaltenes, at least in order to either confirm or reject important differences in weight, molecular structure and other properties compared to solvent precipitated asphaltenes. If the pressure drop asphaltenes are different from the whole fraction of asphaltenes precipitated with excess solvent (40:1) then the whole of the asphaltene fraction should be fractionated based on solubility (and polarity) in order to determine if some fractions are similar (or identical) to the pressure drop/deposit asphaltenes. If one detects the pressure drop fraction inside the solubility fraction, then one can continue working on solvent precipitated asphaltenes. On the other hand, if one does not manage to identify the pressure drop fraction inside the solvent fraction, then the predictions based upon results from solvent asphaltenes may be of lesser value than the results from pressure drop asphaltenes.

3 PREDICTION OF SOLUBILITY PARAMETERS BY MULTIVARIATE DATA ANALYSIS

3.1 Solubility parameters – Basic theory

The use of solubility parameters and other cohesion parameters has just one aim and that is to provide a simple method for correlating and predicting the cohesive and adhesive properties of materials from a knowledge of the properties of the components only.[55] The solubility parameters represent the interaction forces between molecules and are electromagnetic by nature. When an individual molecule is in a medium (gas or liquid), it has what may be called a "cohesive energy" or "self-energy", associated with it. To determine the pair potential w(r) of two identical molecules "1" in a medium "3" ("2" is a second molecule interacting with "1" and "3") one has to take into account the static dielectric constants of the media $\varepsilon_1(0)$ and $\varepsilon_3(0)$, the refractive indices (n_i) of the medium, the molecular radius a and the distance between the two molecules of type "1" (Equation 3-1). The total van der Waals interaction free energy of two identical molecules "1" in medium "3", at frequencies υ, then becomes:

$$w(r) = w(r)_{\nu=0} + w(r)_{\nu>0} \approx \left[3kT \left(\frac{\varepsilon_1(0) - \varepsilon_3(0)}{\varepsilon_1(0) + 2\varepsilon_3(0)} \right)^2 + \frac{\sqrt{3h\nu_e}}{4} \frac{(n_1^2 - n_3^2)^2}{(n_1^2 + 2n_3^2)^{3/2}} \right] \frac{a_1^6}{r^6} \qquad 3\text{-}1$$

Which is strictly valid only for $r >> a_1$.

The refractive index can be defined as (Equation 3-2):

$$n_i = \sqrt{\mu_i' \varepsilon_i'} \qquad 3\text{-}2$$

where μ_i' is the permeability of the medium and ε_i' is the dielectric constant. ε_i can be replaced by n_i^2 since the permeability is very close to unity.[56]

As a rule of thumb, it is known that "like dissolves like". This is apparent from the above equation where one sees that w(r) basically depends on the magnitude of $(n_1^2 - n_3^2)^2$. The

equation tells us that two liquids become immiscible once $(n_1^2\text{-}n_3^2)^2$ becomes too large. This can further be written as (Equation 3-3):

$$\left[\sqrt{(n_1^2-1)^2}-\sqrt{(n_3^2-1)^2}\right]^2 \qquad 3\text{-}3$$

which from the Lorenz-Lorentz equation is roughly proportional to (Equation 3-4):

$$w(r) \propto \left[\sqrt{U_1}-\sqrt{U_3}\right]^2 \qquad 3\text{-}4$$

where U_1 and U_3 are the cohesive energies or latent heats of vaporization of the two liquids.[57] This semi-quantitative derivation forms the basis of the Hildebrand "solvent solubility parameter" δ [$MPa^{1/2}$], which is equal to the square root of the cohesive energy density.[57]
U is defined as the molar internal energy that is the molar potential energy of a material relative to the ideal vapour at the same temperature. The molar cohesive energy, which is the energy associated with the net attractive interactions of the material, is defined as –U, and has a positive value. The value of –U is dependent on the molar vaporization energy, ${}_l\Delta_g U$, required to vaporize one mole of the liquid to its saturated vapour and on the energy, ${}_g\Delta_\infty U$, required to expand the saturated vapour to infinite volume at constant temperature, i.e. the energy necessary to completely separate the molecules.[55] This can be expressed as (Equation 3-5):

$$-U = {}_l\Delta_g U + {}_g\Delta_\infty U = {}_l\Delta_g U + \int_{V={}^g V}^{V=\infty} (\partial U/\partial V)_T \, dV \qquad 3\text{-}5$$

where V is the molar volume. The molar cohesive energy –U can be subdivided also according to the relationship, $-U = {}_l\Delta_g H + {}_g\Delta_\infty H - RT + p_s {}^lV$. Where ${}_l\Delta_g H$ is the molar vaporization enthalpy, ${}_g\Delta_\infty H$ is the enthalpy change (increase) on isothermally expanding one mole of saturated vapour to zero pressure, p_s is the saturation vapour pressure at temperature T, ${}^lV$ is the molar volume of the liquid, and R is the gas constant (8.31441 J/(K*mol).[55]

3.1.1 Hildebrand solubility parameter

The stabilizing or cohesive effect in condensed phases can be expressed in terms of the *cohesive pressure* which is dimensionally identical with the *cohesive energy density* (C = -U/V, cohesive energy per unit volume).[55] Cohesive energy density was the basis of the original definition by Hildebrand and Scott [58] of what is now generally called the Hildebrand solubility parameter or Hildebrand parameter (Equation 3-6).

$$\delta = c^{1/2} = (-U/V)^{1/2} \approx ({}_{l}\Delta_{g}U/V)^{1/2} \qquad 3\text{-}6$$

This parameter was originally intended for nonpolar systems, but the concept has later been extended to all types of systems.[55] The Hildebrand parameter (δ) of a liquid may be readily evaluated if the molar volume and molar vaporization enthalpy have been determined at the required temperature, and if that temperature is well below the normal boiling point of the liquid (Equation 3-7):[55, 58]

$$\delta = ({}_{l}\Delta_{g}H - RT)^{1/2}/V^{1/2} \qquad 3\text{-}7$$

The density and enthalpy information is readily available for some liquids, but for most other liquids and for all polymers, solids, and surfaces it is necessary to use indirect evaluation methods, described in the "CRC Handbook of solubility parameters and other cohesion parameters" by Barton[55]

3.1.2 Hansen solubility parameters

As mentioned, the assumption for the Hildebrand parameter was a nonpolar and nonassociating system. Most real systems are polar or contain polar compounds, like water, acid and base solutions and crude oils. Hansen[59-62] proposed a practical extension of the Hildebrand parameter method to include polar and hydrogen-bonding systems, primarily for use in polymer-liquid interactions. It was assumed that dispersion (D), polar (P) and hydrogen-bonding (H) parameters were valid simultaneously, with the values of each component being determined empirically on the basis of many experimental observations. The D, P and H parameters were related to the Hildebrand, or total (T) interaction parameters by summing the square roots (Equation 3-8):

$$\delta_T^2 = \delta_D^2 + \delta_P^2 + \delta_H^2 \qquad 3\text{-}8$$

The experimental determination of the Hildebrand solubility parameter can be done by methods such as determining the enthalpy of vaporization at the required temperature while controlling the molar volume (Equation 3-7).[55] It can also be determined directly from the vapour pressure. Furthermore, the internal pressure and cohesive pressure is a measure of the total molecular cohesion per unit volume. Cohesive pressure has extremely high values for liquids of high polarity, and very low values for materials such as fluorocarbons where forces of attraction are weak.[55] One has to be aware that all the interacting forces are not necessarily represented in the results obtained by the different techniques. For example, the presence of intermolecular hydrogen bonding in a liquid substantially increases the cohesive pressure, while the internal pressure is comparable to that of liquids without hydrogen bonding.[55]

The most common way to use the solubility parameter concept has been to create a "solubility sphere" based on numerous observations of the miscibility or non-miscibility of a solute in various solvents with known solubility parameters. If the solute is taken as the centre point in a three dimensional coordinate system representing the three components of the Hansen solubility parameters, then a sphere can be drawn around the centre (Figure 3-1).[55] The border of the sphere represents the solubility parameter for which the solute is no longer miscible. The solute is miscible with liquids having solubility parameters occurring within the sphere. The distance of the liquid coordinates ($^i\delta_D$, $^i\delta_P$, $^i\delta_H$) from the centre point ($^j\delta_D$, $^j\delta_P$, $^j\delta_H$) of the solute sphere of solubility is (Equation 3-9):[55]

$$^{ij}R=[4(^i\delta_D - {}^j\delta_D)^2+(^i\delta_P - {}^j\delta_P)^2+(^i\delta_H - {}^j\delta_H)^2]^{1/2} \qquad 3\text{-}9$$

The numerical factor of 4 was inserted to obtain spherical interaction volumes, but was later shown not (always) to be necessary.[55]

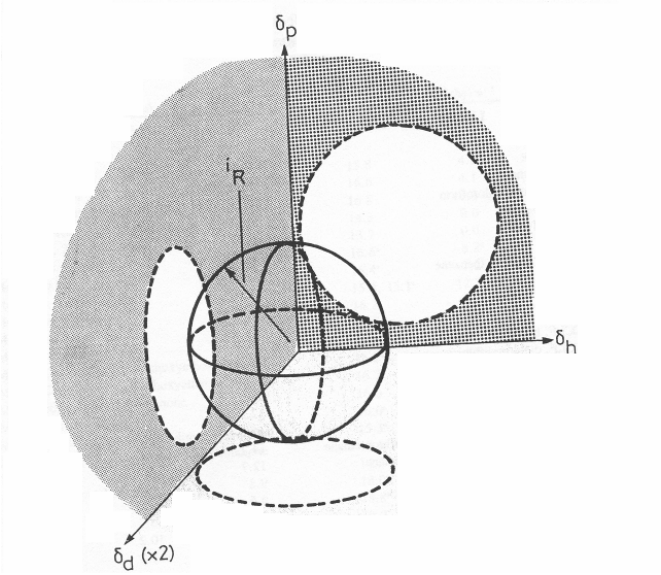

Figure 3-1. The solubility sphere represents the boundaries for the solubility/miscibility of fluids, solids and polymers. The three dimensionality accounts for contributions due to the dispersion, polar and hydrogen bonding parameters.[55]

3.1.3 Solubility parameters for crude oils and asphaltenes

In crude oils the asphaltenes are usually in solution in the reservoir and they often stay in solution all the way to the refinery even when the crude oil has been through several pressure drops. On the other hand, some oils, often the ones with low asphaltene content, may experience asphaltene precipitation during transportation to the refinery.[16, 49] The precipitation is an effect of one or more factors, including pressure reduction, temperature changes, and solvent composition changes (for example when oils from several wells are mixed or gas lift with carbon dioxide is used).[1, 16, 49] What actually happens is that the solubility of the asphaltenes in the crude oil becomes lower leading to clustering, aggregation and ultimately precipitation. Thermodynamic models track those processes by assigning solubility parameters to crude oils and asphaltenes and noting the difference between them.[44] Thus, the solubility of asphaltenes in crude oil can be explained with the solubility parameter concept and the asphaltene precipitation onset can, to a certain degree, be predicted by use of solubility parameters.[1, 44, 45, 63] Separation of asphaltenes is to a large degree dominated by non-polar van der Waals forces (dispersion forces). Thus the refractive index has been used to determine the solvent conditions at which asphaltenes precipitate.[44]

3.2 Multivariate data analysis

Multivariate analysis is required when the simultaneous elucidation of relationship between two or more variables is of interest.[64] This is true for IR and NIR spectra where there can be several thousand variables. Before analyzing, it might be necessary to pre-process the data set. A first-order differentiation of the spectra removes additive shifts in the data, thus removing effects from, for instance, baseline shifts.[64] Any relation between the absorption and concentration remains after differentiation, but there might be a slight decrease in the signal-to-noise ratio. Second-order differentiation removes both baseline shifts and curves. In order to minimize the noise when differentiating, smoothing is often done in combination. The Savitzky-Golay procedure is one method which can be used and it combines differentiation and smoothing in one step.[65]

3.2.1 Principal Component Analysis (PCA)

Principal component analysis (PCA) is a projection method that helps visualize the most important information contained in a data set. PCA finds combinations of variables that describe major trends in the data. Mathematically, PCA is based on an eigenvector decomposition of the covariance matrix of the variables in a data set. For data matrix X with *m* rows of samples and *n* columns of variables, the covariance matrix of X is defined as (Equation 3-10):[64, 65]

$$\mathrm{cov}(X) = \frac{X^T X}{m-1} \qquad 3\text{-}10$$

The decomposition into principal components (PC) called score and loading vectors is the result of the PCA procedure (Equation 3-11).[64, 65]

$$X_{nxm} = t_1 p_1^T + t_2 p_2^T + t_i p_i^T + \ldots + t_k p_k^T + E_{nxm} \qquad 3\text{-}11$$

Here, t_i is the score vector, p_i is the loading vector and E is the residual matrix. *k* must be less than or equal to the smallest dimension of X, i.e. $k \leq \min$. The direction of the first principal component (t_1, p_1) is the straight line in the variable space that best describes the variation in the data matrix. The second principal component is given by the straight line, orthogonal to

the first PC, which best describes the variation not described by the first PC. Plotting the first and second principal components against each other, the score plot is obtained (Figure 3-2). Thus the original data set can be adequately described using a few orthogonal principal components instead of the original variables.[64, 65]

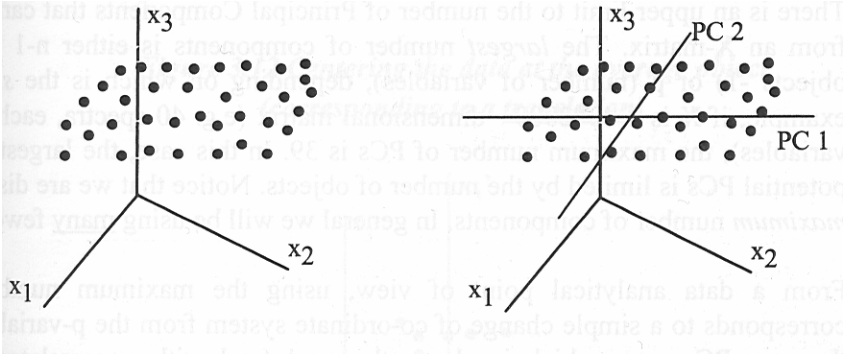

Figure 3-2. Illustration of how the principal component axis are defined in order to construct the score plot. PC 1 is the straight line through the variable space that best describes the variation in the data matrix. PC 2 is the straight line orthogonal to PC 1 which best describes the variation not described by PC 1.[64]

3.2.2 Outlier detection

Some samples can have values that are extremes compared to the other samples in the matrix. They may not be representative for the system at all, or they may be due to errors in measurements. Such samples will often be found in the outskirts of the main "swarm" in the score plot and are referred to as outliers (Figure 3-3).[64] Outliers can be of the "mild" type as to the left in the figure or the "extreme" type to the right. Other ways to detect samples that are very different or have a high influence on the models is to look at the leverage. The leverage is based on the idea that anything can be lifted out of balance if the lifter has a long enough lever.[64] This means that the principal component axes in the score plot can be influenced by a sample that has a high leverage and thus give a bad model.

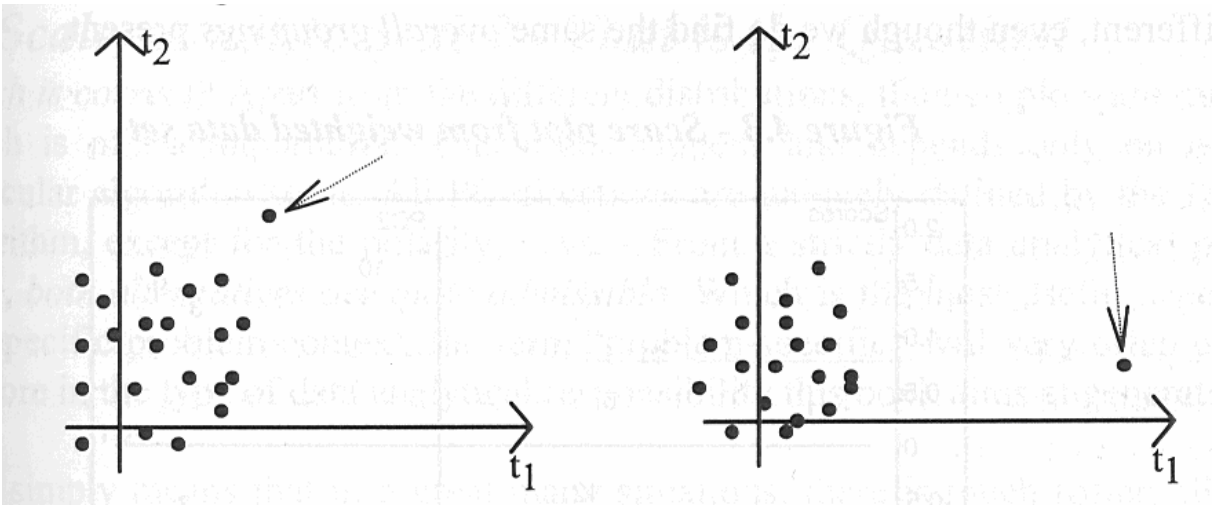

Figure 3-3. The plot shows an example of how outliers are detected in the score plot. In the situation to the left there is a mild outlier which is not easy to detect. To the right the outlier is more obvious.[64]

A sample with high leverage that falls near the PC axis can reinforce the PC model.[66] Special attentions must therefore be paid to samples located far from the other samples in the score plot or have a high leverage (i.e. higher influence). Such samples may contain valuable information or the discrepancy is due to non-representative samples.[65] To decide if a sample is an outlier and should be deleted from the data set, or an extreme that is important in order to get the true picture one have to carefully evaluate the specific samples and preferentially have detailed knowledge of the system under investigation.

3.2.3 Partial Least Squares (PLS) Regression

PLS regression analysis is used to fit a model to observed data in order to quantify the relationship between two groups of variables. It is often difficult, expensive or time consuming to obtain a particular variable (Y-data) that describes the object of interest. These measurements should then be replaced by some indirect measurements (X-data) for example IR and NIR measurements. Y-data are the particular variables of interest, often called the response variables and are the parameters one wants to predict, for example solubility parameters[67] or the determined SARA fractions.[65] PLS regression correlates the X -and Y-data and makes a model that in turn can be used to predict Y-data from new X-data measurements. In PCA the scores and loadings are the vectors that best describe the variance of the X-matrix. In PLS the scores and loadings (called latent variables) are the vectors that have the highest covariance with the response vector y. The decomposition is followed by a

regression between the latent variables and the response. To avoid over-fitting of the PLS model, a full cross validation should be used. With full cross validation the model is checked by repeatedly taking out one sample at the time and then tests them against the model during the modelling process.[65]

3.2.4 Evaluation of the PLS models

A way to check the model is to plot predicted Y-values against the reference Y-values used to make the model. The plot will show how single samples fit the model, both if they have a large impact on the model and if they are well predicted or not; i.e. whether the predicted and reference values are close (Figure 3-4). Also evaluation of the necessary number of PCs should be performed, although commercial software suggests the optimum number for the user for each model.

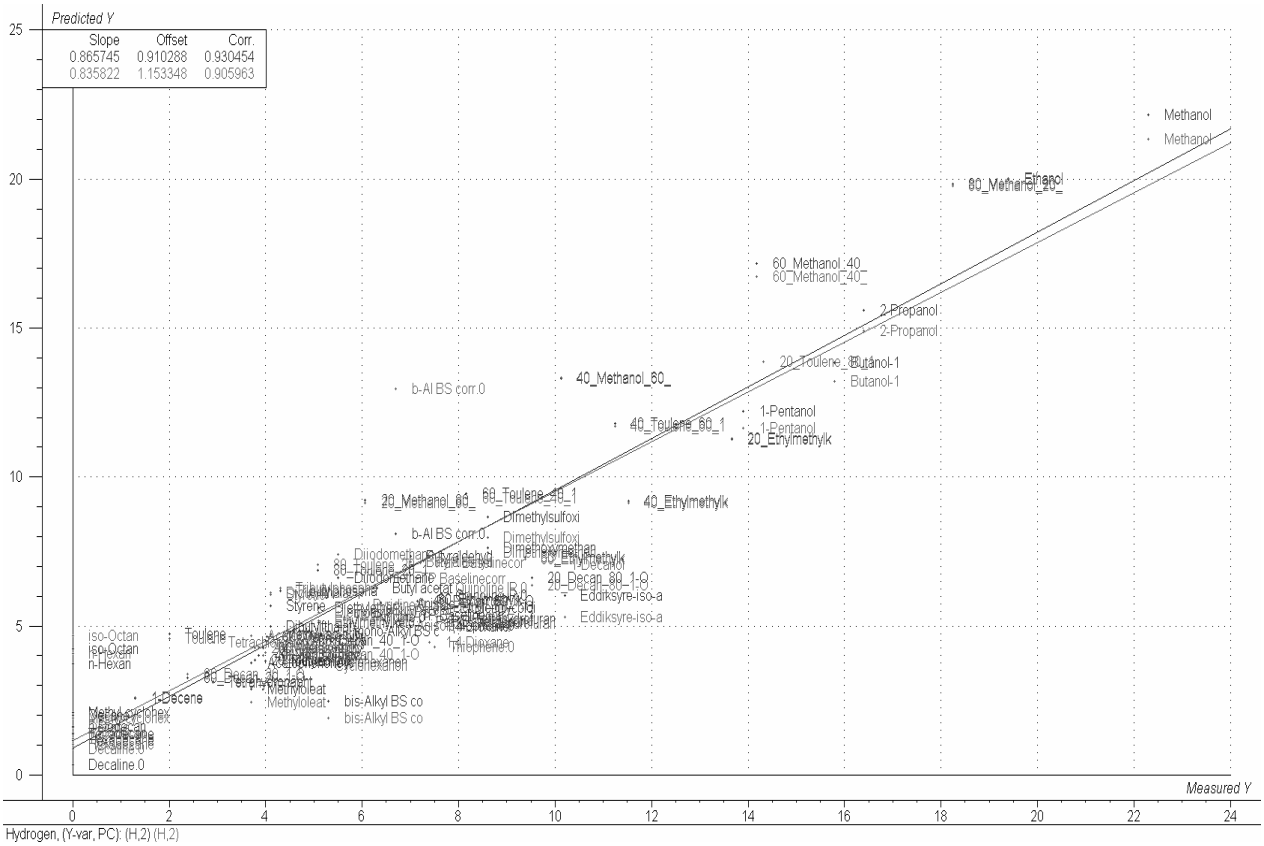

Figure 3-4. Example of a "predicted versus reference (measured) " plot obtained by a partial least squares (PLS-1) regression with full cross validation on the hydrogen bonding parameter and IR spectra of some solvents and solvent mixtures. After deleting some outliers the regression coefficients both for the correlation (0.93) and the validation (0.91) are acceptable. As seen it is difficult to identify each sample in the plot since they are placed above each other here. If a sample is close to the lines, then it is well predicted and if it is far from the lines the model is not suited for prediction on that sample, or it may be an outlier. A sample with a high levereage (for example methanol in this model) may improve the model if that sample is close to the regression line.

Upon creating a PLS model, the X_{cal} and Y_{cal} matrices are the calibration data used to build the model. The RMSEC (Root Mean Square Error of Calibration) is the calibration error in the original measuring units and is found by subtracting the measured y_{cal} values from the predicted y'_{cal} values. One way to check the model is to use a validation data set with known y_{val} variables. The X_{val} variables are put into the model to predict the $y`_{val}$ values. The root mean square error of prediction (RMSEP) from the predicted $y`_{val}$ and the original y_{val} values gives the expected model error for future predictions in the original measuring units (Equation 3-12).[64]

$$RMSEP = \sqrt{\frac{\sum_{i=1}^{n} (y'_{i,val} - y_{i,val})^2}{n}} \qquad 3\text{-}12$$

Standard Error of Performance (SEP) and bias are two other statistical measures closely connected to RMSEP.[64] Bias represents the averaged difference between predicted and measured Y-values for all samples in the validation set, whereas SEP expresses the precision of the results, corrected for Bias (see Esbensen[64] for details). Y-variance shows how large percent of the Y-data that are described by the model for a specific principal component. X-variance tells how many percent of the X-data that is used to describe the Y-variance for a specific principal component.[64]

4 EMULSIONS AND SEPARATION FACILITIES

When crude oil is processed onshore or offshore, one ends up with a mixture of gas, water, oil and solid particles. The oil and water may form emulsions, either water-in-oil (w/o), oil-in-water (o/w) or multiple emulsions consisting of w/o/w or o/w/o.[68] The emulsions are stabilized by components that are inherent in the crude oil or that have been added during the production.[6, 68, 69] This section will shortly describe crude oil-water emulsions and separation techniques using gravity separators and strong electric fields.

4.1 Emulsions

In processing of petroleum water-in-oil (w/o) or oil-in-water (o/w) emulsions can lead to enormous financial losses if not treated correctly. Knowing the particular system and the possible stability mechanisms is thus a necessity for proper processing and flow assurance.[6] The concept of emulsions has been defined by IUPAC (1972) as**:** "a dispersion of droplets of one liquid in another one with which it is incompletely miscible (..). In emulsions the droplets often exceed the usual limits for colloids in size", [70] meaning that they can be large with sizes in the micro meter range.

A system will always move towards the state of lowest free energy. For pure oil and water under normal temperature and pressure conditions this occurs when the phases are separated by a single interface. In order to disperse one of the phases in the other, energy must be supplied. Mixing of two immiscible phases like water and oil represents an increase in the energy state of the system and thus an increase in the Gibbs free energy.[68] A water-in-crude oil emulsion is made by dispersing the water as small droplets in the continuous oil phase through mixing (Figure 4-1).

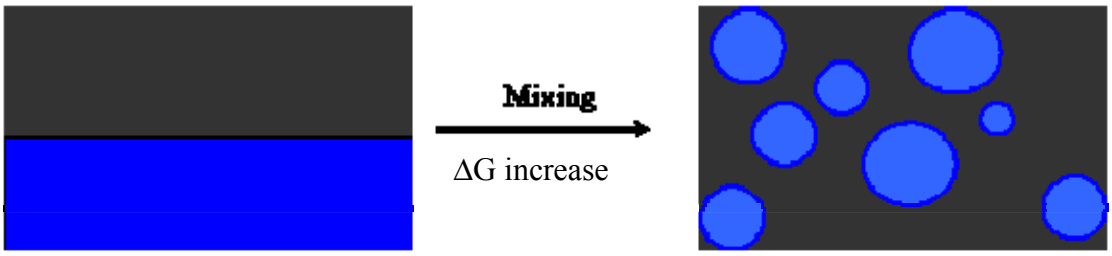

Figure 4-1. Illustration of droplet formation when oil (dark) and water (blue) are mixed. The energy of the system increases (ΔG is positive) as the interfacial area between the two phases is increased.

In the dispersed state, the interfacial area between the dispersed droplets and the bulk phase is much larger than when the phases are separated as two continuous phases. The large interfacial area in the dispersed state (the situation to the right) represents an increase in the systems free energy relative to the situation to the left in the above figure. There is a relationship between the Gibbs energy of the liquid thin film between the water droplets and the continuous oil phase and the changes in temperature, pressure and total area of the film (Equation 4-1).[68] By increasing the area, that is dispersing the water as droplets in the oil phase, the free energy of the system increases.

$$dG^f = -S^f dT + V^f dp^\beta + \gamma^f dA^f + \sum_i \mu_i dN_i^f \qquad 4\text{-}1$$

Here, G^f stands for Gibbs energy of the thin liquid film (f), S for entropy, T for temperature, p^β is the pressure upon the film by the external phase (β), V^f is the volume of the film, γ^f the film tension, A^f the interfacial area of the film, μ_i the chemical potential of each component and N_i the moles of each component. Emulsions are not thermodynamically stable, and will seek to minimise the surface area by separating back into the different phases, thus decreasing the interfacial area and the Gibbs free energy. For an emulsion to separate, the droplets must merge with each other or with the continuous phase, in this case the water phase. Processes that facilitate separation are sedimentation/creaming, flocculation and coalescence (Figure 4-2).[68, 70, 71] Creaming and sedimentation create a droplet concentration gradient due to a density difference between the two liquid phases, which results in a close packing of the droplets. The mechanism of coalescence occurs in two stages; film drainage and film rupture. Interfacially active compounds, such as asphaltenes, resins naphtenic acids and (coated) particles contribute to mechanically strong and elastic interfacial films that act as barriers against aggregation and coalescence.[6, 12, 68, 69, 72, 73]

In order to stabilize water-in-crude oil emulsions an emulsifying agent must be present. Such compounds include scale and clay particles, added chemicals or indigenous crude oil components such as asphaltenes, resins, waxes and naphtenic acids.[71] Asphaltenes are believed to be the main contributor to emulsion stability. McLean and Kilpatrick[74, 75] have postulated that the dominating mechanism whereby crude oil emulsions are stabilized is through the formation of a viscoelastic physically cross-linked network of asphaltenic aggregates at the oil-water interface.[16] Moreover, the aggregation state of the asphaltenes in

the crude oil is decisive with regard to the emulsion stability properties and it is assumed that it is not the individual asphaltene molecules rather than the aggregates that lead to the high w/o emulsion stability.[10, 16, 68, 71] Other factors that usually favour w/o emulsion stability are high viscosity of the bulk phase and relatively small volumes of dispersed phase.[70]

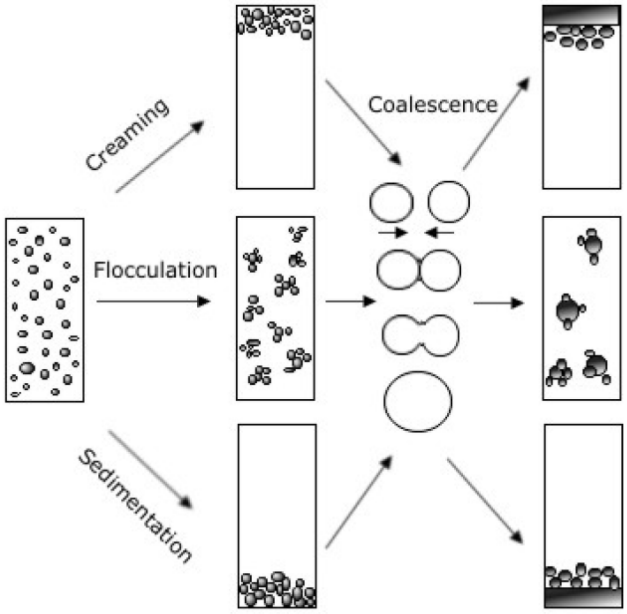

Figure 4-2. Processes taking place in an emulsion leading to emulsion breakdown and separation. Oil droplets will cream and water droplets will sediment. Free water will exist at the bottom and free oil at the top.[70]

For gravity separators the settling and coalescence processes, as well as the obstructions to coalescence described above are valid. If a background electric field is present, as in industrial electro coalescers, the kinematics of droplets and the coalescence of interfaces will be completely different. Several mechanisms which are present in gravimetrically-induced destabilization of emulsions are probably still present, but their relative level of influence may be completely different due to forces induced by strong electric fields.[6]

4.2 Gravity separators

The first process equipment the incoming reservoir fluid enters after the initial pressure reductions is the primary separator. This unit removes most of the water from the oil, which continues to a secondary and eventually a ternary separator. The last one is often equipped with electrodes in order to enhance coalescence.[71] All of these separators are of the type called gravity separators. Gravity separation in oil production is a mature technology, and the

separator vessel is a process component at virtually every installation that produces or treats oil on a large scale. It is also known as “a process component partly designed by chance”.[76] Due to the difficulties in determining the operation window and predicting the efficiency of a separator, industry “vendors” have performed pilot scale work on gravity separators for decades.[76] The main focus is to test equipment in continuous operation where scale-up effects are minimised.

A typical gravity separator is very simple: a large, mostly empty vessel in which a mixture of components are allowed to separate (Figure 4-3).

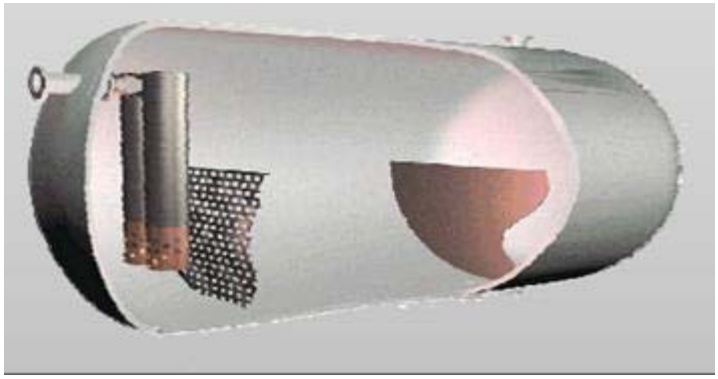

Figure 4-3. Typical gravity separator shown with internals like cyclones and flow distributing devices.

The internals of the gravity separator consist of foam handling devices, flow distributing devices and settling enhancing devices.[71] Water droplets sediment downwards since they are heavier and they ultimately coalesce and enter the free water zone.[68, 71, 76] The theory of settling, residence time and bulk velocities and droplet size distributions have been treated elsewhere and is not to be discussed further in this work.[68, 70, 71, 76]

4.3 Electrostatic coalescence

The electrostatic effects arise from the very different properties of oil and water, water having dielectric permittivity and conductivity values much higher than those of oil. A short description of the process of electro coalescence is given here. For further information the reader should consult the literature.[68, 71, 77-80] Water droplets must possess charge which may be acquired through, dissolved electrolytes, ionization of adsorbed species, preferential adsorption of ions at the interface, or contact with charged electrodes. Furthermore, the continuous phase needs to have a relatively low conductivity in order for dispersed water

droplets to retain a significant amount of charge enabling them to move from one electrode to the other (in DC fields), deform, migrate or other effects charges have on water droplets (Figure 4-4). This is fulfilled in a water-in-crude oil system. After the first stage of approach of the two droplets resulting from the action of the shear, there is a second stage of film thinning and drop deformation until the interfaces destabilize and lead to the generation of a bridge between the drops in a very short time (Figure 5-14).[77]

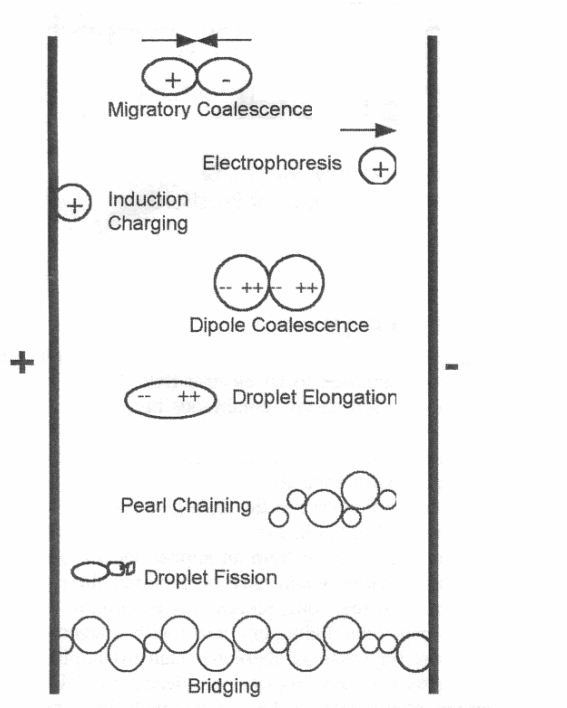

Figure 4-4. The figure shows the different effects an electric field can have on water droplets. The last "step" is the droplets making a bridge between the two poles.[77]

Conventional electrostatic coalescers use a grid of high-voltage electrodes suspended in the water-containing oil layer within the separation vessel, creating the electric field needed for water droplet coalescence. Recent developments of electrostatic units in vessels are the Vessel Internal Electrostatic Coalescer (VIEC) the Low Water Content Coalescer (LOWACC) both by Vetco Aibel.[81]

4.4 State of the art technology for electro coalescence

4.4.1 Vessel Internal Electro Coalescer (VIEC)

The mechanical design of traditional coalescers consists of a bare metal grid suspended horizontally in a large liquid-filled pressure vessel. The grid is suspended in isolators and attached to a 50/60 Hz transformer. With the imminent threat of short-circuiting and other problems, some vendors use isolated or composite electrodes to offset some of these weaknesses.[82]

From an electrical point of view, the use of insulating plates, when an emulsion is present, forms a connection similar to that of two capacitors in series: one capacitor is formed by the insulation layer on the plates whereas the second one is represented by the emulsion between the plate surfaces. The emulsion is characterized by a high dielectric loss factor making the construction of an insulated coalescer operating at 50/60 Hz difficult since the low impedance of the emulsion results in a high voltage drop across the insulation layer.[82]

In VIEC the electrodes are powered by transformers which are molded into a perforated epoxy wall inside the separator (Figure 4-5). Teflon tubes are used in the mould to create holes for the turbulent fluid flow increasing the collision rate of water droplets. Furthermore, the tubes can also act as miniature separators allowing the droplets to settle into a liquid film.[82]

Figure 4-5 VIEC module and frequency converter. The insulated "pipes" is where the electrical coalescence takes place.[82]

The size of the VIEC module is such that it can be carried into the separator through a service manhole and the total typical power consumption of an installation consisting of 40 modules is smaller than 2 kW. Compared with traditional electrocoalescers using heavy 50/60Hz power transformers, the VIEC power supply is small.[82]

Figure 4-6 First stage separator tank with VIEC installed.[82]

VIEC uses a dedicated frequency converter to shift the operating frequency into the kHz region. The combination of high frequency and thick insulation helps the VIEC to better tolerate, and in fact make use of the harsh first stage separator conditions.[82]

In short, VIEC enhances the speed and efficiency of the oil/water separation process by forcing small water droplets to merge, by use of electrostatic coalescence technology. What makes it particularly interesting is that the technology is introduced in the first stage separator, an aspect only made possible by new electrical and mechanical developments. VIEC is currently deployed in different regions worldwide including offshore Brazil, Qatar, China and Norway.[82]

Alongside the VIEC, or more precisely after the VIEC in the same separator tank the Low Water Cut Coalescer (LOWACC) may be placed. The idea behind LOWACC is to construct a single stage separation unit and it is planned to be commercialized from 2008. LOWACC use the even more efficient di-electrophoresis whereby strong electrostatic gradients pull the water droplets to the location of highest field strengths This gradient field force is in the order of magnitude 2-3 times the gravity force and concentrates the dilute water droplets to effectively dehydrate the oil.[81, 83, 84]

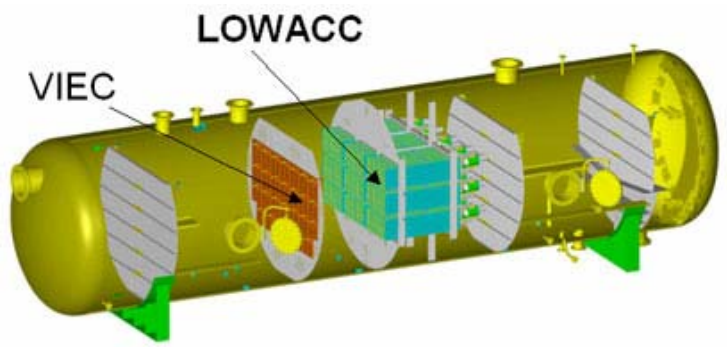

Figure 4-7. The VIEC and LOWACC will be placed in the same separator with the intention to achive full separation using only one vessel.[81]

Recently new contracts have been made where Aibel has promised to deliver the VIEC technology to the Valhall field operated by BP off the coast of Norway. Also Statoil has decided to apply the VIEC technology for a third time. Contractor Aker Kværner Stord AS, through process equipment supplier Midsund Bruk AS, has placed an order for VIEC (Vessel Internal Electrostatic Coalescer) to be installed in the second stage separator on Statoil's new semi submersible production platform on the Gjøa field, a North Sea field consisting of three sets of subsea wells. The large interest for the VIEC is due to the improvements to the oil/water separation process it brings about, with improved control and increased production as the end result. Where heavy oil is involved there are reports of very good results in terms of low water in oil content, cleaner produced water and reductions to the amount of demulsifier chemicals required.[81, 83, 84]

On floating production platforms, large horizontal pressure vessels respond to ship motions, which can cause the liquids inside to slosh around, sometimes causing short-circuiting of the electrodes and also reducing the overall effectiveness of the process.[85] In addition large separator vessels like VIEC gives large investment costs in addition to long residence time.[77] The problems with separating the water starts when the water content in the oil becomes low, and thus the largest problem for an oil/water separator, including electro coalescence, is to treat oil with a low water cut and small drops. Small drops gravitate slowly towards the bottom of a sedimentation tank, and the distances between the droplets will be considerable.[85] Evidently this has been solved by the VIEC (and LOWACC) technology.

In addition to the VIEC another equipment for electrostatic coalescence has recently attracted the interest of the oil companies. The compact electro coalescer (CEC™) has already proved its efficiency and durability at several production sites. The arguments for choosing the CEC™ is basically the same as for the VIEC, that is, reduced energy consumption compared to heating and reduction of demulsifier consumption.[85]

4.4.2 Compact Electrostatic Coalescer - CEC™

In the mid-1990s Statoil patented the idea behind a Compact Electrostatic Coalescer (CEC) and entered a licence agreement with Kværner Process Systems (KPS) to further develop and commercialize the device in association with the University Of Southampton (UK).[85]

Basically the CEC™ enhances separation by applying a high voltage, alternating electric field to an emulsion. Rapid aggregation and coalescence of water droplets lead to faster settling and separation time in the down stream separator. Coalescence occurs quickly under turbulent flow conditions and minimizes the need for emulsion-breaking chemicals. It also leaves the oil with less than 0.3 per cent water content, which is somewhat below the normal refinery requirements. The world's first CEC™ installation took place at the Statoil-operated Glitne field in late 2001 and it is still found to be in perfect working order, having kept the w/o content well below 0.3 per cent using less chemical additives.[85]

Statoil is the owner of the patented CEC™ technology and has issued an exclusive commercial license to Aker Kværner. Continuing on from original research in the 1980s at the University of Southampton in the UK, Aker Kværner has been working with oil company partners on the development and testing of CEC™ technology for the past ten years. At the heart of the CEC™ technology is a series of concentric circular electrodes, housed within a coalescing section inside a 4.2 - 5.5 m tall, vertical vessel (Figure 4-8).[85]

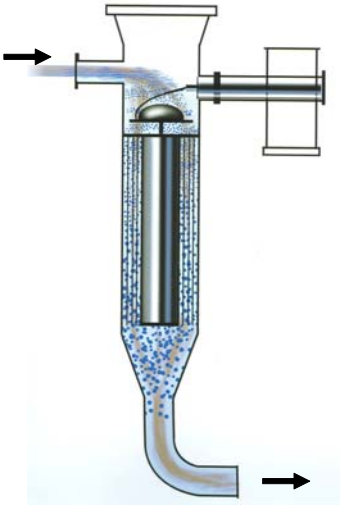

Figure 4-8. A Compact Electro Coalescer (CEC™). Crude oil and water in dispersed state enter at the top. The droplet size of the water droplets has increased tenfold when the dispersion exits the CEC™ at the bottom. The picture has been taken from an Aker Kværner brochure.

Voltages of up to several thousand volts can be applied to the electrodes to create a more intense electrical field in the annular channels and thus a more intense coalescing process than what is achieved in conventional grid units. Water droplets merge several times within a

matter of seconds and increase their size around ten times in the coalescing section. The water droplets and oil then enter a gravity separator for separation, but one with much reduced dimensions compared to a normal electrostatic coalescer. The CEC™ is insensitive to vessel motions, and is not prone to plugging by solids in the well fluids.[86]

Figure 4-9. The CEC™ unit ready for shipment to Chevron's Captain FPSO in the UK sector of the North Sea.[86]

Significant commercial breakthroughs for the CEC™ technology have been made by Aker Kværner recently, with three offshore installations of the unit. In the UK's Captain field, operator Chevron is replacing a conventional coalescer on its floating production facility for treatment of 130,000 bpd (860 m^3/hr) of liquids. Operator Mærsk is installing a 38,000 bpd (250m^3/hr) unit on the Al Shaheen fixed platform in the Arabian Gulf. For the Alvheim field, a new greenfield development offshore Norway, operator Marathon has opted for the CEC™ technology to treat up to 130,000 bpd (860 m^3/hr) of liquids on its new floating production vessel.[86]

5 EXPERIMENTAL METHODS AND INSTRUMENTAL TECHNIQUES

The choice of experimental techniques is in itself a challenge. One thing is that there are numerous standards and methods reported just for the precipitation of asphaltenes which all may give a slightly different composition. Furthermore, for the determination of the molecular weight every method available has its drawbacks leading to potential misinterpretation of results or imprecise predictions. Most often one instrumental technique gives you more questions than answers and necessitates new experiments and characterization methods. This chapter will guide the reader through the experimental procedures and the instrumental techniques that have been used for the studies of asphaltenes and emulsions in this work. Nevertheless, it is beyond the scope of this work to provide a theoretical background for all of these methods and emphasis will be on practical aspects and interpretation of results.

5.1 Precipitation of asphaltenes

The amount of *n*-alkane used in the precipitation of asphaltenes varies but is usually in the range of 40:1 in volumes, with respect to the crude oil.[1] The contact time also affects the amount precipitated, but 12 hours continuous stirring/shaking is usually considered sufficient. After dilution and stirring, the asphaltenes precipitated are filtrated off (using vacuum) through a filter with pore sizes often less than 1 micrometer. After filtration, the filter cake may contain co-precipitated waxes, resins and low molecular weight compounds. These compounds are washed off by flushing with (hot) solvent until the effluent is colourless. It is also possible to transfer the unwashed asphaltenes to a flask and fill with the precipitant and shake for a period of time and do a second filtration and washing procedure, or use soxleth apparatus. In addition to the precipitation of the so called whole asphaltenes, this work reports on a direct step-wise precipitation of asphaltenes, increasing from low to higher dilution ratios with inter-step filtration off of the precipitated asphaltenes.

5.2 Light spectroscopy and neutron scattering

Light spectroscopy using infrared (IR) and near infrared (NIR) light is used in order to obtain information on the chemical structure of organic compounds. In addition, NIR light can be

used to detect particles in a solution due to the scattering of light. The same principles used in light scattering are also available for the scattering of neutrons although the source is different.

5.2.1 Near Infrared Spectroscopy (NIR) and onset of asphaltene precipitation

The solubility and insolubility of asphaltenes in certain solvents is behind the very definition of this class of molecules. Onset of precipitation is a point of interest for the oil industry. With the knowledge of under which conditions the asphaltenes precipitate one can start to determine which mechanisms are more important in the precipitation process. The conditions at which asphaltenes precipitate in a well are different from those in the pipeline, separators or in the laboratory but the driving forces may be the same.

Near infrared light is electromagnetic radiation in the infrared (IR) region close to the visible spectrum. According to the American Society for Testing and Materials (ASTM), it is defined as the spectral region spanning 780 - 2526 nm (12820 - 3959 cm^{-1}).[70] Absorption bands in this region are overtones or combinations of fundamental stretching vibration bands that occur in the region of 3000 to 1700 cm^{-1}. The bonds involved are usually C-H, N-H, and O-H. Because the bands are overtones or combinations, their molar absorptivities are low and detection limits are on the order of 0.1%.[87] The insensitivity and broad adsorption bands can, to a certain degree, be compensated for by using multivariate data analysis.[88] Advantages of using NIR is that there usually is little need for extensive sample preparation and it is fast and non-intrusive. In addition NIR probes combined with fibre optics makes it possible to measure at high temperature and pressure at a distance from the spectrophotometer.

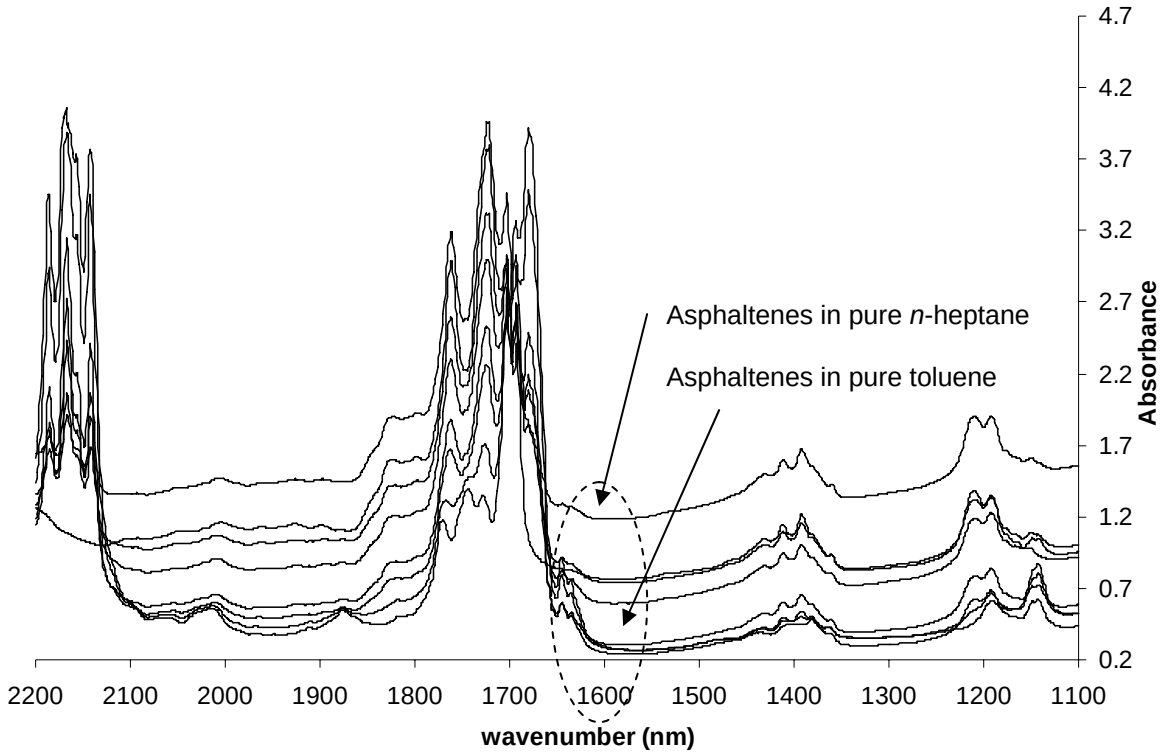

Figure 5-1. Near infrared spectra of asphaltenes in increasing ratios of heptane to toluene. The baseline is elevated when the asphaltenes start to form bigger aggregates that precipitate and scatter light.

In addition to absorption, the NIR light may be scattered when particles are present in the sample. Scattered light, which do not reach the detector will be "measured" as absorbance. This apparent absorbance can bee seen as a baseline elevation in the NIR spectra. The assumption is that the particles are small (in radius r) relative to the wavelength (λ) ($r/\lambda \leq 0.05$). The basic premise for Rayleigh scattering is that the particle is so small that the electro-magnetic field it experiences is uniform over the particle. Within the Rayleigh limit the light extinction can be considered a sum of the absorbance and scattering contributions, represented by the following particle cross-sections (Equation 5-1).[70, 88]

$$\sigma_{tot} = \sigma_{sc} + \sigma_{abs} \qquad 5\text{-}1$$

where σ_{tot}, σ_{sc} and σ_{abs} are the total, scattering and absorption cross-sections, respectively. For crude oils and asphaltene solutions there is practically no absorption of light at 1600 nm, but the light is still scattered when particles are present. Therefore, a baseline elevation can be observed in the NIR spectra when monitoring the aggregation of asphaltenes with subsequent precipitation (Figure 5-1).[70, 88]

5.2.2 Mid Infrared Spectroscopy (IR)

The middle part of the infrared radiation refers to the wave numbers from 400 cm^{-1} to 4000 cm^{-1} and it is this part of the IR spectrum that historically has obtained most focus. Almost all molecules, from the simplest to the more complex, will absorb some light in the IR region. Absorbed light is converted into energy of molecular vibration. A single vibrational energy change is in addition accompanied by a number of rotational energy changes. It is within these vibrational-rotational bands that useful information about functional groups and the structure of molecules can be obtained.[89] IR spectroscopic methods are well suited for analyzing not only pure compounds, but also mixtures of compounds. By proper calibration of the concentration of compounds, functional groups or even indirect properties of materials can be deduced and quantified. The reason for this is that the amount of absorbed light is dependent on factors which can be varied such as the path length of the transmitted light and the concentration of compounds. The absorbance is therefore directly related to the concentration of a compound or a functional group as is described by the Beer-Lambert law (Equation 5-2).[87, 89, 90]

$$\text{Absorbance} = \log\frac{I_0}{I} = \varepsilon c l \qquad 5\text{-}2$$

Here I_0/I is the ratio of the light detected by the sensor to the light emitted, ε is molar absorbtivity, c is the concentration of the compound or functional group of interest, and l is the length the light passes through the sample.[90]

There are two types of molecular vibrations: stretching and bending. The various stretching and bending modes can be found in the literature.[89] A typical IR spectra of asphaltenes (Figure 5-2) will have a broad and weak absorption band in the 4000 cm^{-1} to 3100 cm^{-1} (NH, OH and SH) two sharp peaks at 2921 cm^{-1} (CH_2) and 2852 cm^{-1} (CH_3), furthermore the region of 1750 cm^{-1} to 1100 cm^{-1} includes various absorption bands related to polar functional groups. In the region of 750 cm^{-1} to 875 cm^{-1} three peaks are present from CH deformation vibrations of aromatic compounds.

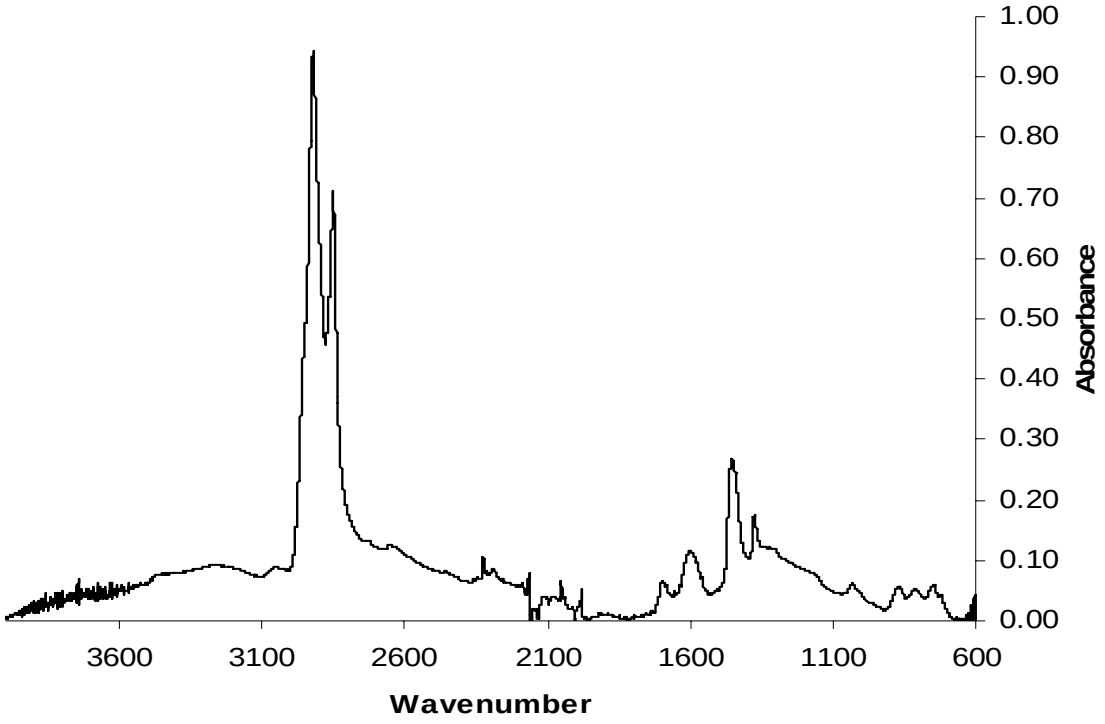

Figure 5-2. Example of a infrared spectrum of an asphaltene sample.

Only those vibrations resulting in a rhythmical change in the dipole moment of the molecule are detectable in the IR.[6, 89]

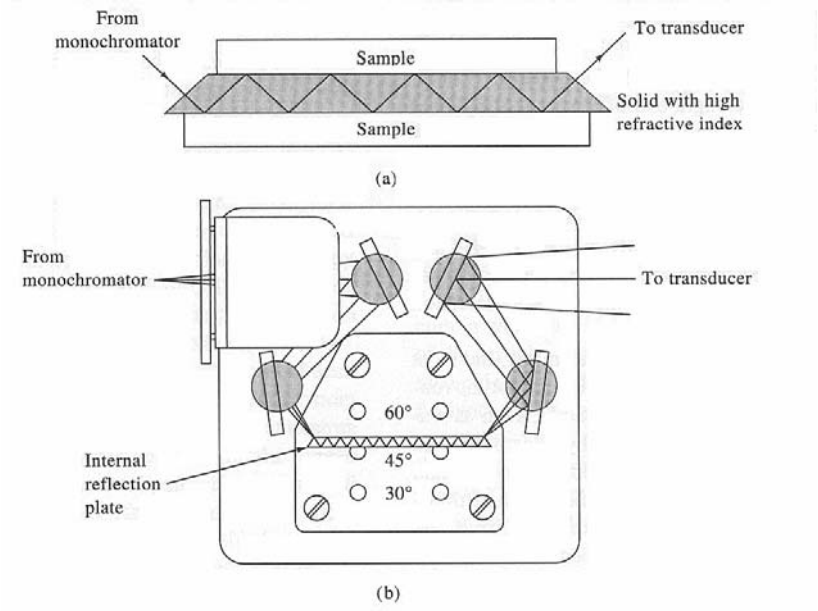

Figure 5-3. Principle of the attenuated total reflectance. a) Sample mounted on reflection plate, b) internal reflection adapter. By adjusting the incident angle, the radiation undergoes multiple internal reflections before passing from the crystal to the detector. Cells for liquids and solids are availible.[87]

One type of IR measurement is the Attenuated Total Reflectance (ATR) spectroscopy which is an internal-reflection technique used for samples that are difficult to deal with such as solids of limited solubility, films, thread and powders etc. The principle of the method is that when a beam of radiation passes from a less to a denser medium, reflection occurs (Figure 5-3). The fraction of the incident beam that is reflected increases as the angle of incidence becomes larger and beyond and certain critical angle, reflection is complete. The beam acts as if it penetrates a small distance into the less dense medium before reflection occurs. The penetrating radiation is called the evanescent wave. If the less dense medium absorbs the evanescent radiation, attenuation of the beam occurs at wavelengths corresponding to absorption bands.[87]

5.2.3 Small Angle Neutron Scattering (SANS)

Light scattering is the scattering of photons, but the theory is much the same for the scattering of neutrons or x-rays. Neutrons are scattered by the nuclei of the atoms and by the magnetic moments of the atoms. The typical wavelength of the (SANS) method is 0.4 nm with a range of the scattering vector *s* of $7*10^{-3}$ to $9*10^{-1}$ nm. The scattering vector *s* is defined as (Equation 5-3)

$$s = \frac{4\pi}{\lambda}\sin(\theta/2) \qquad 5\text{-}3$$

where λ is the wavelength of the incident radiation and θ is the angle of "observation" relative to the horizontal plane. Often the s, which is a dimensional quantity, is converted to a non-dimensional quantity called Q by multiplying with a suitable reference dimension (L_{ch}). L_{ch} is the characteristic dimension that represents the size of the scatterers.[91] Neutrons allow probing of structures at much shorter length scales than possible with light, so that SANS is more suitable for determining aggregate size of asphaltenes as compared by using NIR light. Furthermore, the particles and fluid are effectively transparent to neutrons (and x-rays) so that more complicated scattering theories like Mie and Rayleigh-Debye is avoided.[91]

SANS can be used to determine the radius of gyration of particles. This is done by plotting the logarithm of *I(Q)* versus Q^2 called the Guinier plot, represented by Equation 5-4. The straight

line obtained in the Guinier region (Figure 5-4) is used to calculate the size of the particles by solving the equation for R_G (Equation 5-4).[92]

$$I(Q) = I_0 e^{-Q^2 \frac{R_G^2}{3}} \qquad 5\text{-}4$$

Furthermore, the form factor P(Q) can be deduced from the scattering vector as a function of Q to derive simple geometries of (primary) spherical particles (Figure 5-4). Kilpatrick and Gawrys presented work where they tested models for various intra-particle structure factor models and concluded that asphaltenic aggregates are polydisperse oblate sylinders.[93]

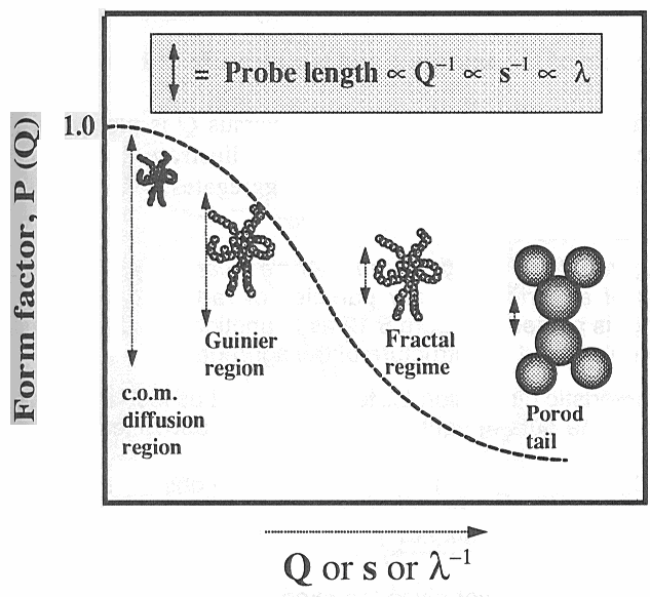

Figure 5-4. Schematic representation of P(Q) versus Q for fractal objects. The regions shown are the centre-of-mass (c.o.m) region, the Guinier region (used in this work), the fractal region and the Porod region. The probe length is the yardstick corresponding to the measurements.[91] As illustrated, the Guinier region probe the nano aggregates in the solution, i.e. the asphaltene aggregates.

Errors in the results are typically less than 1 Å, which makes SANS suitable for measuring the size of asphaltene aggregates. One drawback of the SANS is that one has to use relatively high concentrations, about 1 weight percent in deuterated toluene. This means that the concentration is above the critical concentration for asphaltene aggregation which might be less that 100 mg/L in toluene, depending on source and type of asphaltene.[16]

5.3 Nuclear Magnetic Resonance (NMR)

Nuclear magnetic resonance spectroscopy (qualitative study of interaction between radiation and matter) and spectrometry (quantitative measurements of the interactions between radiation and matter) is just another form of absorption spectroscopy like IR. To get a thorough introduction to NMR the reader should consult textbooks on the theme.[87, 89, 94, 95]

5.3.1 A short description of the principle of NMR

The basis of nuclear magnetic resonance is that under appropriate conditions, in a magnetic field, a sample can absorb electromagnetic radiation in the radio frequency (rf) region at specific frequencies governed by the characteristics of the sample, thus altering its energy state. Absorption is a function of certain nuclei in the molecule. A plot of the frequencies of the absorption peaks versus peak intensities constitutes an NMR spectrum.[89] As in light spectroscopy each part of the spectrum can be assigned to some chemical/physical state of the molecules. A simplified description of a nucleus is that it is a "magnet" with dipoles. This "magnet" is generated when the charge (which all molecules have) spins on the nuclear axis.[89]

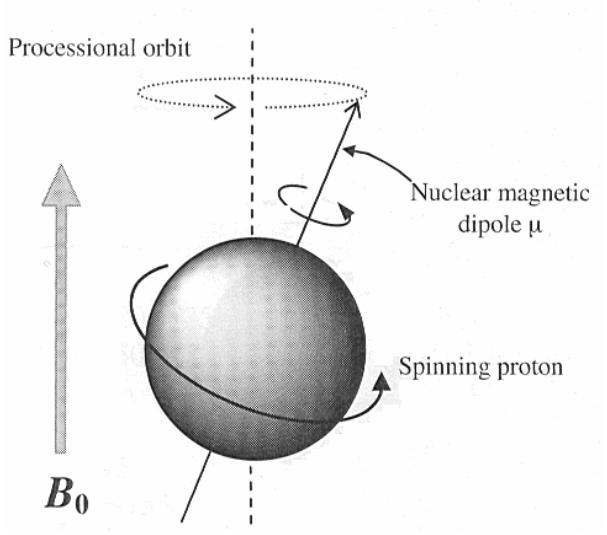

Figure 5-5. The figure shows a classical representation of a proton (^{1}H) precession in a magnetic field of magnitude B_0 in analogy with a precessing spinning top[89]

The angular momentum of the spinning charge leads to the concept of spin numbers where proton (^{1}H) and carbon-13 (^{13}C) have net spins of 1/2. This means that they can have two energy levels.[89] Radio frequency, which is energy in the form of electromagnetic radiation, can alter the energy level of a nucleus by pushing the magnetic dipole out of its original state,

thus raising it to a higher energy state. In an external magnetic field the nuclei will align itself according to this field and by applying radio frequency pulses it is possible to effect a transition between the energy levels (spin states) in a stationary magnetic field (Figure 5-6).[89]

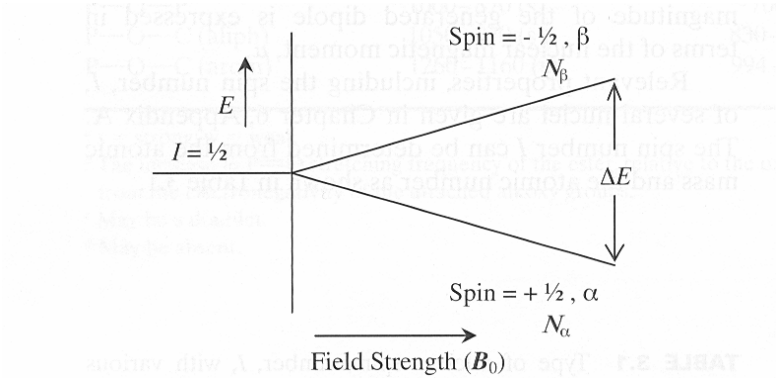

Figure 5-6. Two proton energy levels in a magnetic field of magnitude B_0. N is population of spins in the upper (N_b) and lower (N_a) energy states. The direction of the magnetic field (B_0) is up, parallel to the ordinate, and the field strength (B_0) increases to the right. Larger magnetic fields increase the ΔE and thus increase the resolution of the acquired spectra.[89]

The fundamental NMR equation (Equation 5-6) correlating the applied radiofrequency υ, with the magnetic field strength is derived from the equation relating the energy difference between the two states (for spin 1/2 nuclei) (Equation 5-5) since $\Delta E = h\nu$.[89]

$$\Delta E = (h\gamma / 2\pi)B_0 \qquad 5\text{-}5$$

$$\nu_1 = \frac{\gamma}{2\pi} B_0 \qquad 5\text{-}6$$

h is Planck`s constant, γ is the gyromagnetic ratio which is the proportionality constant between the magnetic moment, μ, and the spin number *I*. B_0 is the magnetic field strength (Tesla).[89] Immediately following the rf pulse, the excited nuclei begins to return to their ground state and radiate the absorbed energy in a process called relaxation. A detector collects this energy producing a free induction decay (FID), which is the sum of all the nuclei radiating over time. The information in the FID is Fourier transformed to a readable spectrum, which is a function of frequency. Figure 5-7 shows comparisons of different wave forms that are Fourier transformed.

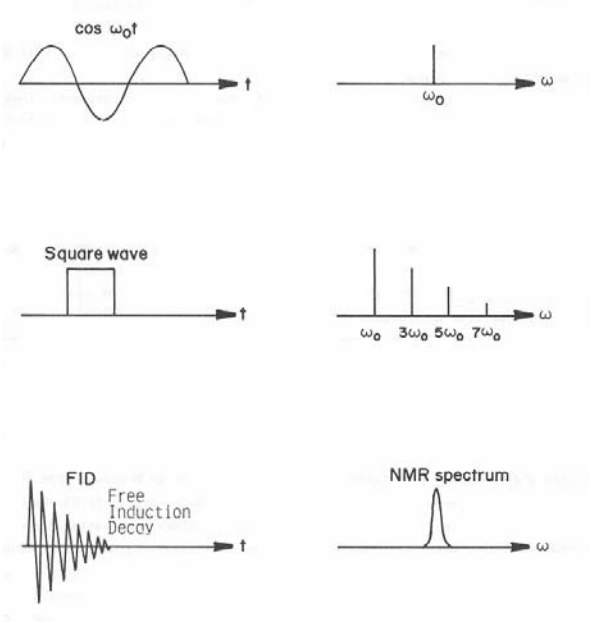

Figure 5-7. A simple representation of how the Fourier Transformation looks like when applied to different wave functions.[96]

The return of the nuclei to the relaxed state, that is; when the dipoles are aligned with the magnetic field, is called spin-lattice relaxation.[89] The rate at which equilibrium is restored is characterized by the spin-lattice or longitudinal relaxation time, T_1. The spins do not only exchange energy with the surrounding lattice, but also amongst themselves. This is generally a faster process than spin-lattice relaxation, and is characterized by the spin-spin relaxation time, T_2.[89] The relaxation processes induce a voltage that is detected by a suitably tuned coil of wire, amplified, and the signal can then be displayed as the free induction decay (FID) (Figure 5-7). This gives rise to characteristic spectra, which are functions of several factors; i) the type of nucleus, ii) the chemical environment of the nucleus, and iii) on the spatial location in the magnetic field if that field is not uniform.[70, 87, 89, 96]

5.3.2 Application of NMR to crude oil and asphaltene systems

With higher magnetic fields, both proton and carbon NMR are used in the study of structure and properties of crude oils and crude oil constituents. Higher fields and larger magnets give better resolution and faster and more detailed characterization can be obtained. For proton NMR, the sample needed is relatively small due to the high abundance of the "right" proton nuclei in nature, which is the ^{1}H. For carbon NMR the ^{13}C has only an abundance of 1.1% to that of ^{12}C (which can not be used due to the lack of net spin) and a sensitivity of 1.6% to that of ^{1}H. The overall sensitivity of the carbon-13 NMR to the proton NMR is about 1/5700.[89]

This results in the need for high concentrations and a large number of scans to obtain an acceptable signal-to-noise ratio (S/N). This, unfortunately, makes it impossible to perform experiments on low concentrations of asphaltenes within a reasonable time frame.

The practical use of proton and carbon NMR techniques that have been used in the present work will be dealt with in a pragmatic manner.

5.3.3 ^{1}H proton NMR on asphaltenes

Chemical shifts in ^{1}H NMR give information about the chemical environment of the proton nuclei. The nuclei are shielded to a very small extent by its electron cloud, the density of which varies with the chemical environment and the variation gives rise to differences in chemical shift positions.[89] Virtually this means that it is possible to distinguish between CH, CH_2 and CH_3 due to the individual absorptions of the protons. The variation and the position of the peaks are called chemical shifts positions.[89] Chemical shifts are referred to as parts per million (ppm) and are the chemical shift of a peak in Hz divided by the designated frequency of the spectrometer in MHz.[89, 96] Proton NMR chemical shift values are usually in the range of 0-10 ppm. Resolution is important for qualitative analysis and higher designated frequencies of the spectrophotometer result in an increased resolution of the spectrum.[96] Related to heavy oil systems the chemical shifts positions are not sharp peaks as in pure compounds. Due to the heterogeneity of the oil samples the protons do not form discrete peaks. Instead, broader peaks are found which makes it difficult to determine exactly what type of protons is analyzed (Figure 5-8). Therefore, higher fields and higher frequencies of the spectrophotometer are important in order to do qualitative NMR.

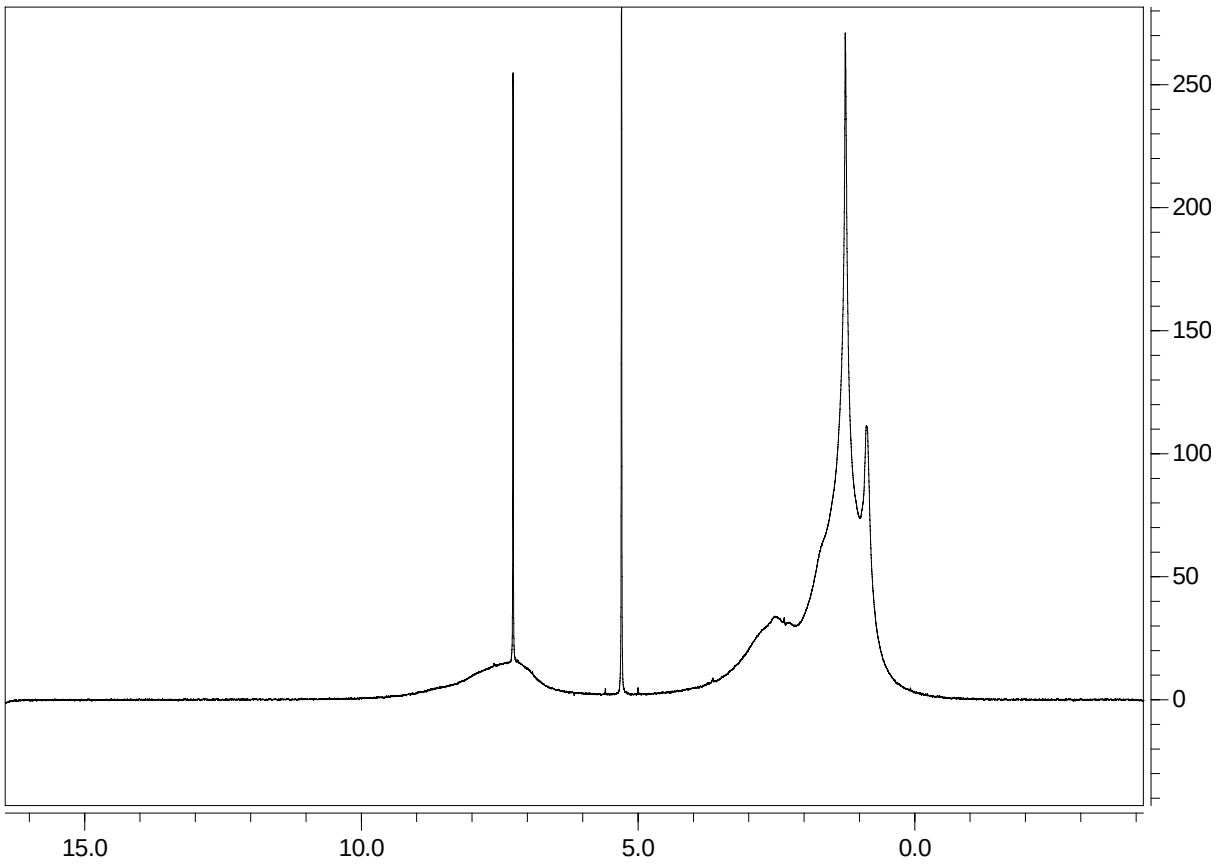

Figure 5-8 Proton NMR spectra of a asphaltene sample. Hydrogens bound to aromatic carbons reveals a broad peak (9.9-6.5). The sharp peak in the aromatic region is the solvent $CDCl_3$. The aliphatic region (4.5 – 0.5 ppm) can be divided in three parts based on the relative position of the hydrogens to aromatic carbons.

For mixture of compounds like in asphaltenes the resolution is not high enough in order to obtain single peaks for each chemical shift assigned by the chemical environment. Therefore simplifications are often used, in the form of designated shift ranges, when analyzing the spectra of asphaltenes. A common approach is to divide the fractions into four groups (Table 5-1).[97, 98]

Table 5-1. The chemical shift regions recognized for various protons in crude oils and asphaltenes.[97]

H-type	Chemical Shift (ppm)
Total aromatic hydrogen	9.9-6.5
Total aliphatic hydrogen	4.5-0.5
Total hydrogens on the α-position of an aromatic ring	4.5-1.9
Total hydrogen on the β-position of an aromatic ring	1.9-1.0
Total hydrogen on the γ-position of an aromatic ring	1.0-0-5

Hydrogens are bound to aromatic carbons where a broad peak is found for asphaltenes. Furthermore the aliphatic region is divided into three sub regions representing protons alpha (α), beta (β) and gamma (γ) to the aromatic ring (Figure 5-9).

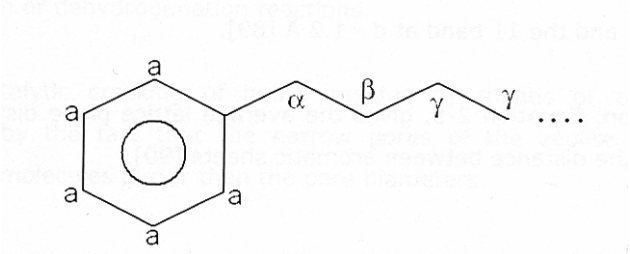

Figure 5-9. A simple illustration showing the position of the aromatic hydrogens (a) and the aliphatic region which is divided into three sub regions representing protons positioned alpha (α), beta (β) and gamma (γ) to the aromatic ring. [98]

The proton spectra will give information about the ratio of aromatic to aliphatic hydrogens. In addition some information can be obtained on the chain length of alkyl side chains. This is important information, but due to the fact that crude oils and asphaltenes are mixtures of thousands of different chemical structures, the proton NMR will create more questions than answers. Therefore, the next logical step is to do a carbon NMR study of the samples.

5.3.4 ^{13}C carbon NMR on asphaltenes

Generally, carbon-13 shifts can not be used as criteria for aromaticity since there is no difference between aromatic (128.5 ppm for benzene) and comparable alkene carbon nuclei (127.5) Chemical shifts of aromatic compounds occur between 120 and 150 ppm, but the

inclusion of electron releasing and electron withdrawing substituents as well as multiplet substitution expand this shift range considerably so that the shifts for aromatic carbons are found in the 90-185 ppm range.[94] However, the fact that alkene structures are non-existent in crude oils explains why the region 90-185 ppm is suitable for determination of total aromatic content of crude oil components.

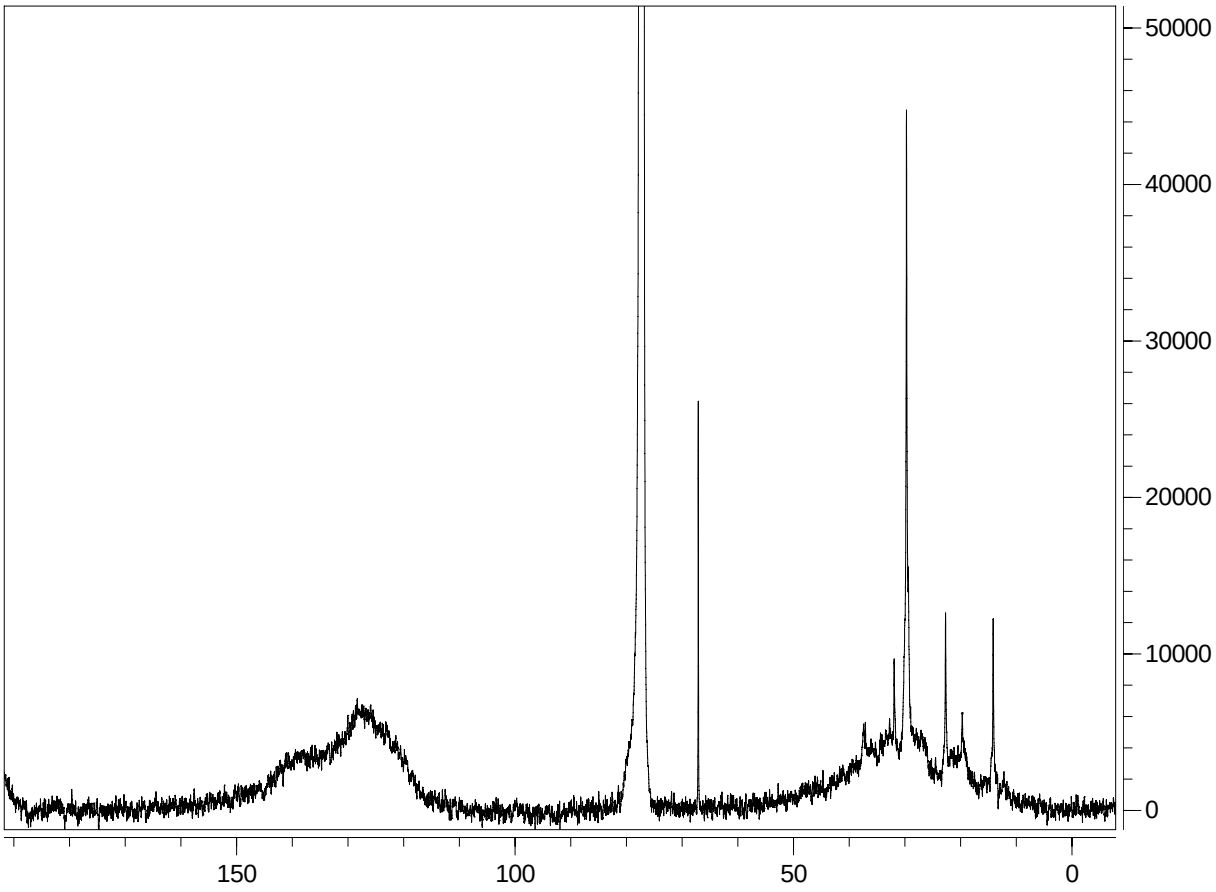

Figure 5-10 Carbon-13 NMR spectra of an asphaltene sample. The shift range is from -5 to 190 ppm. The aromatic a aliphatic shifts are shown below (Table 5-2). The peak at 77 ppm is the internal standard 1,4-dioxane and the sharp peak at 67 is the solvent $CDCl_3$.

Carbon-13 NMR gives a lot more information on the skeleton of the hydrocarbon molecules compared to proton NMR. For asphaltenes a broad peak in the aromatic (170-110 ppm) region with a shoulder is obtained, while more distinguished peaks appear in the aliphatic region (70–0 ppm) (Figure 5-10). Coupled with different pulse sequences and two dimensional NMR spectroscopic methods[37, 96], detailed information on crude oil components can be deduced. For asphaltenes as a solubility fraction, it is not only difficult, but impossible to determine the molecular structure. At best an average structure, which may or may not be relevant to the properties of the asphaltenes, can be determined.

Despite the depressing fact that one is unable to determine the structure of asphaltene molecules, the carbon-13 NMR technique is still a powerful tool.[97, 99] Carbon-13 NMR combined with various pulse sequences may give detailed information about asphaltenes. This is valuable information when comparing asphaltenes from various sources such as crude oils from different origins, coal asphaltenes and coke products obtained downstream the distillation column at the refinery.

Several distinct features of the carbon skeleton can be identified and quantified by application of the normal carbon-13 method (Table 5-2). Both terminal and branched methyl (CH_3), secondary or methylene (CH_2) and tertiary (CH) carbon can be determined. In addition it is assumed that the shift range from 150 – 178 ppm is due to carbons with substituted heteroatoms. The degree of substitution on the aromatic core may also be determined from the shift ranges of 138 – 150 ppm.[97] By integrating over the various shift ranges and applying correlations and equations including the knowledge of the CHNOS ratio and molecular weight, an average structure of asphaltene "molecules"can be determined.[97]

Table 5-2. The chemical shift regions recognized for various ^{13}C carbons in crude oils and asphaltenes.[97]

C-type	Chemical Shift (ppm)
Total aliphatic carbon	10.0-70.0
Total methyl (CH_3) carbon	10-22.7
Total terminal methyl carbon	14.3
Total branched methyl carbon	19.7
Total tertiary (CH) carbon	28.2
Total secondary (CH_2) carbon	29.7
Total aromatic carbon	100-178
Total alkyl-substituted aromatic carbon	138-150
Total heteroatom-substituted aromatic carbon	150-178

Other pulse sequences and variations of two dimensional techniques[100] may be used to extract even more detailed information from the asphaltenes.

5.3.5 Distortionless Enhancement by Polarization Transfer (DEPT)

Additional pulse sequences are often used in combination with the normal carbon-13 sequence. One of these is the DEPT sequence. DEPT has the following characteristics: CH carbon signals exhibit maximum enhancement of γ_H/γ_C at $\theta = \pi/2$, (γ_H and γ_C are the gyro magnetic ratios for proton and carbon and θ is the proton shift angle), CH_2 carbons exhibit a maximum enhancement at $\theta = \pi/4$, and CH_3 carbons a maximum enhancement of 1.15 γ_H/γ_C at $\theta = 0.196\ \pi$, respectively.[94] For coupled spectra, peak intensities are observed with their characteristic normal ratio and the lines have the same phases as in the normal FT spectrum. For example, a CH_3 (1:3:3:1) quartet becomes an enhanced 1:3:3:1 quartet.[94] The enhancement can be varied uniformly, i.e. the same for each line within a multiplet, by adjusting the pulse angle, θ. The variation with θ for CH, CH_2 and CH_3 has the following mathematical dependencies: sin θ for CH; sin 2θ for CH_2 and sin (θ + sin 3θ) for CH_3.[94] As a consequence CH_2 and CH_3 signals are zero when $\theta = \pi/2$ (90°) and CH_2 signals are inverted by changing θ from $\pi/4$ (45°) to 3 $\pi/4$ (135°); CH and CH_3 signals are unaffected (Figure 5-11).[94, 101]

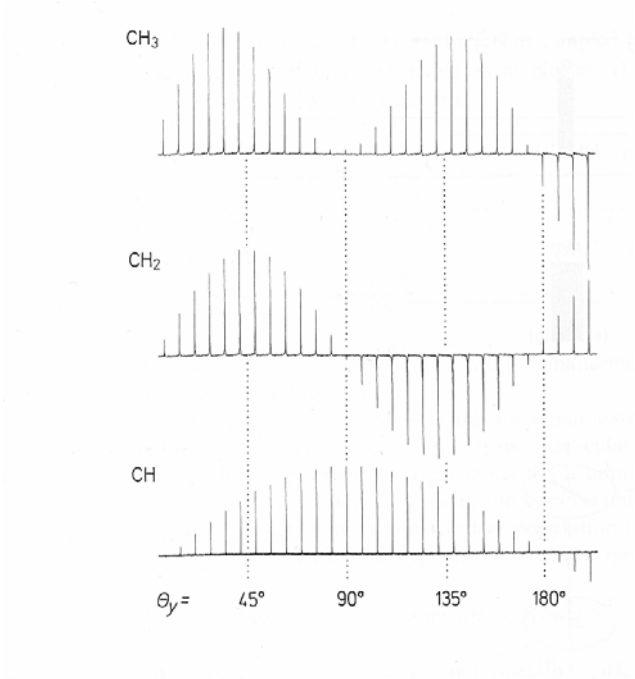

Figure 5-11. Signal intensities of CH, CH_2 and CH_3 groups as function of the polarization transfer angle (PTA) θ_y. As seen, at a PTA of 135° the CH_2 are phased down. In addition the intensity of the CH carbons are not at full intensity. This has to be taken into account when analyzing the spectra quantitatively. [94]

These dependencies can be used to generate individual CH, CH_2 and CH_3 subspectra.[101] For DEPT-135 used in this work, the pulse angle θ was 3 $\pi/4$ or 135°. The DEPT-135 gives

negative CH_2 and positive CH and CH_3 but no signal from quaternary carbon (Figure 5-12).[89, 94, 96, 102]

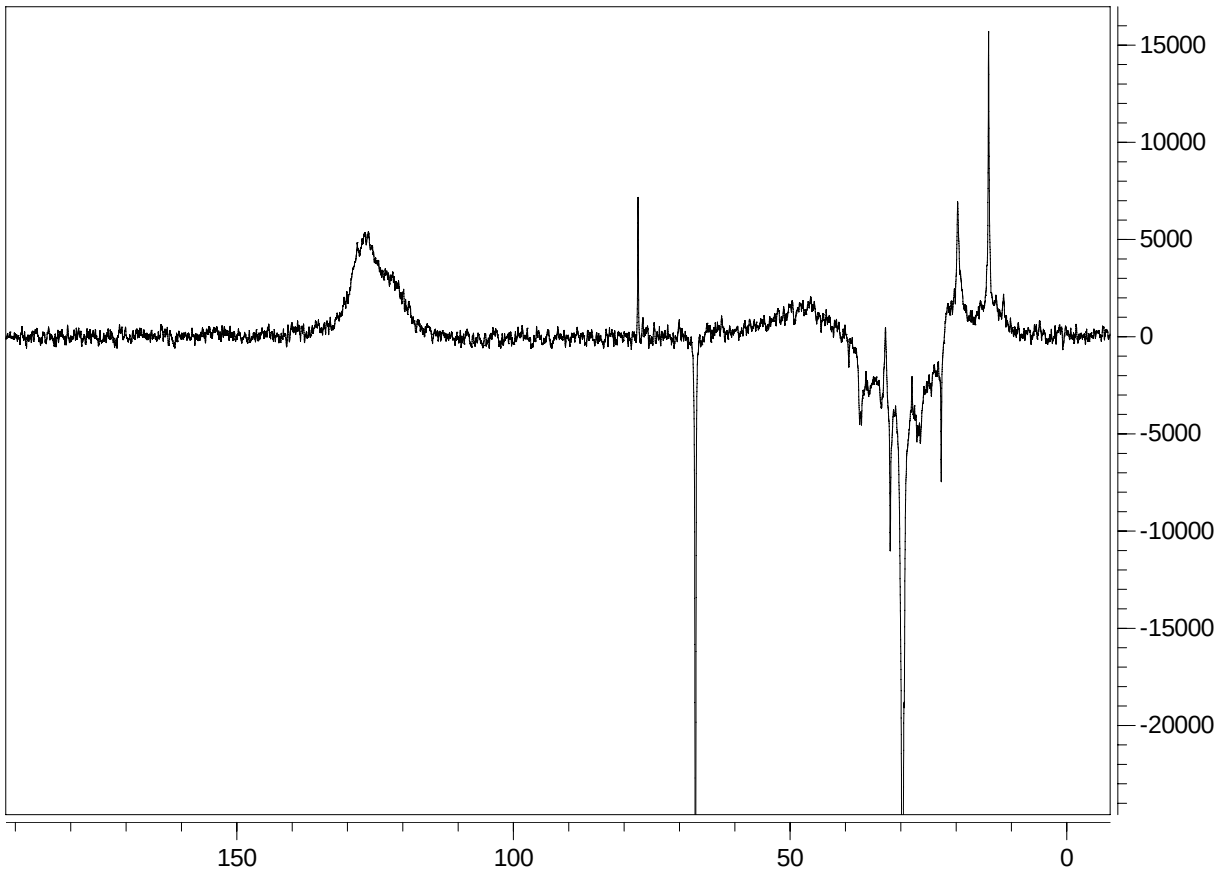

Figure 5-12 DEPT-135 NMR spectra of an asphaltene sample. The signals from CH_2 are phased down, while there is no signal from quarternary carbons.

Signals observed in the ^{13}C spectra and not in the DEPT-135 spectra will therefore belong to quaternary carbons.[94] In the literature DEPT and ^{13}C NMR sequences have been used in combination to deduce information from coal asphaltenes, maltenes and pitches.[99, 102-105]

5.4 Interfacial tension by the pendant drop technique

When two immiscible liquids like oil and water are in contact, the free energy change when expanding their interfacial area (i.e. dispersing one phase in the other) by unit area is known as their interfacial energy or interfacial tension γ_{wo}.[57] The method used for determining the interfacial tension in this work was the pendant drop method with an axisymmetric drop shape analyzer (ADSA). A balance of the gravity force (proportional to the density difference) with

the pressure difference (ΔP) across the interface, given by the Laplace pressure equation[57] (Equation 5-7),

$$\Delta P = \gamma\,(1/R1+1/R2) \qquad 5\text{-}7$$

provides the interfacial tension, γ, between the two phases. The radii of the curvature, R_1 and R_2, are determined from geometrical considerations/correlations depending on the shape of the droplet whereas the density differences between the two phases, Δρ, must be known or measured independently.[6, 68] The instrumental setup used consists of a syringe containing the oil phase and a water bath (Figure 5-13). The syringe is used to push the oil phase into the water phase, resulting in an oil droplet hanging upward from a needle in the water phase. The syringe is closed with a valve to prevent the droplet from changing volume. A camera is used to record pictures of the droplet. Some precautions must be taken when performing the measurements such as avoiding leakage from the needle, proper calibration and concentration vs. interfacial area effects.[6]

Figure 5-13. Setup of the CAM 200 from KSV Instruments. A syringe with the oil phase is placed in a quartz crystal container containing the water phase. A (high speed) camera takes pictures of the droplet. The interfacial tension is calculated from the shape of the droplet and the difference in density between the two phases.

5.5 Mass spectrometry

In mass spectrometry a compound is ionized and the ions are separated on basis of their mass/charge (m/z) ratio and the number of ions representing each m/z "unit" is recorded as a spectrum. Often mass spectrometers are coupled with some form of chromatographic instruments such as gas chromatographer (GC-MS) or a liquid chromatographer (LC-MS).[89]

In this work the method used was laser desorption ionization (LDI) with time-of-flight (TOF) mass spectrometry. With laser desorption a pulsed laser beam is used to ionize samples for mass spectroscopy. A CO_2 laser, emitting in the far-IR region or a frequency-quadruple neodymium/yttrium aluminium garned (Nd/YAG) laser emitting in the ultra violet (UV) region at 266 nm may be used. Without matrix assistance the method is limited to low molecular weight molecules (< 2000 g/mol). The TOF mass spectrometers measures the time that accelerated ions use to "drift" down a tube to a detector. Knowing the exact time and position of ionization and the length of the tube the mass can be calculated (Equation 5-7),

$$t = \left(\frac{L^2 m}{2zeV} \right)^{1/2} \qquad 5\text{-}8$$

where L is the length of the tube, m the mass of the ion, z the charge and V the potential used for the acceleration.[89] Detailed information on the setup used in this work is to be found in Hortal et. al.[106]

5.6 Characterization of emulsions and emulsion stability

Emulsions can be characterized by various methods. The bottle test is a simple test where the emulsion height is monitored as a function of time. Other characterization methods measure the droplet size using NMR self diffusion experiments or light scattering techniques. Techniques used for measurements of emulsion stability in this work were the bottle test including centrifugation, and critical electric field measurements. Droplet size determination was performed using microscopy.

5.6.1 Bottle tests

The bottle test is a simple method for screening but is not to be used to emulate the real production process.[68] The bottle test is usually performed by making an emulsion and then measuring the height of the emulsion layer as a function of time. The method is efficient when a fast screening of, for example, the effect of different water cuts or emulsion inhibitors is to be tested rapidly. If the emulsions are very stable, centrifugation may be used to force the water to separate.

5.6.2 Critical electrical field

Application of an electric field up to several thousands kV/cm is used as a common process in the oil industry to increase the flocculation and coalescence rate of the water droplets present in a continuous oil phase (see section 4.3). The electric field strength needed to cause such coalescence can be used as a measure of the emulsion stability. In low electric fields, water droplets surrounded by a rigid interfacial film will attain a chain-like configuration. When increasing the electric field, the droplets will bridge the gap between the electrodes leading to a sudden increase in the current (Figure 5-14). This critical electric field, called E-critical, is measured in a E-critical cell (Figure 5-15) and gives an indication of the emulsion stability of a w/o emulsion.[88]

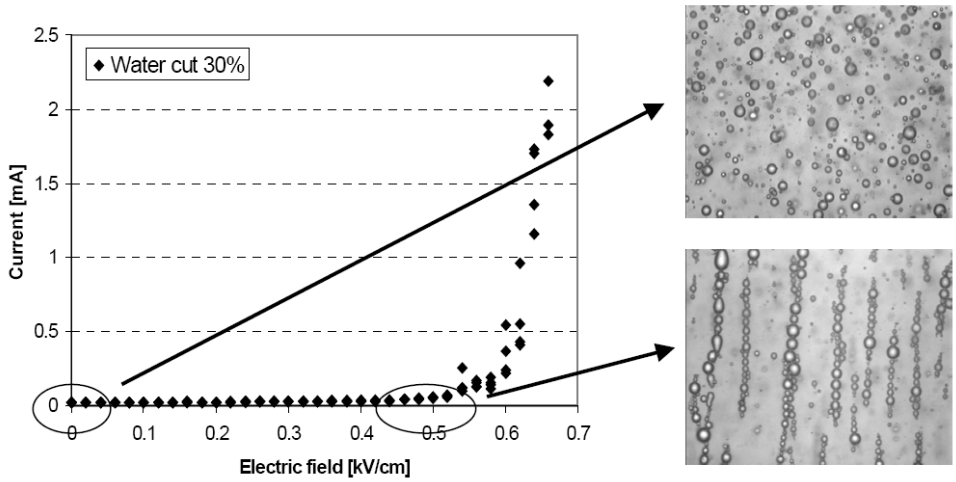

Figure 5-14. Water droplets in an emulsion attain a chain-like configuration when the electric field reaches a critical limit (the E-critical).[88]

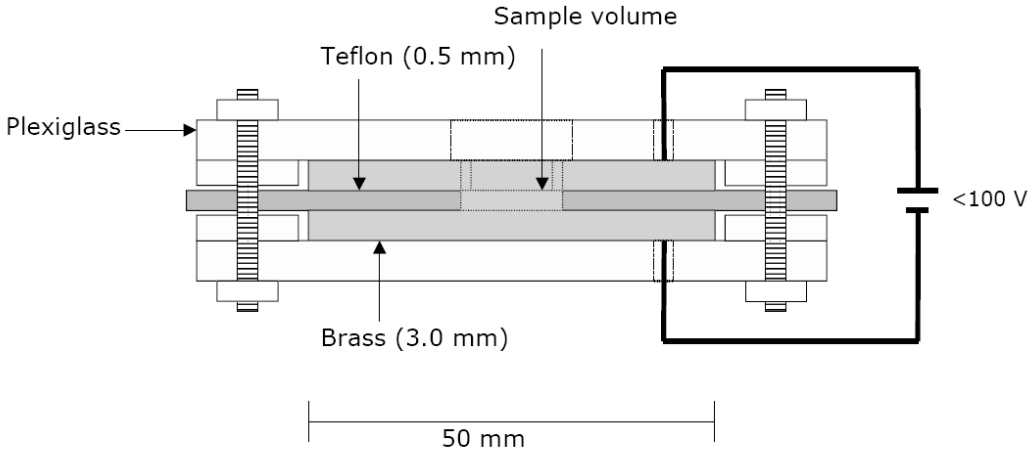

Figure 5-15. An electric field cell for emulsion stability measurements similar to the one used in this work.[88]

5.6.3 Digital Video Microscopy (DVM)

A digital video microscope with a resolution of about 1 μm was used in this work (paper 5). DVM can be used for direct determination of particle sizes and shapes and can be used to determine droplet size distributions of crude oil emulsions. The drawback by using DVM on emulsions instead of an in situ or online method is that the sample usually has to be diluted and measurements are not taken exactly at the time of formation of the emulsion leading to some uncertainties with regard to the real droplet size distribution. Nevertheless, the DVM (or other direct measurement techniques) is mandatory in order to have some direct measure of droplet sizes for correlation with indirect techniques like NMR self diffusion or light scattering techniques.

6 MAIN RESULTS

The results obtained during the PhD period are presented in the papers enclosed. Furthermore the status of each manuscript is given in the "list of papers" section. In the manuscripts, details on procedures, experimental techniques, and more detailed discussions with regard to the results are to be found. This chapter highlights the most important results and conclusions in each manuscript. Moreover, the research and results are original work by the authors.

6.1 Paper 1: Solubility parameters based on near infrared and infrared spectra. I. Correlation to polar solutes and binary mixtures

Near infrared (NIR) and infrared (IR) spectra were recorded for a set of solvents and binary solvents with various polarity and functional groups. Solubility parameters for the solvents were found in the literature. The intention of the study was to make an attempt to correlate and predict solubility parameters for solvents and solvent mixtures based on their respective IR and NIR spectra. Furthermore, it was of interest to see how IR spectra of crude oils and their respective SARA fractions were arranged in a score plot by principal component analysis (PCA). In addition, the solubility parameters of the crude oils and the SARA fractions were predicted based on the respective models.

Hansen solubility parameters for several solvents were correlated to their respective IR and NIR spectra. Partial least square (PLS) regression was used and the results were evaluated by the correlation coefficient (R^2), root mean square error of prediction and other statistical parameters obtained by using the Unscrambler™ software by CAMOS. A correlation matrix was used to build the model while a test set was used as a "blind" reference to test the prediction ability of the models. The results of PLS regression were presented in the manuscript for the models based on IR (Table 6-1) and NIR (Table 6-2) data respectively.

Table 6-1 (Table 2 in Paper 1). Results from PLS-1 modelling and predictions based on the correlation of the solubility parameters to IR data.

Solubility parameter	Tot [$MPa^{1/2}$]	D [$MPa^{1/2}$]	H [$MPa^{1/2}$]	P [$MPa^{1/2}$]
Number of PC	3	3	2	3
Correlation val.	0.91	0.85	0.98	0.94
Correlation pred.	0.89	0.26	0.93	0.70
RMSEV [$MPa^{1/2}$]	1.3	0.5	1.8	1.1
RMSEP [$MPa^{1/2}$]	2.6	1.3	3.9	3.6
Dev (averaged)	1.21	0.50	1.75	3.59
Bias	0.03	-0.33	1.55	-0.42
Y-variance val. %	95	90	91	98
X-variance val. %	54	67	37	59

Table 6-2 (Table 4 in Paper 1). Results from PLS-1 modelling and predictions based on the correlation of solubility parameters to unmodified NIR data.

Solubility parameter	Tot [$MPa^{1/2}$]	D [$MPa^{1/2}$]	H [$MPa^{1/2}$]	P [$MPa^{1/2}$]
Number of PC	4	4	2	4
Correlation val.	0.92	0.88	0.95	0.95
Correlation pred.	0.92	0.53	0.91	0.78
RMSEV [$MPa^{1/2}$]	1.8	0.6	1.7	1.1
RMSEP [$MPa^{1/2}$]	2.6	1.1	3.5	3.8
Dev (averaged)	1.47	0.71	2.26	1.50
Bias	-0.42	0.12	1.19	-0.56
Y-variance %	87	81	90	89
X-variance. %	80	84	67	82

Furthermore, the solubility parameters of SARA fractions and crude oils were predicted using the models developed (Table 6-3 and Table 6-4).

Table 6-3 (Table 6 in Paper 1). Results from prediction of the solubility parameters on the crude oils presented as the lowest and highest predicted value.

Parameter	Min. – Max. [$MPa^{1/2}$]	Average [$MPa^{1/2}$]
Hildebrand	16.3 – 16.9	16.6
Dispersion	16.2 – 16.4	16.3
Hydrogen bonding	5.0 – 6.0	5.5
Polar	0.4 – 1.3	0.8

Table 6-4 (Table 7 in Paper 1). Results from prediction of the solubility parameters on the SARA fractions presented as the lowest and highest predicted value.

Fraction	Hildebrand [$MPa^{1/2}$]	Dispersive [$MPa^{1/2}$]	Hydrogen [$MPa^{1/2}$]	Polar [$MPa^{1/2}$]
Saturates	16.4 – 16.7	16.2 – 16.4	4.7 – 5.6	0.0 - 0.7
Aromatics	16.7 – 16.9	16.4 – 16.6	4.9 – 5.4	0.7 – 1.0
Resins	17.3 – 18.6	15.6 – 16.4	5.9 – 8.1	1.2 – 2.3
Asphaltenes	18.0 – 19.1	15.0 – 15.8	7.6 – 10.3	1.2 – 3.2

The conclusion of this study was that IR and NIR spectra in general can be used for correlation to Hansen solubility parameters. Furthermore, IR and NIR spectra can be used to distinguish between crude oils and crude oil components

6.2 Paper 2: Asphaltenes Precipitated by a Two-Step Precipitation Procedure. 1. Interfacial Tension and Solvent Properties

Asphaltenes were precipitated into two fractions using a two-step precipitation procedure. The first fraction was obtained by mixing 3:1volumes of n-pentane/crude oil followed by filtration. In the following step the second fraction was precipitated out from the filtrate using 18:1 volumes of n-pentane/crude oil. Whole asphaltenes were also precipitated using a 40:1 *n*-pentane-to-crude oil ratio. Amount of each fraction was determined for comparison with the whole asphaltenes (Table 6-5). Three crude oils (named WA, NS-A and NS-B) were used and the asphaltene fractions obtained were characterized with regard to onset of precipitation, interfacial tension ($\gamma_{o/w}$) and radius of gyration of the aggregates.

Table 6-5. (Table 1 in paper 2). Percent weight of asphaltenes for the first fraction (3:1), second fraction (18:1) and the asphaltenes precipitated by the standard procedure of excess (40:1) *n*-pentane. Since the fractions are only precipitated with up to 18:1 *n*-pentane-to-crude oil there is not likely that the first and second fraction will sum up to the whole as shown for the WA and NS-B asphaltenes. While for the NS-A they do sum up to the whole fraction.

Oil	wt % first fraction (3:1)	wt% second fraction (18:1)	Sum wt% first and second fraction	wt% whole fraction (40:1)
WA	0.8	0.9	1.7	2.0
NS-A	1.0	0.8	1.8	1.8
NS-B	0.4	0.5	0.9	1.6

First of all, the onset of precipitation (NIR) for the asphaltenes was tested to verify that the first fractions taken out, in fact were the less soluble of the fractions (Figure 6-1). Interfacial tension measurements were conducted using the pendant drop method where the interfacial tension of toluene, containing 100 mg/L of asphaltenes, towards water (pH 7 buffered, 3.5 wt% NaCl) was recorded over 12 hours. Asphaltenes that precipitated at the 3:1 dilution ratio (first fractions) had a faster initial reduction of the $\gamma_{o/w}$, while the second fractions (18:1 dilution ratio) led to a lower $\gamma_{o/w}$ over time (Figure 6-2). Whole asphaltenes seemed to hold properties of both the first and the second fractions. They had a fast initial reduction like the first fractions and reduced the value of the interfacial tension more, indicating that there were also compounds which will not influence the value of $\gamma_{o/w}$ after a longer period of time. The SANS measurements showed that the aggregates of the first fractions were larger than the aggregates of the second fractions (Table 6-6).

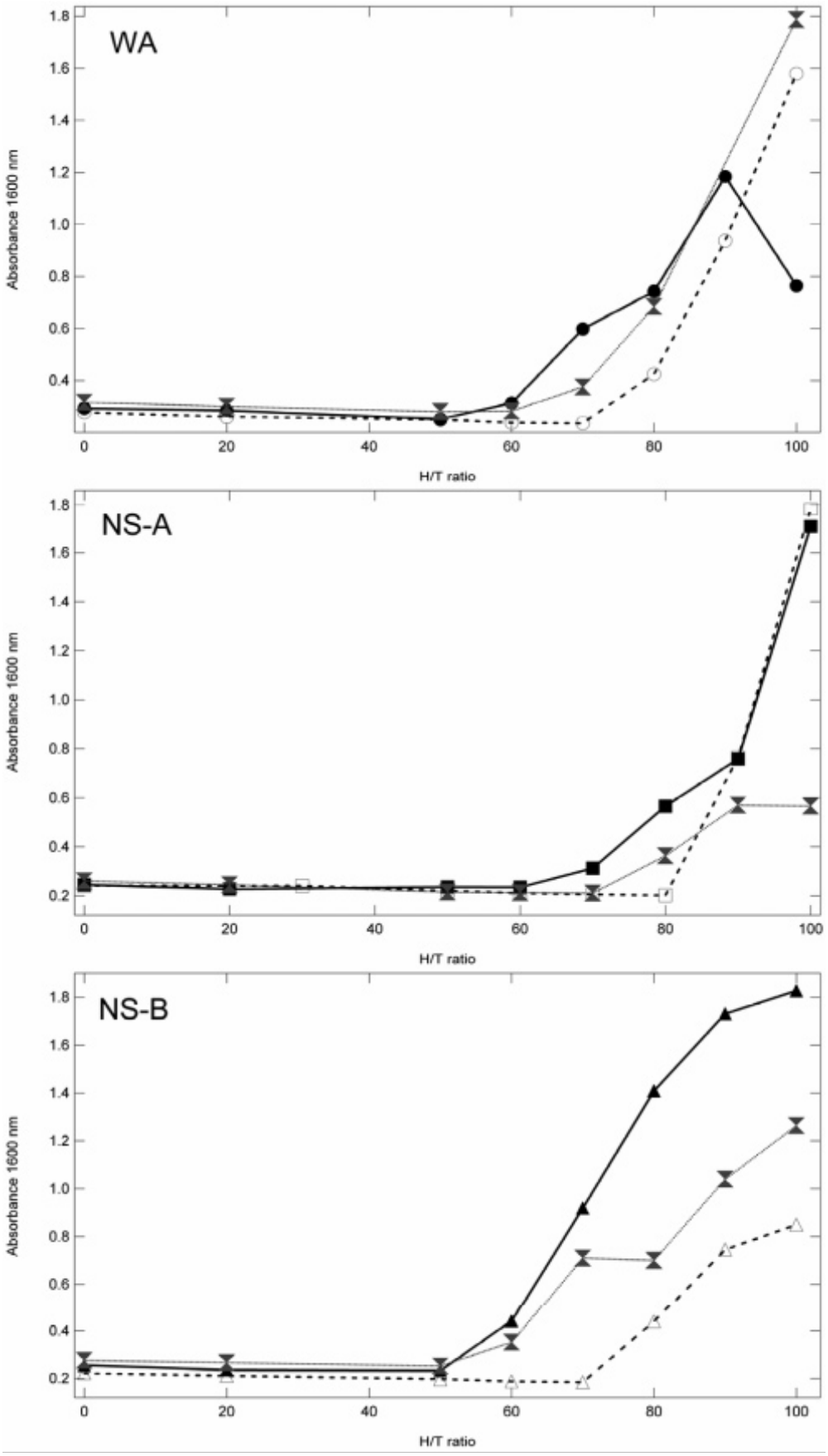

Figure 6-1 (Figure 2 in Paper 2). The figure shows the precipitation onsets for the first and second fractions and whole asphaltenes. Filled markers represents the first fraction, open markers the second fraction and the hourglass the whole asphaltenes.

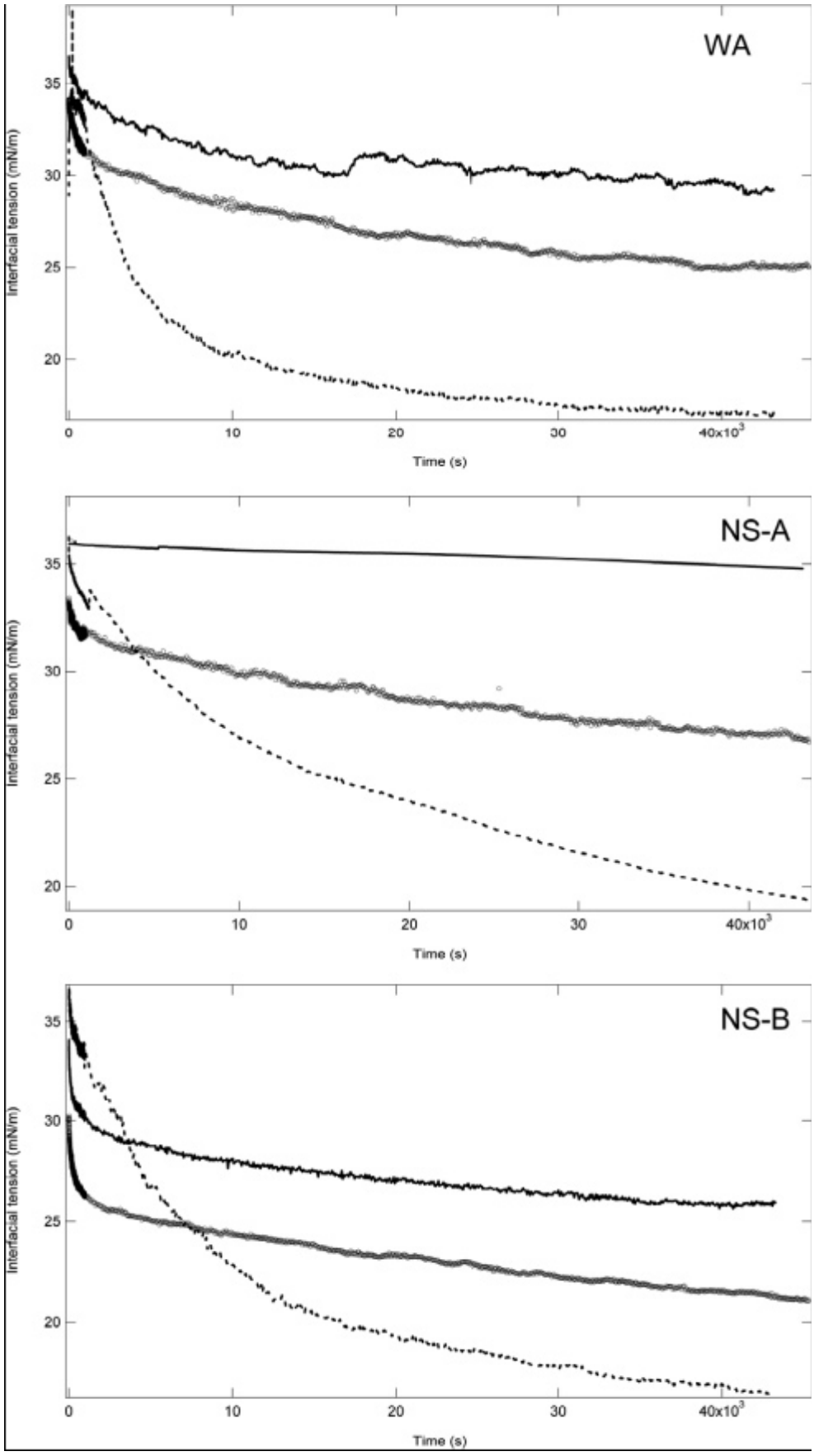

Figure 6-2 (figure 3 in Paper 2). Interfacial tension as a function of time for the asphaltene fractions. Black is the first fractions, dotted markesr the second fractions and grey represents the whole asphaltenes.

Table 6-6 (Table 4 Paper 2). Calculated R_G from the SANS measurements using the Guinier approximation. The uncertainty of the instrument is ± 1 Å. N.D (not determined) indicating the values were outside the detection limit fo the instrument. This meant that these samples contained aggregates which were much larger (>700 Å) than the other samples.

Asphaltene fraction	R_G (Å)
WA first	30
WA second	25
NS-A first	N.D
NS-A second	N.D
NS-B first	26
NS-B second	21

The conclusion of this work was that the precipitation procedure used was suitable for fractionating asphaltenes by a direct step-wise precipitation from the crude oils without first precipitating the whole fraction. It was also shown that the solvent properties of the two solubility fractions were quite different. The first fractions that precipitated upon addition of a small amount of *n*-pentane was less soluble in the precipitation onset experiments, formed larger aggregates and had a different (lower) interfacial activity as compared to the second, more soluble fractions. The assumptions made based on the results were that the first fractions would contain molecules with a higher molecular weight, and be more polar and more aromatic. These assumptions were tested using NMR, FT-IR, LDI-MS and elemental analysis presented in the next section.

6.3 Paper 3: Asphaltenes Precipitated By a Two-Step Precipitation Procedure. 2. Physical and Chemical Characteristics

The intention of this study was to search for explanations in the molecular structures and physical properties of the asphaltenes for the results obtained in paper 2. The aim was to map and quantify, as far as possible, the functional groups, aromaticity, polarity and size of the asphaltene solubility fractions. What is important to keep in mind is that asphaltenes are mixtures of thousands of different, yet relatively similar compounds. Any attempt of measuring the properties, or analyzing the size or structure will result in values that are average of all the compounds in the asphaltene sample. FT-IR was used to determine and quantify functional groups, elemental analysis was performed to determine the relative amount of the CHNOS compounds, and LDI-MS was used to determine the average molecular weight of the asphaltenes in the samples. Proton (^{1}H), carbon-13 (^{13}C) and DEPT-135 NMR was used to analyze and quantify the aromaticity, type of aliphatic groups, and the carbon skeleton in general. It was shown that the relative amounts of the polar heteroatoms S, N and O were slightly higher in the first (least soluble) fractions than in the second fractions and whole asphaltenes (Table 6-7)

Table 6-7 (Table 2 Paper 3). Relative values of hydrogen and heteroatoms to the carbon atoms in the asphaltene samples.

Sample	H/C*100	N/C*100	S/C*100	O/C*100	(N+S+O)/C*100
WA whole	9.5	1.8	1.4	2.0	5.2
WA first	10.6	1.8	2.6	1.8	6.3
WA second	9.9	1.7	2.5	1.7	5.9
NS-A whole	9.3	1.2	2.3	2.0	5.4
NS-A first	9.5	1.2	2.3	2.2	5.7
NS-A second	9.1	1.2	2.3	2.0	5.5
NS-B whole	9.7	1.7	2.5	3.1	7.3
NS-B first	10.1	1.8	4.4	3.9	10.0
NS-B second	10.3	1.7	3.9	3.7	9.2

LDI-MS showed that the average molecular weight is higher for the first fractions compared to the second fractions the whole asphaltenes (Table 6-8).

Table 6-8 (Table 3 Paper 3). Number averaged molecular weights in g/mol of the asphaltenes obtained by laser desorption ionization mass spectrometry using a laser pulse with the energy of 20 µJ.

Fraction	WA	NS-A	NS-B
First Fraction (3:1)	825	840	470
Second Fraction (18:1)	720	745	460
Whole Fraction (40:1)	500	700	445

First fractions of the asphaltenes were (for WA and NS-B) more aromatic and had more heteroatoms substituted to the aromatic core and contained slightly more heteroatoms. There were no indications from the results that the alkyl chains substituted on the aromatic were longer for the second fraction. However there were indications that they had a higher degree of branching and contained more of hydroxylic and carboxylic functional groups. The second fractions were also more substituted.

All the parameters obtained are an average of the molecular mixture in the samples, thus there are no guarantee that the relative differences commented upon in this work are the ones responsible for the properties determined in the previous work. For example comparing the aromaticity of the first and second fractions one finds, according to the assumptions, that for the WA and NS-B the less soluble fraction has a higher aromaticity, while for the NS-A the aromaticities are equal for the two sub-fractions. NS-A was also the crude oil where the sub-fractions added up to the total weight of the whole asphaltenes (Table 6-5) and which also formed very large aggregates according to SANS measurements indicating that the asphaltenes from this crude oil (NS-A) behaved different from the two other crude oils. The precipitation procedure using 3:1 and 18:1 may not divide the solubility fractions of asphaltenes in the same manner for different oils. In fact, the results indicated that there was a trend that the WA and NS-B asphaltene sub-fractions followed each other with regard to the relative values in properties, while the NS-A was different in the respect that the determined values between the first and second fractions were either more equal or more different so that the same conclusions could not be drawn. Nevertheless, the trends found that support the

assumptions are that the less soluble fractions which formed larger aggregates (SANS) were less interfacial active (pendant drop) were more aromatic, more polar (in the aromatic core) and had a higher average molecular weigh. The second fractions had alkyl groups that were probably more branched and contained a somewhat larger portion of naphtenic rings and had more of the hydroxyl and carboxylic groups on the aliphatic parts which could explain the higher interfacial activity.

There is probably no single reason for the precipitation of asphaltene that can be explained by the molecular structure or weight. The results in paper 2 and 3 indicate that it is of great interest and importance to fractionate asphaltenes with respect to the less and more soluble asphaltenes. Furthermore, it is not yet determined what the ultimate character of the least soluble asphaltene fraction is, and if this fraction is the most harmful with regard to adsorbtion to surfaces and emulsion stability. The procedure presented here were extended to a four-step precipitation procedure (Paper 4) where it was shown that the interfacial activity was not linearly dependent on the order of the solubility fraction.

6.4 Paper 4: A new procedure for direct precipitation and fractionation of asphaltenes from crude oil

This manuscript describes a new procedure for the direct precipitation and fractionation of asphaltenes from crude oils and is based on the experience of the work described in papers 2 and 3. The intention here was to further investigate which part of the second fraction was more interfacially active. It was not taken for granted that it would be the most soluble fraction when doing an extended step-wise precipitation procedure.

The precipitation procedure was principally similar to the one described in paper 2, only here with four dilution and filtration steps. Precipitation followed by inter-step filtration off of the precipitated material was performed step-wise after an addition of 3:1, 10:1, 15:1 and 20:1 *n*-pentane-to-crude oil named fraction 1, 2, 3 and 4 respectively. These fractions were analyzed with regard to precipitation onset (Figure 6-3 and Figure 6-4) in toluene/heptane mixtures and interfacial tension (Figure 6-5 and Figure 6-6). Two oils were tested in this study, the NS-A and the NS-B crude oils from paper 2 and 3.

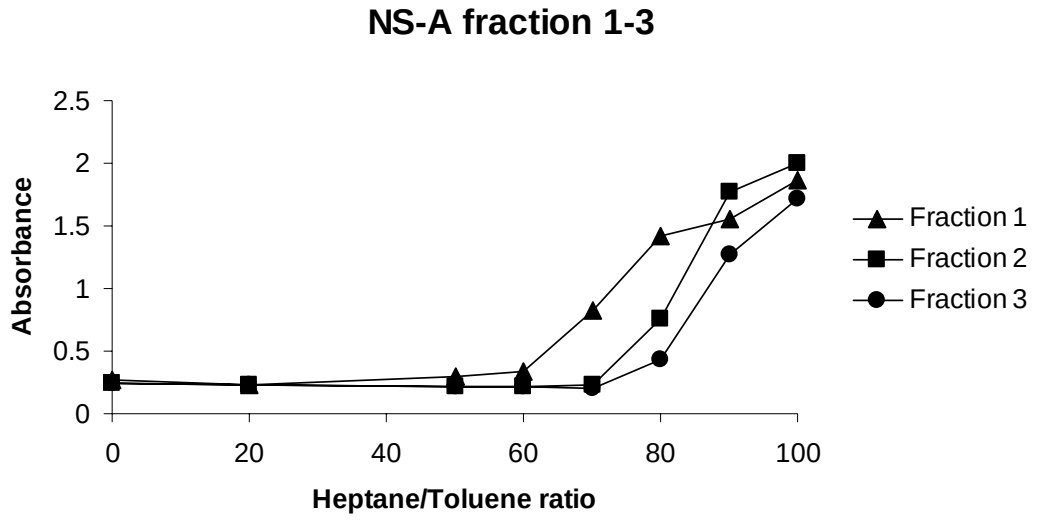

Figure 6-3 (Figure 2 in paper 4). Determination of precipitation onset for NS-A asphaltene fractions in toluene at increasing heptane ratios measured as increase in absorbance at 1600 nm.

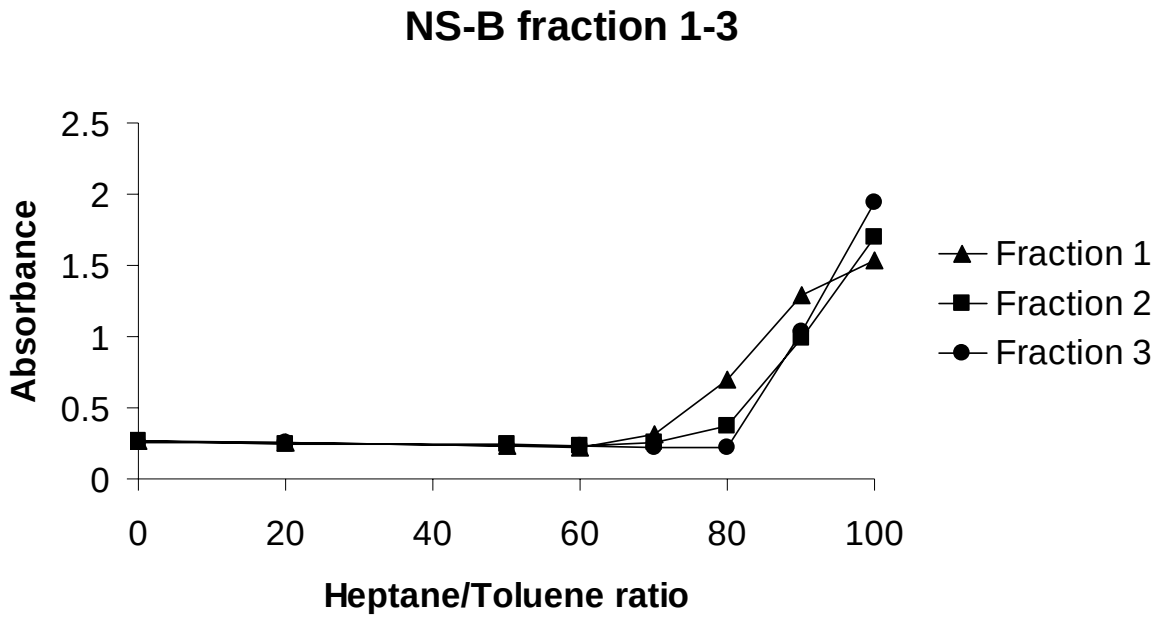

Figure 6-4 (Figure 3 in paper 4). Determination of precipitation onset for NS-A asphaltene fractions in toluene at increasing heptane ratios measured as increase in absorbance at 1600 nm.

The results from the precipitation onset experiments verify that the solubility of the fractions is in the order of which they were precipitated. The reason why fraction four is not present in these experiments is that there were not enough mass of the samples. This was still not considered to be of importance for the overall results and conclusions since this fraction probably would have the highest solubility, and did not have a lower interfacial tension. Although in other measurements, there can not be ruled out that this fraction is of importance.

For the interfacial tension experiments, which were the most important in this investigation, there were enough samples of all four fractions.

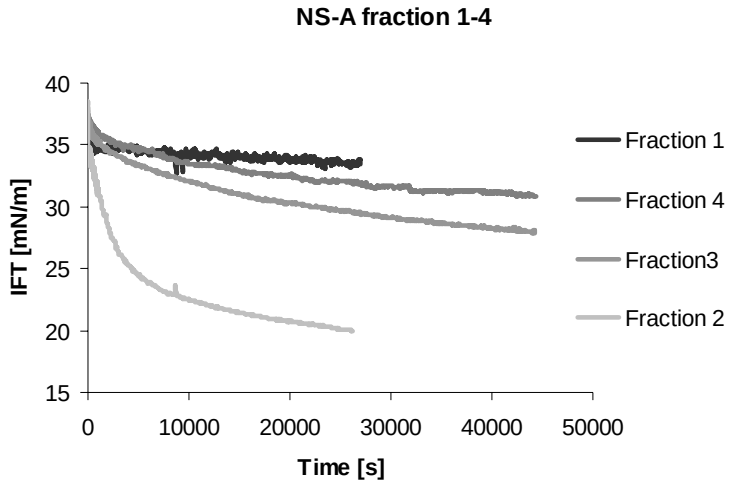

Figure 6-5 (Figure 3 in paper 4). Interfacial tensions of 100 mg/L solutions of asphaltene fractions from NS-A in toluene. Water phase is pH 7 buffered water containing 3.5 wt% NaCl.

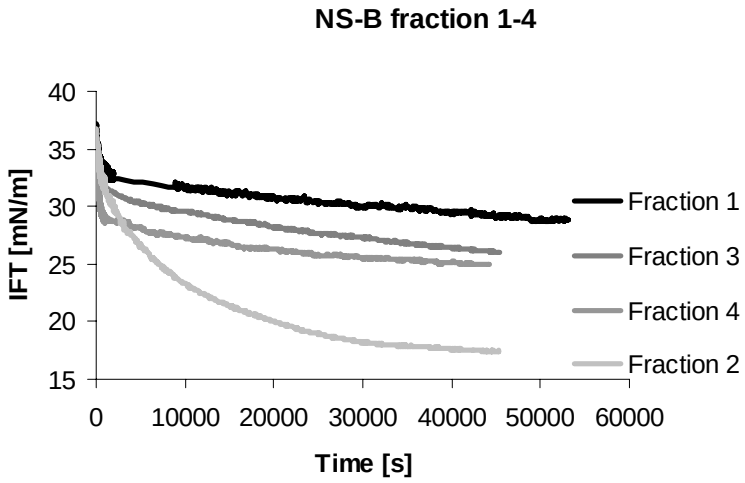

Figure 6-6 (Figure 4 in paper 4). Interfacial tensions of 100 mg/L solutions of asphaltene fractions from NS-B in toluene. Water phase is pH 7 buffered water containing 3.5 wt% NaCl. This figure is misprinted in the published manuscript, where Figure 3 is printed twice.

As seen, there is a great difference in the interfacial tensions for the different fractions from both crude oils. It is remarkable that fraction 2, the 10:1 middle fraction exhibited the highest interfacial activity, measured after 12 hours. The measured interfacial activity at the end of the experiments (equilibrium value) was plotted as a function of the *n*-pentane-to-crude oil ratio (Figure 6-7)

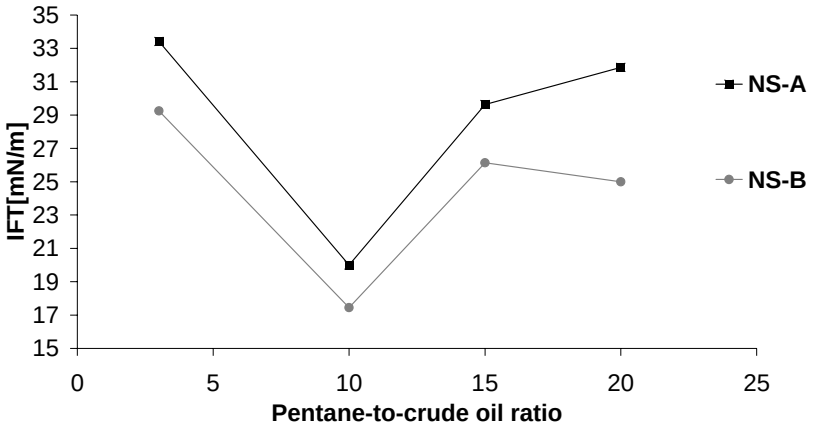

Figure 6-7 (Figure 5 in paper 4). The plot shows the interfacial tension of each fraction at the end of the experiment time. It is clear that the second fraction, that is the fraction precipitated after the 3:1 fraction was taken out of the solution and when a 10:1 ratio of pentane-to-crude oil was added, was the most interfacially active compound in these experiments.

It was neither the least nor the most soluble fractions, within the fractions studied, which were the most interfacially active compounds. This is in fact very well in accordance with general surfactant chemistry. For a compound to be interfacially active, it has to have both water soluble and oil soluble parts. This principle might be transferred to these results by suggesting that it is neither the least nor the most soluble fraction that is the more interfacial active, but a middle fraction.

The conclusion of these results is that more effort should be put into the fractionation of asphaltenes when one wants to study both properties and structure. The common 40:1 fraction may mask important features of asphaltenes resulting in erroneous assumptions based on properties studies and the structure elucidation of the asphaltenes. This has large technical consequences within crude oil production and processing.

6.5 Paper 5: A laboratory-scale vertical gravity separator for emulsion characterization

A flow loop was build where water and oil are pumped separately using positive displacement pumps and then mixed in a tee before flowing through a choke valve where shear may be induced in order to form a dispersion which separates in the test separator. The water and oil then are led (separately) back to the feed separator (see Figure 6-8). The main goals of the manuscript were to explain the setup and give a report on the droplet sizes created.

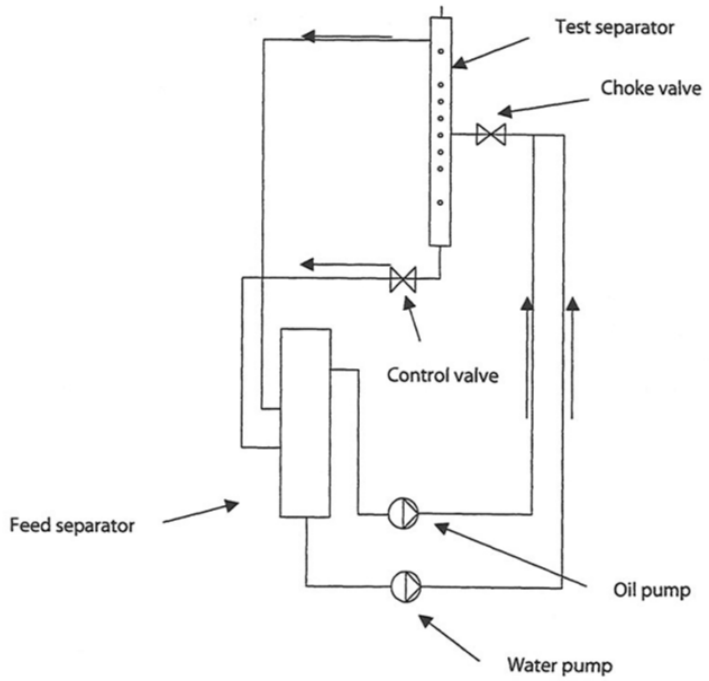

Figure 6-8. (Figure 1 in Paper 5). Flow scheme of the separator system with the main process units. Arrows indicate the flow directions

Table 6-9 report on the model systems, water cuts and pressure drops used in the experiments. In Table 6-10 the theoretical maximum drop sizes for pressure drops from 0.25 to 4.5 bars are presented.

Table 6-9 (Table 1 in Paper 5). Process parameters for the model systems used.

TABLE 1
Process parameters for the model system used

System	Water cuts %	Pressure drops %
Model system 1[a]	10, 20, 30, 40, 50	5, 10, 15, 25, 50, 90
Model system 2[b]	30	10, 25, 30, 40, 50, 60, 70, 80, 90
Model system 3[c]	10, 20, 30, 40, 50	5, 10, 15, 25, 50, 90

[a]500 ppm oil 18, 30 vol% toluene.
[b]5000 ppm oil 18, 20 vol% toluene.
[c]5000 ppm oil 3, 30 vol% toluene.

Table 6-10 (Table 2 in Paper 5). Maximum droplet sizes that can survive after the choke valve, calculated for various pressure drops.

TABLE 2
Calculated maximum drop size at different pressure drops for infinite dilution

	DP (bars)						
	0.25	0.5	0.75	1.25	2.5	4.0	4.5
Max drop size (10^{-6} m)	93	71	60	49	37	31	29

The droplet sizes were determined experimentally using DVM on diluted solutions (Table 6-11, Table 6-12 and Table 6-13).

Table 6-11 (Table 3 in Paper 5). Mean droplet sizes determined for the process parameters tested on system 1

TABLE 3
Mean droplet size for different water cuts and pressure drops of model system 1

	Model system 1					
	DP 5	DP 10	DP 15	DP 25	DP 50	DP 90
WC 10	9.8	4.4	5.4	7.0	11.9	4.1
WC 20	10.8	6.1	5.5	5.3	2.6	4.7
WC 30	11.6	8.1	5.8	4.7	4.3	6.8
WC 40	9.6	9.0	6.2	6.2	4.7	4.1
WC 50	7.2	8.1	6.4	5.4	N.D	N.D

Table 6-12 (Table 4 in Paper 5). Mean droplet sizes determined for the process parameters tested on system 2

TABLE 4
Mean droplet size for different water cuts and pressure drops of model system 2

	Model system 2								
	DP 10	DP 25	DP 30	DP 40	DP 50	DP 60	DP70	DP80	DP90
WC 30	13.5	8.6	9.0	6.0	7.3	5.4	10.6	11.0	11.9

Table 6-13 (Table 5 in Paper 5). Mean droplet sizes determined for the process parameters tested on system 3

TABLE 5
Mean droplet size for different water cuts and pressure drops of model system 3

	Model system 3					
	DP 5	DP 10	DP 15	DP 25	DP 50	DP 90
WC 10	7.1	10.4	7.8	4.5	4.1	4.8
WC 20	6.7	5.6	6.6	7.8	6.4	5.8
WC 30	9.8	6.3	5.1	7.3	7.8	5.6
WC 40	12.2	10.1	8.7	6.1	8.2	6.2

The droplet sizes determined were from 2 to 90 microns approximately which was confirmed by theoretical calculations of maximum droplet sizes at the relevant pressure drops. The mean diameter droplet size was between 2.6 and 13.5 microns depending on the model system and the process parameters (flow rate, pressure drop and water cut). The trend (but not in all cases) was that increasing the pressure drop led to droplets with smaller mean diameter and a more narrow size distribution. Increasing the water cut at a certain pressure drop for a certain system gave an increase in the mean diameter of the droplets.

6.6 Paper 6: Electrostatic coalescence under flowing conditions: An investigation of the effect of a high electric AC field on the efficiency of two different demulsifiers

A compact electro coalescer was constructed with the intention to simulate a down-scaled (vertical slice of) CEC™ (Figure 6-9) with length of one third of the commercial CEC and a flow channel which also should resemble the CEC™ with respect to dimension and electric field strength (Figure 6-10).

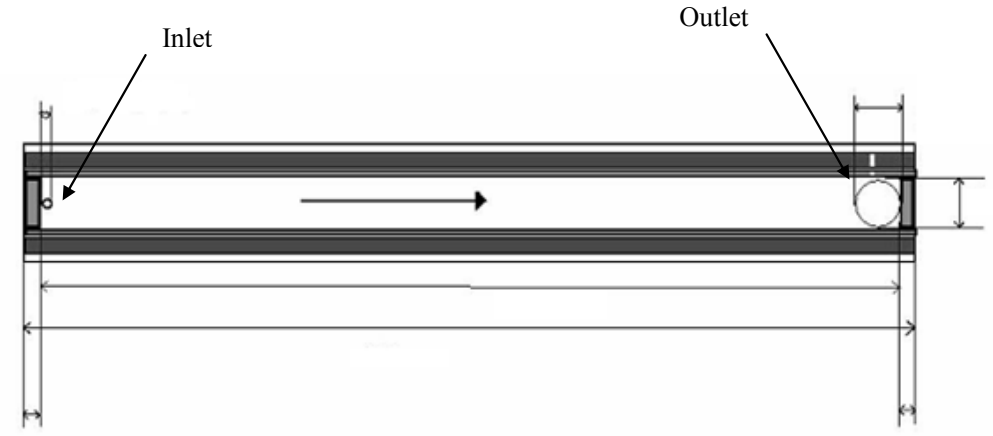

Figure 6-9. A water-in-oil (w/o) emulsion is produced by shear over a choke valve and led to the inlet of the lab scale CEC. The CEC will work as small separator even when there is no electric field over the two spaced plates. The oil and water exits through a opening approximately equal in area to the CEC.

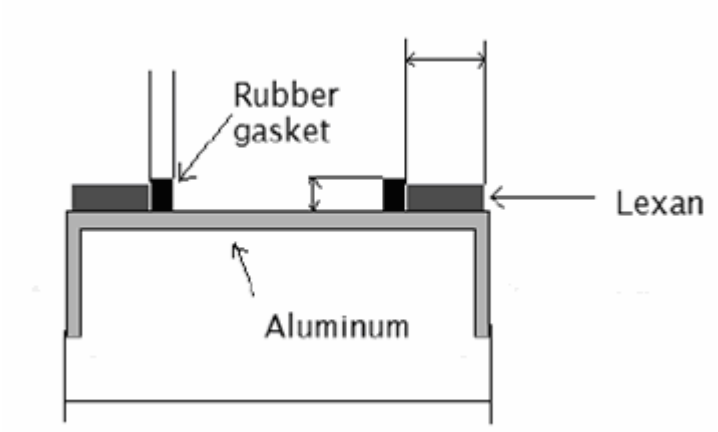

Figure 6-10. The flow channel is formed by placing one coated steel plate and one bare alumina plate against each other spaced by two rubber gaskets.

The power supply which produces the necessary voltage consist of four 220 V transformers in parallel giving approximately 1000 V and 150 VA. A simplified Magtech unit (similar to the

Magtech Controllable Transformer) was used to control the power to the transformers. The Magtech unit was placed outside a Lexan cage in which the separator rig including the CEC were placed to preserve safety regulations (Figure 6-11).

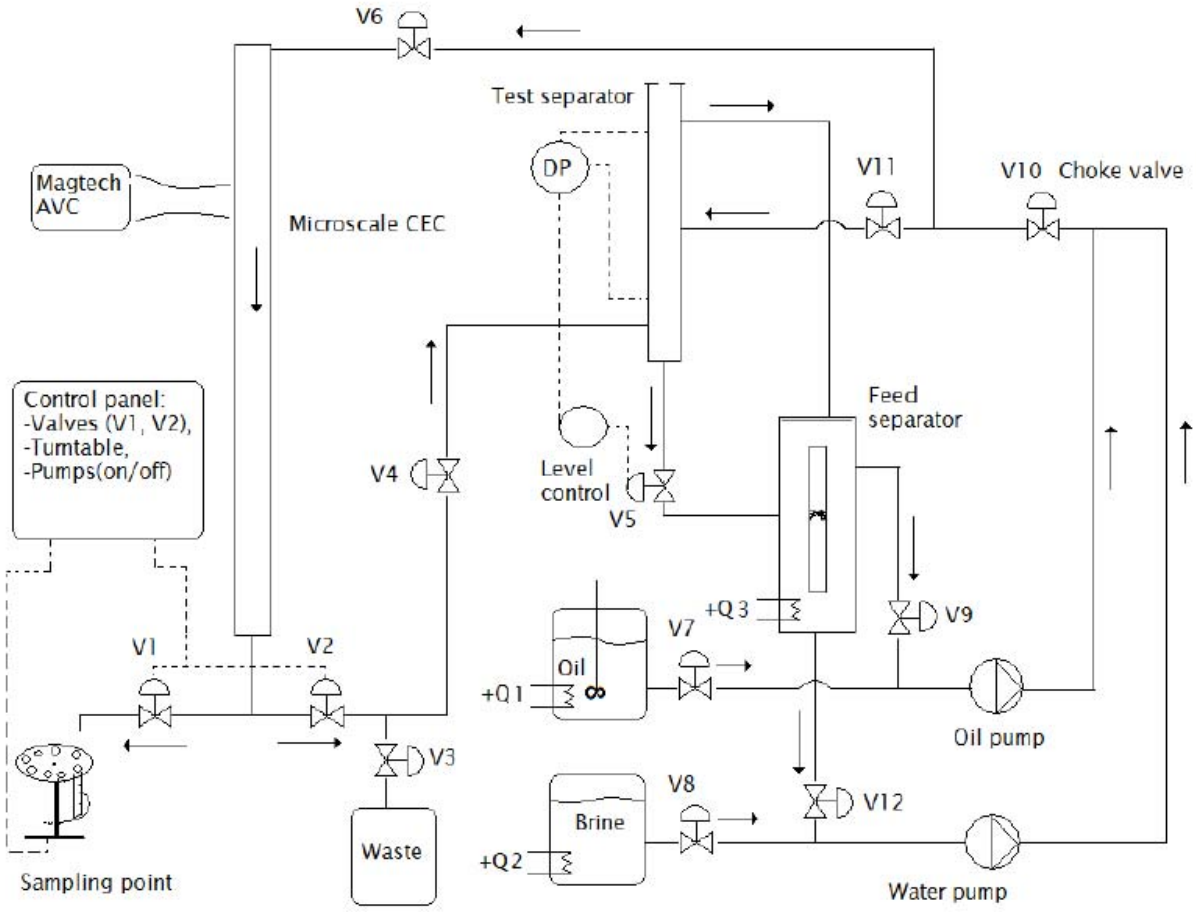

Figure 6-11. The flow scheme indicates the direction of flow for the oil and brine solutions which were pumped separately and mixed in a tee in front of valve 10 (V10). The choke valve produces a pressure drop which results in high shear and dispersion of the oil and brine. V11 was closed in the test so that the flow was directed through V6 to the CEC. The test and feed separators were not used in this study. The sampling point (V1) and waste (V2) valves are indicated. The oil and brine reservoirs were heated to 60 °C.

One crude oil blend was used and two different demulsifiers (A and B) were tested. The crude oil with and without demulsifiers were emulsified with brine at a water cut of approximately 30 vol%. The system with the CEC on and 20 ppm demulsifier B managed to separate most free water, 83% of total water cut (Table 6-14) and was considered the best demulsifier for the crude oil blend if electrostatic coalescence is to be involved. If no electrostatic coalescence is involved the most efficient system was with demulsifier A and CEC off (35% of total water cut). Without demulsifiers, but with the CEC on 46% of total water cut was separated out compared to 0% for no CEC or demulsifier.

Table 6-14. The efficiency of the systems with the CEC turned on and off with the two demulsifiers was measured as the relative amount of water separated with regard to the water cut determined by centrifugation. The water resolved is shown in percent with the standard devation. The system with demulsifier B and the CEC turned on showed to be the most efficient system in terms of amount free water after 10 minutes.

Sample	Crude oil (% water resolved divided by water cut)	Crude oil + 20 ppm demulsifier A (% water resolved divided by water cut)	Crude oil + 20 ppm demulsifier B (% water resolved divided by water cut)
CEC off	0 ± 0.0	35 ± 3.7	0 ± 0.0
CEC on	46 ± 13.1	5 ± 5.3	83 ± 15.7

The pH of the water phases were measured after centrifugation of 5 samples. Results are presented as the mean values with standard deviation (Table 6-15). For the crude oil and the crude oil with demulsifier A, the pH of the water phase decreases from approximately 5.3 to 4.9 for the tests with the CEC off and on respectively. For the system with demulsifier B the pH of the water phase is lower (5.0) when the CEC was not in use, and increased when the CEC had been used (5.5). The reason for the increase in pH for the system with demulsifier B and CEC on may be due to the effect the electric field has on the demulsifier and also by the fact that it was more efficient in separating out the water from the emulsion.

Table 6-15. The pH of the water phases after centrifugation. The systems without demulsifier and with demulsifier A showed a decrease when the CEC was turned on, while the system with demulsifier B had an increase in the pH of the water.

Sample	Crude oil (% water resolved divided by water cut)	Crude oil + 20 ppm demulsifier A (% water resolved divided by water cut)	Crude oil + 20 ppm demulsifier B (% water resolved divided by water cut)
pH of water phase after centrifugation	5.3 ± 0.12	5.4 ±0.07	5.0 ± 0.03
pH of water phase after centrifugation	4.9 ± 0.09	4.9 ± 0.03	5.5 ± 0.04

E-critical measurements were performed as a consistency check for the results obtained with the CEC. Also here the system with demulsifier B had at 30 % water cut much lower

emulsion stability under an electric field than any of the other systems. The E-critical results (Figure 6-12) are, to a certain degree, confirmations of the results obtained with the CEC.

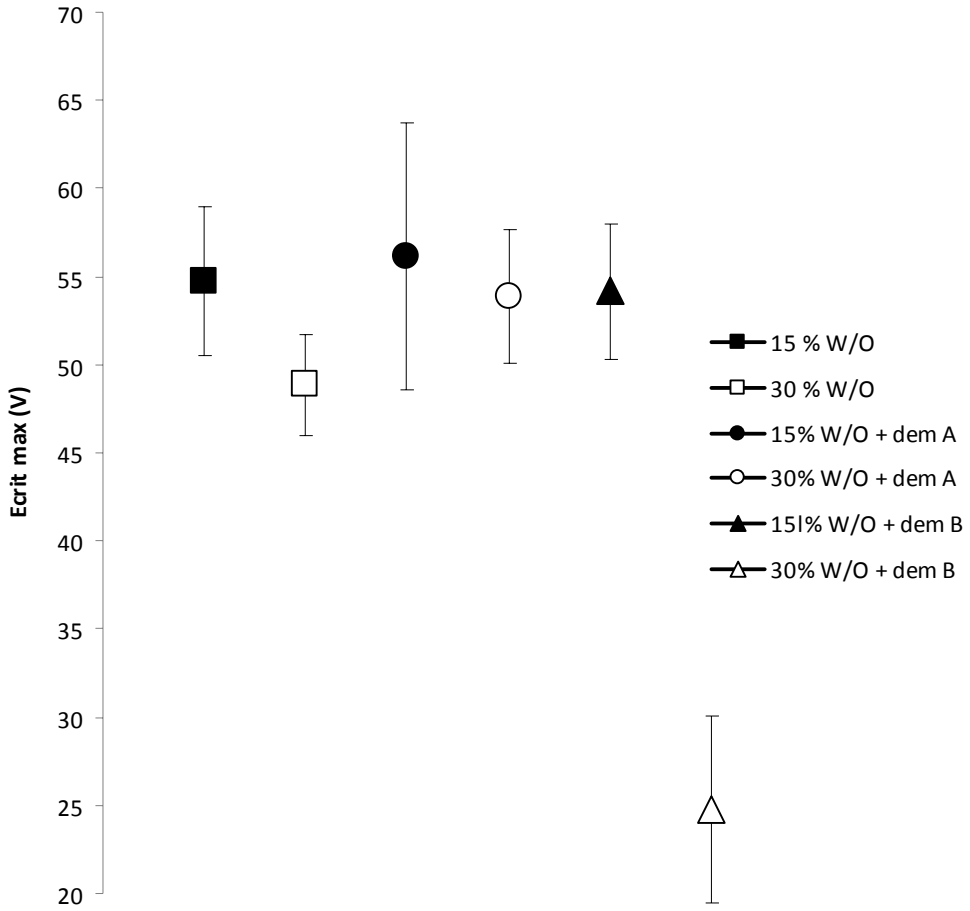

Figure 6-12. As seen the systems containing 30 vol% water cut have a lower E-critical value than the ones with lower (15 vol%) water cut. Furthermore, the system with demulsifier B and 30 % water cut was much more unstable than the other emulsions supporting the results obtained with the CEC.

The equipment made is considered to be of great use for testing crude oils and demulsifiers under various conditions including high electric fields as in the CEC™ technology. It must though be mentioned that the results not necessarily can be used for direct scale up, but that they provide cost efficient methods for testing systems than would not have been feasible on larger equipment.

7 CONCLUDING REMARKS

In this thesis two important, and to a high degree interconnected topics in the crude oil processing chain have been treated. Asphaltenes are a source of concern due to their tendency to precipitate in the well and block pores, or to precipitate in the stream and plug pipes or stabilize emulsions. Crude oil emulsions are multiphase systems consisting of water droplets in oil or oil droplets in water containing solids and gas. Asphaltenes are one of the components which contribute to the stability of crude oil emulsions.

In the first paper it was shown that the Hansen solubility parameters can be correlated to infrared and near infrared spectra. The models made were used to predict values for the solubility parameters of crude oils and SARA fractions (Paper 1). Paper 2 describes a direct precipitation procedure where asphaltenes were precipitated and filtrated off in two steps in order to obtain two solubility fractions. It was shown that the more soluble of the two fractions was more interfacially active and formed smaller aggregates. This work was followed up by characterization of the molecular weights and chemical structures of the two fractions including the whole asphaltenes. Elemental analysis, IR, LDI-MS and NMR techniques indicated that the less soluble fraction consisted of molecules with larger average molecular weight, higher aromaticity and more polar aromatic cores (Paper 3). A new fractionation procedure was further attempted using four steps within the dilution range of 20:1 *n*-pentane-to-crude oil. The results (paper 4) suggested that a middle fraction, namely fraction 2 which consisted of the asphaltenes precipitated at a ratio of 10:1 (and after the 3:1 asphaltenes were removed from the solution), was the most interfacial active.

Paper 5 describes the design of and determination of droplet size distributions and theoretical maximum droplet sizes at various pressure drops for a separation rig built for studies of crude oil emulsions. Later a Compact Electro Coalescer (CEC), which should resemble the commercial CMC™ by Aker Kværner, was built and added to the separation rig in order to have the opportunity to test emulsions under high electric fields (Paper 6). Paper 6 indicated that it is not trivial which demulsifier to use when a high electric field is used in the coalescence process. The most important aspect of the separation rig with the CEC is that it is a cost efficient and relatively fast method of testing crude oils and their behaviour in combination with demulsifiers and high electrical fields.

REFERENCES

1. Speight, J. G., *The chemistry and technology of petroleum*. Marcel Dekker: Boca Raton, Fla., 2007; p 945 s.
2. http://www.spe.org/spe/jsp/basic/0, 1104_1008218_1108884,00.html
3. Witze, A. *Nature* **2007,** 445, (7123), 14-17.
4. Giles, J. *Nature* **2004,** 429, (6993), 694-695.
5. Sachsenhofer, R. F.; Gratzer, R.; Tschelaut, W.; Bechtel, A. *Marine and Petroleum Geology* **2006,** 23, (1), 1-15.
6. Hannisdal, A. Particle-stabilized emulsions and heavy crude oils: characterization, stability mechanisms and interfacial properties. Norwegian University of Science and Technology, Faculty of Natural Sciences and Technology, Department of Chemical Engineering, Trondheim, 2006.
7. http://www.statoil.com/statoilcom/technology/SVG03268.nsf?OpenDatabase&lang=en. **2005**.
8. Nomura, M.; Rahimi, P. M.; Koseoglu, O. R. In *Heavy hydrocarbon resources: characterization, upgrading, and utilization*, Washington, D.C., c2005, American Chemical Society: Washington, D.C., pp X, 240 s.
9. Moulijn, J. A.; Diepen, A. v.; Makkee, M., *Chemical process technology*. Wiley: Chichester, 2001; p XII, 453 s.
10. Sjöblom, J.; Aske, N.; Auflem, I. H.; Brandal, Ø.; Havre, T. E.; Sæther, Ø.; Westvik, A.; Johnsen, E. E.; Kallevik, H. *Advances in Colloid and Interface Science* **2003,** 100-102, 399-473.
11. Ruiz-Morales, Y.; Wu, X.; Mullins, O. C. *Energy & Fuels* **2007,** 21, (2), 944-952.
12. Buckley, J. S.; Wang, J. X. *Journal of Petroleum Science and Engineering* **2002,** 33, (1-3), 195-202.
13. Stasiuk, L. D.; Snowdon, L. R. *Applied Geochemistry* **1997,** 12, (3), 229-&.
14. Hannisdal, A.; Hemmingsen, P. V.; Sjöblom, J. *Ind. Eng. Chem. Res.* **2005,** 44, 1349-1357.
15. Hannisdal, A.; Ese, M. H.; Hemmingsen, P. V.; Sjoblom, J. *Colloids and Surfaces a-Physicochemical and Engineering Aspects* **2006,** 276, (1-3), 45-58.
16. Mullins, O. C.; Y.Sheu, E.; Hammami, A.; Marshall, A. G., *Asphaltenes, Heavy Oils, and Petroleomics*. Springer Science+Business Media, LLC: New York, 2007.
17. Crick, F., *What mad pursuit: a personal view of scientific discovery*. Weidenfeld and Nicolson: Lond., 1989; p 182 s.
18. Speight, J. G., *The Chemistry and Technology of Petroleum*. Marcel Dekker: New York, 1999.
19. Morgan, T. J.; Millan, M.; Behrouzi, M.; Herod, A. A.; Kandiyoti, R. *Energy & Fuels* **2005,** 19, (1), 164-169.
20. Badre, S.; Goncalves, C. C.; Norinaga, K.; Gustavson, G.; Mullins, O. C. *Fuel* **2006,** 85, (1), 1-11.
21. Mullins, O. C. *Fuel* **2007,** 86, (1-2), 309-312.
22. Dickie, J. P.; Yen, T. F. *Analytical Chemistry* **1967,** 39, (14), 1847-&.
23. Strausz, O. P.; Mojelsky, T. W.; Lown, E. M. *Fuel* **1992,** 71, (12), 1355-1363.
24. Moschopedis, S. E.; Fryer, J. F.; Speight, J. G. *Fuel* **1976,** 55, (3), 227-232.
25. Yen, T. F.; Chilingarian, G. V., *Asphaltenes and asphalts*. Elsevier: Amsterdam, 1994; p b.
26. Yen, T. F. *Energy Sources* **1974,** 1, (4), 447-463.

27. Bunger, J. W. In *Chemistry of asphaltenes: based on a symposium sponsored by the Division of Petroleum Chemistry at the 178th Meeting of the American Chemical Society, Washington, D.C., September 10-11, 1979*, Washington, D.C., 1981, Bunger, J. W.; Li, N. C., Eds. American Chemical Society: Washington, D.C., pp VIII, 260 s.
28. Speight, J. G.; Moschopedis, E. *Fuel* **1980,** 59, (6), 440-442.
29. Storm, D. A.; Decanio, S. J.; Detar, M. M.; Nero, V. P. *Fuel* **1990,** 69, (6), 735-738.
30. Groenzin, H.; Mullins, O. C. *Energy & Fuels* **2000,** 14, 677-684.
31. Groenzin, H.; Mullins, O. C. *Energy & Fuels* **2003,** 17, 498-503.
32. Strausz, O. P.; Peng, P.; Murgich, J. *Energy & Fuels* **2002,** 16, (4), 809-822.
33. Ascanius, B. E.; Garcia, D. M.; Andersen, S. I. *Energy & Fuels* **2004,** 18, (6), 1827-1831.
34. Karaca, F.; Islas, C. A.; Millan, M.; Behrouzi, M.; Morgan, T. J.; Herod, A. A.; Kandiyoti, R. *Energy & Fuels* **2004,** 18, (3), 778-788.
35. Acevedo, S.; Gutierrez, L. B.; Negrin, G.; Pereira, J. C.; Mendez, B. *Energy & Fuels* **2005,** 19, (4), 1548-1560.
36. Rakotondradany, F.; Fenniri, H.; Rahimi, P.; Gawrys, K. L.; Kilpatrick, P. K.; Gray, M. R. *Energy & Fuels* **2006,** 20, (6), 2439-2447.
37. Sheremata, J. M.; Gray, M. R.; Dettman, H. D.; McCaffrey, W. C. *Energy & Fuels* **2004,** 18, (5), 1377-1384.
38. Mullins, O. C. *SPE International* **2005,** SPE 95801, 1-10.
39. Yen, T. F.; Erdman, J. G.; Pollack, S. S. *Analytical Chemistry* **1961,** 33, (11), 1587-&.
40. *http://www.statoil.com/statoilcom/technology/svg03268.nsf/Attachments/memoir1flowassurance/$FILE/flow%20assurance.pdf* **2002**.
41. Aske, N.; Kallevik, H.; Johnsen, E. E.; Sjoblom, J. *Energy & Fuels* **2002,** 16, (5), 1287-1295.
42. Pina, A.; Mougin, P.; Behar, E. *Oil & Gas Science and Technology-Revue De L Institut Francais Du Petrole* **2006,** 61, (3), 319-343.
43. Joshi, N. B.; Mullins, O. C.; Jamaluddin, A.; Creek, J.; McFadden, J. *Energy & Fuels* **2001,** 15, (4), 979-986.
44. Buckley, J. S. *Energy & Fuels* **1999,** 13, (2), 328-332.
45. Wang, J. X.; Buckley, J. S. *Energy & Fuels* **2001,** 15, (5), 1004-1012.
46. http://www.cpchem.com/enu/docs_drilling/heavyoils.pdf.
47. Ting, P. D.; Joyce, P. C.; Jog, P. K.; Chapman, W. G.; Thies, M. C. *Fluid Phase Equilibria* **2003,** 209, (2), 309-309.
48. Ting, P. D.; Joyce, P. C.; Jog, P. K.; Chapman, W. G.; Thies, M. C. *Fluid Phase Equilibria* **2003,** 206, (1-2), 267-286.
49. Ting, P. D.; Hirasaki, G. J.; Chapman, W. G. *Petroleum Science and Technology* **2003,** 21, (3-4), 647-661.
50. Evdokimov, I. N.; Eliseev, N. Y.; Akhmetov, B. R. *Fuel* **2006,** 85, (10-11), 1465-1472.
51. Evdokimov, I. N. *Petroleum Science and Technology* **2007,** 25, (1-2), 5-17.
52. Merino-Garcia, D.; Correra, S. *Journal of Dispersion Science and Technology* **2007,** 28, (3), 339-347.
53. Klein, G. C.; Kim, S.; Rodgers, R. P.; Marshall, A. G. *Energy & Fuels* **2006,** 20, (5), 1965-1972.
54. Aquino-Olivos, M. A.; Andersen, S. I.; Lira-Galeana, C. *Petroleum Science and Technology* **2003,** 21, (5-6), 1017-1041.
55. Barton, A. F. M., *Handbook of Solubility Parameters and Other Cohesion Parameters*. 2nd ed. ed.; Boca Raton: Florida, 1991.
56. Synovec, R. E.; Yeung, E. S. *Analytical Chemistry* **1983,** 55, (9), 1599-1603.

57. Israelachvili, J. N., *Intermolecular and surface forces*. Academic Press: London, 1991; p xxi, 450 s.
58. Hildebrand, J. H.; Scott, R. L., *Solubility of Nonelectrolytes*. 3rd ed. ed.; Reinhold: New York, 1950.
59. Hansen, C. M. *J. Paint. Technol.* **1967,** 39, (505), 104-117.
60. Hansen, C. M. *J. Paint. Technol.* **1967,** 39, (511), 505-510.
61. Hansen, C. M. *J. Paint. Technol.* **1967,** 39, (505), 511-514.
62. Hansen, C. M., *Hansen Solubility Parameters: A User`s Handbook*. Boca Raton: Fla., 2000.
63. Mitchell, D. L.; Speight, J. G. *Fuel* **1973,** 52, (2), 149-152.
64. Esbensen, K. H.; Guyot, D.; Westad, F.; Houmøller, L. P., *Multivariate data analysis - in practice: an introduction to multivariate data analysis and experimental design*. Camo: Oslo, 2001; p XX, 598 s.
65. Aske, N.; Kallevik, H.; Sjoblom, J. *Energy & Fuels* **2001,** 15, (5), 1304-1312.
66. Wold, S.; Esbensen, K.; Geladi, P. *Chemometrics and Intelligent Laboratory Systems* **1987,** 2, (1-3), 37-52.
67. Fossen, M.; Hemmingsen, P. V.; Hannisdal, A.; Sjoblom, J. *Journal of Dispersion Science and Technology* **2005,** 26, (2), 227-241.
68. Sjöblom, J., *Emulsions and emulsion stability*. Taylor & Francis: Boca Raton, Fla., 2006; p 668 s.
69. Acevedo, S.; Borges, B.; Quintero, F.; Piscitelly, V.; Gutierrez, L. B. *Energy & Fuels* **2005,** 19, 1948-1953.
70. Auflem, I. H. Influence of asphaltene aggregation and pressure on crudeoil emulsion stability. Department of Chemical Engineering, Norwegian University of Science and Technology, Trondheim, 2002.
71. Sjöblom, J., *Encyclopedic handbook of emulsion technology*. Marcel Dekker: New York, 2001; p XIV, 736 s.
72. Buckley, J. S. *Current Opinion in Colloid & Interface Science* **2001,** 6, (3), 191-196.
73. Buckley, J. S.; Liu, Y. *Journal of Petroleum Science and Engineering* **1998,** 20, (3-4), 155-160.
74. McLean, J. D.; Kilpatrick, P. K. *J. Colloid Interface. Sci.* **1997,** 189, 252-253.
75. McLean, J. D.; Kilpatrick, P. K. *J. Colloid Interf. Sci.* **1997,** 196, 23-34.
76. Arntzen, R. Gravity separator revamping. Department of Chemical Engineering, Norwegian University of Science and Technology, Trondheim, 2001.
77. Urdahl, O.; Nordstad, K.; Berry, P.; Wayth, N.; Williams, T.; Bailey, A.; Thew, M. *Spe Production & Facilities* **2001,** 16, (1), 4-8.
78. Atten, P. *Journal of Electrostatics* **1993,** 30, 259-269.
79. Atten, P.; Lundgaard, L.; Berg, G. *Journal of Electrostatics* **2006,** 64, (7-9), 550-554.
80. Berg, G.; Lundgaard, L. E.; Becidan, M.; Sigmond, R. S. *Proceedings of 14th international conference on dielectric liquids* **2002**, 220–224.
81. http://www.aibel.com/. *Press Release* **2007**.
82. Piasecki, W.; Florkowski, M.; Fulczyk, M.; Sipowicz, J.; Sundt, H. K. *http://www02.abb.com/global/gad/gad02077.nsf/lupLongContent/14551B90633A3AF6C1256F51002CEA8F*.
83. http://www.aibel.com/global/seitp/seitp161.nsf/0/ea03515fda8ed69fc125723e0038fe9a/$file/Newsinbrief_Dec06_screen.pdf. *A global newsletter from Vetco Aibel* **2006**.
84. http://www.vetcoaibel.com/global/noofs/NOOFS187.NSF/99ad595c32e0c2d9c12566e

1000a4540/138dac51a7ed02c3c1256ee400364cd6/$FILE/LOWACC%20-%20Low%20Water%20Content%20Coalescer.DOC.
85. http://www.statoil.com/statoilcom/technology/SVG03268.nsf?OpenDatabase&lang=en
86. http://www.akerkvaerner.com/Internet/MediaCentre/Featurestories/OilandGas/Makingeverydropcount.htm.
87. Skoog, D. A.; Nieman, T. A.; Holler, F. J., *Principles of instrumental analysis*. Saunders College Publ.: Philadelphia, 1998; p XV, 849, [93] s.
88. Aske, N. Characterisation of crude oil components, asphaltene aggregation and emulsion stability by means of near infrared spectroscopy and multivariate analysis. Department of Chemical Engineering, Norwegian University of Science and Technology, Trondheim, 2002.
89. Silverstein, R. M.; Webster, F. X.; Kiemle, D. J., *Spectrometric identification of organic compounds*. Wiley: Hoboken, N.J., 2005; p X, 502 s.
90. Barrow, G. M., *Physical chemistry*. McGraw-Hill: New York, 1996; p XVII, 910 s.
91. Hiemenz, P. C.; Rajagopalan, R., *Principles of colloid and surface chemistry*. Marcel Dekker: New York, 1997; p XIX, 650 s.
92. Sheu, E. Y. *Journal of Physics-Condensed Matter* **2006,** 18, (36), S2485-S2498.
93. Gawrys, K. L.; Kilpatrick, P. K. *Journal of Colloid and Interface Science* **2005,** 288, (2), 325-334.
94. Breitmaier, E.; Voelter, W., *Carbon-13 NMR Spectroscopy, High-Resolution Methods and Application in Organic Chemistry and Biochemistry*. Third ed.; VCH: New York, 1987.
95. Keeler, J., *Understanding NMR spectroscopy*. Wiley: Chichester, 2005; p XV, 459 s.
96. Petrakis, L.; Allen, D., *NMR for liquid fossil fuels*. Elsevier Science Publishers B.V.: Amsterdam, 1987.
97. Michael, G.; Al-Siri, M.; Khan, Z. H.; Ali, F. A. *Energy & Fuels* **2005,** 19, (4), 1598-1605.
98. Wangen, E. S. Characterisation and pyrolysis of heavy oils. Norwegian University of Science and Technology, Trondheim, 2007.
99. Christopher, J.; Sarpal, A. S.; Kapur, G. S.; Krishna, A.; Tyagi, B. R.; Jain, M. C.; Jain, S. K.; Bhatnagar, A. K. *Fuel* **1996,** 75, (8), 999-1008.
100. Berger, S.; Braun, S.; Kalinowski, H.-O., *200 and more NMR experiments: a practical course*. Wiley-VCH: Weinheim, 2004; p XV, 838 s.
101. Doddrell, D. M.; Pegg, D. T.; Bendall, M. R. *Journal of Magnetic Resonance* **1982,** 48, (2), 323-327.
102. Barron, P. F.; Bendall, M. R.; Armstrong, L. G.; Atkins, A. R. *Fuel* **1984,** 63, (9), 1276-1280.
103. Nishizawa, T.; Sakata, M. *Fuel* **1991,** 70, (1), 124-128.
104. Masuda, K.; Okuma, O.; Nishizawa, T.; Kanaji, M.; Matsumura, T. *Fuel* **1996,** 75, (3), 295-299.
105. Kotlyar, L. S.; Morat, C.; Ripmeester, J. A. *Fuel* **1991,** 70, (1), 90-94.
106. Hortal, A. R.; Martinez-Haya, B.; Lobato, M. D.; Pedrosa, J. M.; Lago, S. *Journal of Mass Spectrometry* **2006,** 41, (7), 960-968.

Paper I, II, III, IV and V are not included due to copyright.

Electrostatic Coalescence Under Flowing Conditions: A Study of the Effect of a High Electric AC Field on the Efficiency of Two Demulsifiers

Martin Fossen[1,a], Christian Bjørn Melbye[2], Morten Hana[2] and Johan Sjöblom[1]

[1]Ugelstad Laboratory, Department of Chemical Engineering, Norwegian University of Science and Technology, Trondheim, Norway

[2]Aker Kværner Process Systems, Lysaker, Norway

ABSTRACT

A lab scale compact electro coalescer was designed for the study of crude oil emulsions under a high alternating current voltage field. The main intention of this study was to design the equipment and test the effect two different demulsifiers had on the separation efficiency of the w/o emulsion. Results indicated a dependence between demulsifier and the high electric field present in the separator. The crude oil was mixed with a brine solution and emulsified over a choke valve with a pressure drop of 2 bar. Without demulsifier and the electric field off, no water was separated. With the electric field on 46% of the water phase separated. Of the systems tested, demulsifier B with the electric field on was the most efficient with 83% of the water separated from the emulsion. Demulsifier A did probably loose its function under the electric field since 0% water was separated out compared with 35% water when no electric field was present.

Key words:
CEC, electro coalescence, crude oil, demulsifiers.

SHORT TITLE

Electrostatic coalescence and demulsifiers

INTRODUCTION

Water-in-oil w/o emulsions are well known phenomena and of continuous concern for the processing of crude oils.[1-4] Water, and salts in the water phase, may lead to pipeline corrosion and additional cost of transportation and separation.[5] Co-produced water is

[a] Correspondence: Martin Fossen, Ugelstad Laboratory, Department of Chemical Engineering, Norwegian University of Science and Technology, N-7491 Trondheim, Norway, E-mail: martin.fossen@nt.ntnu.no

dispersed as small droplets in the crude oil when the fluids flow through pipes, chokes and valves. This dispersion is again stabilized by indigenous species in the crude oil like asphaltenes, resins, waxes and acids. Water-in-oil emulsions are also formed in the process of desalination where the removal of catalyst poisons such as sodium, iron and arsenic is achieved by dispersion of freshwater in the oil.[6]

The water present in the oil has to be removed by destabilization of the emulsion before further processing and refining. Traditionally, the primary method to separate oil from water in offshore installations both on platforms and in sub-sea projects is by the application of gravity separators in several stages.[7] Long residence time to achieve separation is the reason for why the gravity separator vessels can become very large.[8] It is of interest to increase the droplet size to improve the settling and coalescence rates both in front of, and within the gravity separators. To obtain a faster coalescence rate and more efficient separation several approaches, including electrical induced coalescence techniques, are used. Electrical coalescence is considered the most energy efficient method for braking of w/o emulsions compared to pH adjustments, gravity or centrifugal settling, filtration, heat treatment and chemical demulsifiers.[6, 9] In 1911 the first patent on electro coalescence was filed from the observation of a high potential which was applied to a pair of wire electrodes in an water-in-oil emulsion.[9] Although the mechanisms for this phenomenon is not yet clearly understood some generalizations are present. One is that in an electric field, the induced electrostatic force between two conducting drops is inversely proportional to approximately the fourth power of the separation distance between the drops. Furthermore, the electric-induced force also increases with the square of the drop size, dominating the van der Waals force in the coalescence of large drops.[9, 10] The application of an electrical field can (and usually will) therefore increase the speed of the droplet growth and the overall efficiency of gravity separators.

Conventional electro coalescers are large vessels containing electrodes, between which a “treating space” exists where dispersed water droplets grow mainly by electro coalescence and a “settling zone” where gravitational phase separation takes place under low velocity flow condition. The residence time in such vessels is typically 10-30 minutes.[11] Urdahl et.al. suggested that the electro coalescence step and phase separation process could be decoupled in order to obtain electric field induced droplet growth in turbulent flow and to perform the phase separation in a conventional separator.[11] Later Urdahl et. al. presented the basic ideas behind the compact electro coalescer (CEC).[12]

In this work a lab scale CEC has been developed for utilization in basic research on crude oil emulsions and for practical testing of specific crude oils and demulsifiers. The AC field and frequency is controlled by a device from Magtech and the strength of the field is controlled by the operator and can be varied from 0-1000 V. The CEC was designed to resemble a vertical part of the commercial CEC™ and the height and distance between the electrodes were approximately one third of the CEC™. One crude oil which formed very stable emulsions was tested at 30 vol% water cut (WC) alone and in combination with two different demulsifiers. It is shown that it is not trivial what type of demulsifier that should be used when a high electric field is used in the coalescence process.

THEORY

Sedimentation of water droplets

Gravity will act on water drops with the force being a function of the volume (V) of the drop and the difference in density ($\Delta\rho$) between the water drop and the oil phase and the gravitational constant (g) (Equation 1).

$$F = V\Delta\rho g \qquad 1$$

For a water droplet of diameter (d), the speed of sedimentation is controlled by the terminal velocity (v_{st}) which in the Stokes regime is described as (Equation 2):

$$v_{st} = \frac{d^2\Delta\rho g}{18\mu_c} \qquad 2$$

An increase in the difference in the density between the water and oil and a lower viscosity (μ_c) of the continuous oil phase will increase the v_{st}. To speed up the sedimentation process in the gravity separators the droplet size must be increased and eventually the viscosity of the oil phase must be reduced and the droplet-droplet collision frequency increased.[7, 8] The squared dependence of droplet diameter in stokes law (Equation 2) clearly show that the settling speed will increase with increasing droplet size.[1, 9] diluents and temperature can be used to increase $\Delta\rho$, decrease the viscosity and increase the dispersion rate of demulsifying chemicals.[6, 9]

The hydrostatic pressure within the droplets is determined by the interfacial tension, γ, between the oil and water and the radius of the drop (Equation 3). This hydrostatic pressure affects the critical field strength described below.

$$\Delta P = \frac{2\gamma_o}{r} \qquad 3$$

Charging of water droplets and possible mechanisms for electrocoalescence

When a water drop hits a metallic plate with an electric field the particle will receive a net charge Q (Equation 4). Due to interfacial tension the water drop is spherical with radius r unless electrical of mechanical forces change the shape of the drop. The permittivity (ε) of the oil phase and the electric field (E_0) applied determines the net charge. The more elongated the particle is in the direction of the field, the higher the charge. Other processes that lead to charging of water drops are charge transfer from other bodies, streaming electrification, adsorption of polar ions on the drop surface, and by drop break up.[2]

$$Q = \frac{2}{3}\pi\varepsilon r^2 E_0 \qquad 4$$

This charge will force the drop to align both to the electric field and to other charged particles and droplets in close distance to the droplet.

Decreasing the closest distance between two droplet surfaces (D) will increase the forces, F (N), induced by the electric field by approximately the fourth power of the distance reduced as shown by, (Equation 5)

$$F = \frac{24\pi\varepsilon_0\varepsilon_1 r^6 E^2}{(D+2r)^4} \qquad 5$$

where ε_0 is the permittivity of vacuum and ε_1 is the permittivity of the continuous phase (i.e the oil), E is the electric field strength (V/m). Furthermore the electrostatic force will increase by the sixth power of the radius of the droplets.[9] The increase in the force between charged droplets may increase the contact time during impact. If probability of a collapse of the film between drops increases with time this may be a main reason for the observed higher coalescence rate. Furthermore, the forces between the drops will help draining away the oil

film between the drops so that the surfaces collide.[8] As most of the charge will be located at the point closest to the neighbour drop, the forces will be concentrated in that point resulting in the surface being pulled towards the other drops. The radius of curvature will be smaller, which again enhances the field resulting in an increase in the surface charge increasing the forces and so on.[8] Another proposed mechanism for electro coalescence is called eletctrostriction and is a result of thinning of the interfacial memebrane. Surface layer like Helmholtz and Stern layers will consist of hydrophilic compounds, ionic and dipolar, where the local electric fields may become high. An external applied field may change the thickness of such layers thereby increasing the chance of breaking it and getting the drops to coalesce.[8] Yet another mechanism is the effect of shock waves from electric breakdown between water drops. As the drops approach, the electric field between them increases and a breakdown of the oil film eventually will occur. The potential electrostatic energy is released into a small explosive event and pressure waves that may tear up the interfacial film can occur.[8]

Critical field strength for droplet disintegration

Electrically stressed water droplets in oil enhance the coalescence rate of w/o emulsions, probably due to a combination of dipole interaction between the water droplets and breaking of the surface layers at droplet contact. [13] However, water droplets will respond to electric stress on its surface by elongation. If the field strength becomes too high, the water droplet will deform into a thin thread and burst into smaller drops.[9, 13] The reason for this is that when the field is too high (determined by r and γ_o) the electric stress overwhelms the recovery force due to interfacial tension (Equation 4).[9]

$$E_c = 0.648\sqrt{\frac{\gamma_o}{2\varepsilon r_0}} \qquad 6$$

The E_c is dependent on the radius of the droplets, where smaller droplets result in a higher critical electric field due to a larger hydrostatic pressure (Equation 3).[8, 9]

Effects of applied electric field and electrode design

Considerations of electrode design and insulation type have been subject for several investigations.[9] Whether insulation should be used at all is dependent on the electric field used. Types of electrical fields that have been considered for the electrical coalescence of water

droplets include alternating current (AC) with insulated electrodes, direct current (DC), AC/DC which combines the high water cut tolerance of the AC and the efficiency of the DC, and pulsed DC which tolerated high WC due to insulated electrodes.[1, 2, 6, 9, 14] Insulation is used mainly to prevent short circuiting due to droplet bridging[12] or water slugs in the coalescer. Without insulation, current limiting instrumentation is required to prevent the effective electrostatic field across the emulsion to break down during the short circuiting period.[12] Additionally, insulation reduce the current drain on the system, allowing the use of lower-rated transformers. Nevertheless, insulation of the electrode limits the type of electrostatic excitation which may be used. If a DC field is applied to an insulated system, interfacial polarization occurs where the insulation is charged to the opposite polarity of the adjacent electrode and greatly reduces the electric field across the actual emulsion. This limits the electrostatically enhanced coalescence process. The solution is to apply a time-varying electric field which prevents charge build up on the insulating layer.[12] For an AC field the frequency must be optimized with regard to the thickness and material of the coating to obtain maximum charge density.[9] Furthermore the behaviour of emulsions in AC fields may depend on the type of crude oil and chemical additives such as demulsifiers.

Laminar and turbulent flow regimes

In the gravity separators the flow regime is laminar so that water droplets are allowed to settle towards the dense layer where the coalescence occurs. When designing the separation vessels one must allow for the droplets to settle and coalesce during the residence time. Since both the settling and coalescence steps may be slow processes, the gravity separators tend to be very large and most often several separators in series are needed. However, during the last decades shear movement in the emulsion is applied as a method to create more frequent drop collisions.[1, 2, 11, 14] Increasing the Reynolds number in order to enter the turbulent flow regime does not automatically lead to re-dispersion of water droplets. Turbulent shear is an efficient mechanism for bringing small droplets into contact with one another which may lead to their coalescence. Although the droplets are brought together, the contact time may not be long enough for coalescence to occur under turbulent flow conditions. By coupling the turbulent flow with an applied electric field, the mutually attractive electrostatic force, arising from polarization, increases without limit as the distance between the droplets reduces and thus the droplets may be in contact long enough for coalescence to occur.[11]

Demulsifiers and their behaviour under high electric fields

Commercially available demulsifiers are chemical cocktails where one expects to find synergistic effects of one or more active components that are dissolved in a oil phase. Demuslifiers are often classified as low molecular weigh (LMW) or high molecular weigh (HMW) and pure solvents. HMW molecules include polymers and macro molecules (block copolymers) including polyelectrolytes with MW usually > 5000 g/mol. LMW are usually oil soluble surfactants that are interfacially active by replacing stabilizing compounds at the water/oil interface or they may change the wettability of stabilizing compounds.[1] The HMW chemicals are often efficient film modifiers reducing the rheology of the interfacial film surrounding the water drop. Furthermore the HMWs may also be flocculants collecting drops and thus increase the contact time between water drops. It is belived that some of the chemicals displace the asphaltic material from the interface followed by the formation of demulsifier micelles which solubilize and/or stabilize the asphaltene compounds in the oil.[1]

The effect of a high electric field on demulsifiers used in the breaking of emulsions and dewatering and desalting is of great interest although little is published on this subject. Kim et. al. showed that for a selected demulsifier the application of a AC field on a emulsion increased the separation efficiency.[15] Yunusov et. al. suggested that the mechanical strength of the surface layer of the water drops was decreased so that the elongation of the droplets was increased at increasing demulsifier concentration.[16] Desalting of crude oils in combination with electric fields has also been studied by others.[17, 18]

Partly due to the operational and economic aspects of the oil industry and the fact that most demulsifiers tested are commercial products, little work has been done on systematic testing of demulsifiers with known structures under an electric field. Often, simple bottle tests are used where the demulsifiers are considered based on the relative amount of water separated from the emulsions at specific water cuts. Moreover final chemical selection and evaluations based on widely accepted bottle test methods may fail to select the proper chemical demulsifier for electrostatic coalescence and separation.[6] Additional tests must be performed if the detailed knowledge about the emulsions and the effect the demulsifiers have on the system is to be understood. Rheological behaviour of the emulsion is of interest, as well as the interfacial properties of the emulsion stabilizing indigenous compounds of the crude oils like asphaltenes, resins, waxes and carboxylic acids, and solid particles that are oil wetted.[5, 6, 19-22] Also the concentration at which the demulsifiers are most efficient must be checked[23, 24] and all this should be done under the most realistic conditions possible, that is under an electric field of the type used in the process equipment present or planned in the production.

Critical electric field (E-critical) measurements

E-critical measurements were used to determine the relative stability of the emulsions in an electric field. When water droplets stabilized by rigid interfacial films in a stationary emulsion are exposed to an electric field they form chains, bridging the electrodes. The critical electric field is often used as a measure of the emulsion stability and the critical value is the voltage needed to create a current across the electrodes.[25]

MATERIALS AND METHODS

Equipment

The intention of this work was to build the CEC and test it with regard to separation efficiency. The additional equipment used is described in a previous publication.[26] The CEC was custom made and consist of two flat plates, one steel plate with coating and one bare alumina plate.

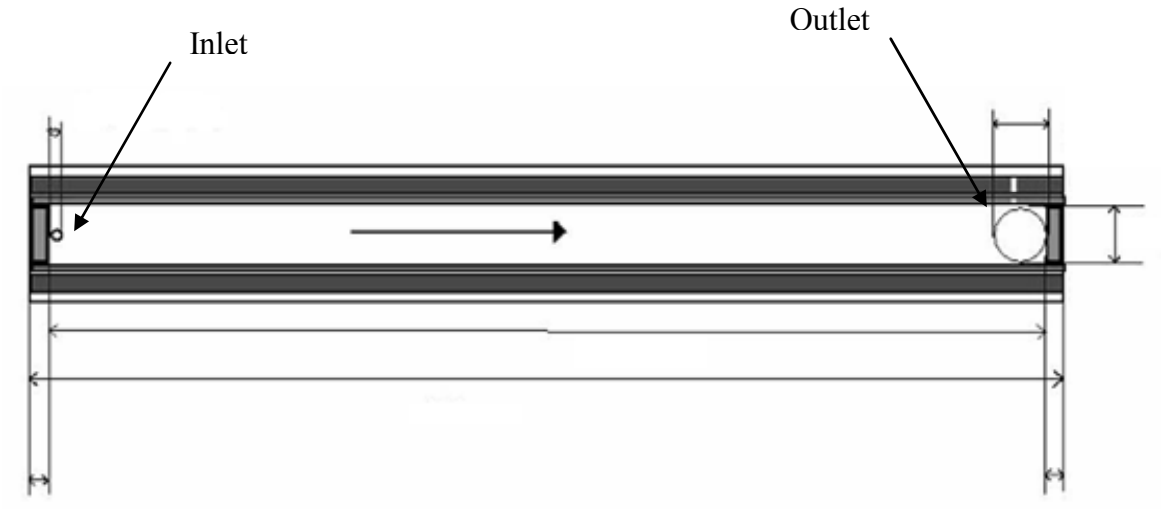

Figure 1. Sketch of the lab scale CEC. The CEC is in a vertical position when in use and the indicated flow direction (arrow) is downwards. The inlet and outlet are indicated and they were connected to the flow loop with flexible tubing.

The plates were spaced with a Lexan spacer and a gasket was glued along each side. The plates were clamped together so that a flow channel was formed between the plates.

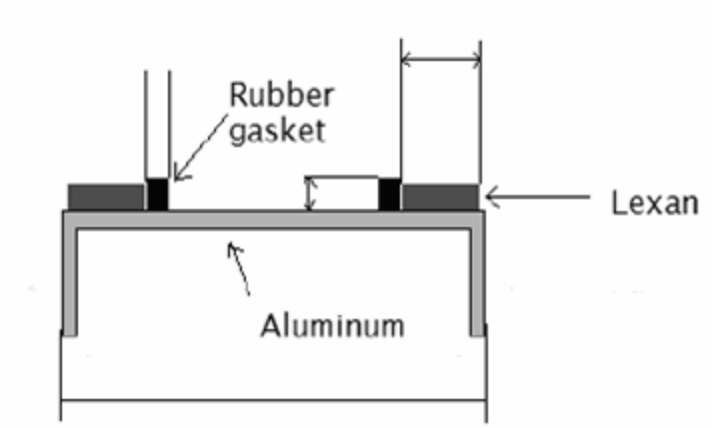

Figure 2. The flow channel when looked at in the flow direction. The coated steel plate was clamped together with the alumina plate, separated by the gaskets forming the flow channel

The plates were connected to an electric field which also was scaled down in order to mimic the electric field in the real CEC™. The CEC is constructed as a vertical slice of the full size CEC™, but with the flow rate of 24 - 60 l/h used in the experiments the flow in the lab scale CEC was calculated to be laminar instead of turbulent. The setup of the equipment was modified for the experiments but is based on the vertical gravity separator used in previous studies (Figure 3).[26]

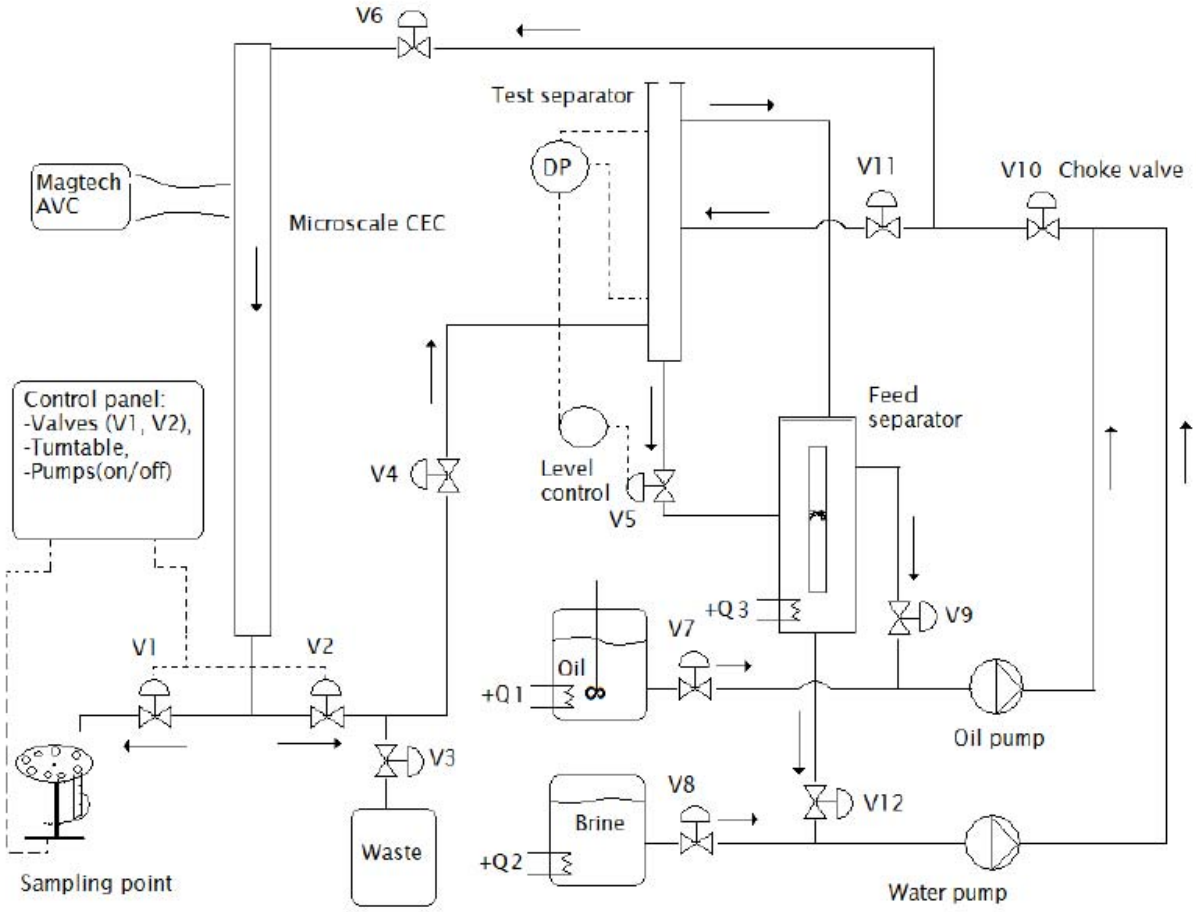

Figure 3. The flow scheme indicates the direction of flow for the oil and brine solutions which were pumped separately and mixed in a tee in front of valve 10 (V10). The choke valve produces a pressure drop which results in high shear and dispersion of the oil and brine. Valve V11 was closed in the test so that the flow was directed through V6 to the CEC. The test and feed separators were not used in this study. The sampling point (V1 open) and waste (V2 open) valves are indicated. The oil and brine reservoirs were heated to 60 °C.

Power supply

The lab scale CEC is controlled by a power supply consisting of four 220 V transformes and a Magtech Controllable Transformer (MCT)[b] with a variable output voltage of 0-1kV with a 50hz sinusoidal AC.[27]

Critical electric field (E-critical) and pH measurements

[b] http://www.magtech.no/

E-critical cell:

In the experiments, a E-critical cell developed by Aske[25] was used to determine the emulsion stability. The E-critical method was used to obtain a measurement of the relative stability of the emulsions with and without demulsifiers, at 15% and 30% water cut. The cell consisted of a teflon plate with a 10 mm diameter hole in the centre, with a brass plate on each side. A small drop of the emulsion was placed in the hole and the plates were carefully pressed together. The thickness of the teflon plate was 0.10 mm. and glued to the lower brass plate. The system was held together with isolating teflon plates. The power was supplied by a Agilent 6634B system-DC that can increase the applied voltage in user defined steps from 0-100V. The E-critical value was identified by a sudden increase in conductivity.[25]

pH measurements

The pH of the separated water phases after centrifugation were measured on a Thermo Orion 420A pH meter. The electrode used in the experiment was a combined electrode. Thermo Orion triode™ pH electrode with a Ag/AgCl internal reference system and a temperature probe. The pH meter was calibrated before the measurements.

Materials

The crude oil mixture and demulsifiers were supplied by the oil company. A blend consisting of four crude oils was tested with regard to emulsion stability after mixing with a brine solution. In addition two different demulsifiers, A and B, were tested both with and without the electric field on. A blend of crude oil was used which had an API gravity of 26.7 and a specific gravity of 0.89 kg/dm^3 at 60° F. The crude oil was by the oil company seen as a potential problem oil with regard to emulsion stability and the intention was to try to test it under an electric field using the lab scale CEC. The crude oil was tested initially with regard to emulsion stability and it showed to be very stable with little tendency to destabilize, even after several days at room temperature. Of the two demulsifiers, B was labelled as the most environmentally friendly.

Mixtures of crude oil and 20 ppm demulsifier A and B were made by adding 1000 µl 10vol% demulsifier in toluen to 5.0 litres of the crude oil mixture. The 5L container was then shaken for at least 1 hour at 200 round per minute (rpm) at room temperature using an agitator table. Distilled water was used for preparing all aqueous samples. The synthetic brine was made in order to have a water phase that resembled the produced water of this specific well. The pH of the brine was measured to be 6.8.

Procedure and test conditions

The experiments were performed by running the oil once through the system in order to have "fresh" oil for each test. The temperature of the brine and oil in the reservoir was 60°C. The temperature dropped somewhat on the way from the reservoir to the sampling point due to heat lost to pipes and equipment. There was no circulation of the hot fluid to keep the system warm, but in each test the system was run for approximately one and a half minute in order to obtain steady state at the sampling point downstream the CEC. Tests indicated that the temperature of the fluid at the sampling point had dropped to about 40°C. Differential pressure over the choke valve was 2 bar and the liquid flow rate was 1 l/min. The water cut used was approximately 30 vol% (Determined by centrifugation). It must be mentioned that there were challenges with keeping the pressure drop constant due to sudden increases in the pressure drop over the choke valve. This pressure was assumed to rise due to the formation of an emulsion with a high viscosity downstream the choke valve.

The sampling was performed by filling five 100 ml graded cylinders and five 50 ml centrifugation tubes. The graded cylinders were transferred to an incubator holding 60°C and were left there for 10 minutes after which the height of the free water phase was measured. The 50 ml containers were centrifuged for 30 minutes at 4000 rpm at room temperature. There could be a time delay of 30 minutes before the samples were centrifuged. The amount water separated by centrifugation was assumed to be approximately the same as the water cut delivered by the pumps.

The emulsions used in the E-critical studies were made using the Ultraturax hand blender on preheated to 60°C brine and oil at 24,000 rpm for 2 minutes.

RESULTS AND DISCUSSION

Water resolved

The amount water resolved after 10 minutes in the incubator is shown as percent of the water cut determined after centrifugation (Table 1). The results are based on 5 samples from each run.

Table 1. The efficiency of the systems with the CEC turned on and off with the two demulsifiers was measured as the relative amount of water separated with regard to the water cut determined by centrifugation. The water resolved is shown in percent with the standard

devation. The system with demulsifier B and the CEC turned on showed to be the most efficient system in terms of amount free water after 10 minutes.

Sample	Crude oil (% water resolved divided by water cut)	Crude oil + 20 ppm demulsifier A (% water resolved divided by water cut)	Crude oil + 20 ppm demulsifier B (% water resolved divided by water cut)
CEC off	0 ± 0.0	35 ± 3.7	0 ± 0.0
CEC on	46 ± 13.1	5 ± 5.3	83 ± 15.7

For the crude oil without demulsifier added the CEC improves the separation efficiency from 0 % to 46 % water resolved. When demulsifier A is added 35 % water was resolved with the CEC off. With demulsifier A, and the CEC on only 5 % of the water was resolved which indicates that the demulsifier A is incompatible with a high electric field. For demulsifier B no water was resolved when the CEC was off. The efficiency of demulsifier B increased dramatically when the CEC was on and 83 % of the water was resolved. This indicates that the system with demulsifier B and the CEC on was the most efficient system at 30 % water cut and the current conditions.

The experiments were performed on the separation rig described previously.[26] What is different is that in this work a real crude oil was used instead of Exxsol D60. This made the flow meters unreliable for the oil phase since they were not calibrated for the density or viscosity of the crude oil. The water cut, therefore had to be determined manually through centrifugation. In addition, the water pump broke down after the first tests with the pure crude oil system due to dry running. Therefore another water pump had to be used which resulted in a different flow rate in the experiments with the demulsifiers. The flow rate with the pure crude oil was 24 l/h and for the crude oil with demulsifiers it had to be 60 l/h to obtain 30 vol% water cut. The retention time in the CEC was twice as long for the first tests compared to the tests with the two demulsifiers A and B. This has of course a large impact on the droplet growth and time for coalescence in the CEC, but since the systems with the two demulsifiers were run under the same conditions the main interest of the experiment was preserved.

Since no information is available on the chemistry of the demulsifiers, except an explanation of how two different types of demulsifiers may work, the discussion is based on

assumptions and can not give detailed explanation on why the demulsifiers work or not. It may look strange that for demulsifier A the amount resolved water is higher with the CEC off than when it was on. A possible explanation for this is that demulsifier A is affected by the electric field and loses its function.[6] One can imagine that the demulsifier and the electric field are working against each other. In simple terms one can think of Type A demulsifiers which work as flocculants for water droplets and Type B demulsifiers which work to coalesce water droplets i.e. act at the droplet-droplet interface to form bigger droplets. Taking Type A (flocculant) the chemical works as a chain which grabs the small water droplets and collects them together. When the 'floc' is big enough it settles out under gravity (this is not unlike the way polyelectrolytes work in water clarification to remove suspended fines). Unfortunately the very nature of the way this type of chemical works is at odds with operating well in an electric field, and hence is not optimal for electrocoalescence. Indeed something like the CEC may destroy its effectiveness altogether - the electric field and chemical work against one another. For the Type B, the electric field brings the droplets together and if the chemical present is active at the droplet-droplet contact then it will promote coalescence and droplet growth i.e. the chemical and coalescer work synergistically.[c] In order to test this hypothesis, one should do experiments with the two proposed types of demulsifiers, that is a polymer flocculent (Type A) and a compound which works more at the droplet interface (Type B).

The system with the CEC on and 20 ppm demulsifier B managed to separate the largest amount of free water and is thus considered the best demulsifier for the crude oil blend if electrostatic coalescence is to be involved. If no electrostatic coalescence is involved the most efficient system was with demulsifier A. The system without demulsifier but with the CEC on separated more water than the system with demulsifier A and the CEC on, which indicates that if the choice is between these two systems no demulsifiers should be used. It must be mentioned that it is dangerous to draw finite conclusions on the behaviour of the systems under process conditions based on the experiments performed on this kind of equipment. Nevertheless it is of great importance when several systems are to be tested against each other before scaled up experiments are to be performed. Furthermore, such tests give the opportunity to test more chemicals and crude oils at several water cuts for a fraction of the costs an up-scaled test would require.

pH of the water phases

[c] Possible explanation after discussion with the oil company and chemical vendor.

The pH of the water phases were measured after centrifugation of 5 samples. The results are presented as the mean values with standard deviation (Table 2).

Table 2. The pH of the water phases after centrifugation. The systems without demulsifier and with demulsifier A showed a decrease when the CEC was turned on, while the system with demulsifier B had an increase in the pH of the water.

Sample	Crude oil (% water resolved divided by water cut)	Crude oil + 20 ppm demulsifier A (% water resolved divided by water cut)	Crude oil + 20 ppm demulsifier B (% water resolved divided by water cut)
pH of water phase after centrifugation	5.3 ± 0.12	5.4 ±0.07	5.0 ± 0.03
pH of water phase after centrifugation	4.9 ± 0.09	4.9 ± 0.03	5.5 ± 0.04

For the crude oil and the crude oil with demulsifier A the pH of the water phase decreases from approximately 5.3 to 4.9 for the tests with the CEC off and on respectively. The system with demulsifier B shows the opposite trend. Here the pH of the water phase is lower (5.0) when the CEC was not in use, and increased when the CEC had been used (5.5). The reason for the increase in pH for the system with demulsifier B and CEC on may be due to the effect the electric field has on the demulsifier and also by the fact that it was more efficient in separating out the water from the emulsion.

E-critical measurements

The E-critical measurements were performed as a consistency check for the results obtained with the CEC. The results (Figure 4) show clearly that the system with demulsifier B has much lower emulsion stability under an electric field than any of the other systems. The E-critical results are, to a certain degree, confirmations of the results obtained with the CEC (Table 1).

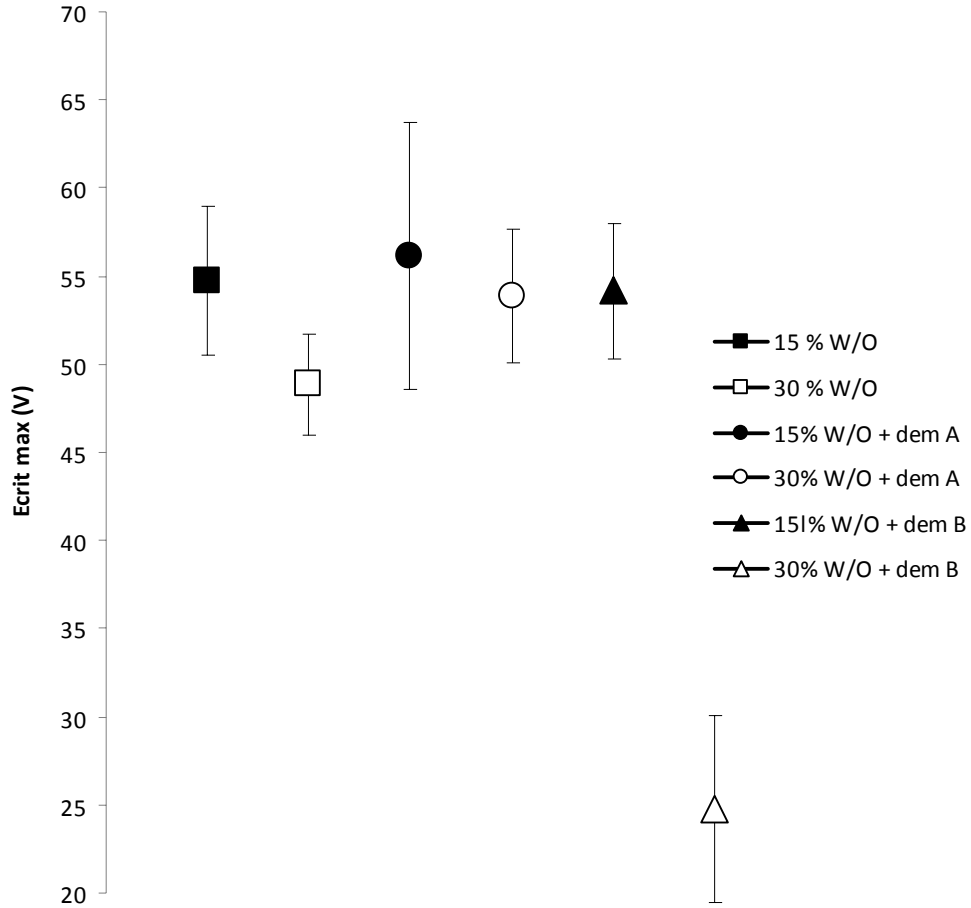

Figure 4. The E-critical measurements were performed on the E-critical cell developed by Aske.[25] As seen the systems containing 30 vol% water cut have a lower E-critical value than the ones with lower (15 vol%) water cut. Furthermore, the system with demulsifier B and 30 % water cut was much more unstable than the other emulsions supporting the results obtained with the CEC.

Furthermore, for the other systems tested all obtain relatively similar E-critical values, even the system containing 15 vol% water and demulsifier B. For all the systems the ones with 30 vol% water cut have a lower E-critical value than the ones with 15 vol% water cut. This indicates that there is a need for the droplets to be close to each other in order to coalesce and that high water cut, or turbulent flow conditions may improve the coalescence rate.

General consideration of the lab scale CEC and suggestions for further work

One cannot assume that all droplets are neutral since they may become charged at contact with the isolated electrodes in a induction charging process, or in collision with the bare electrode. However, as crude oil is somewhat conductive, Atten[14] concludes that the

charge leak rapidly, and the effect of charged droplets can be ignored. Due to the AC field eventual charged droplets will not have a net movement due to electrophoresis, but will oscillate in place between the electrodes. The lab scale CEC has flat electrode plates and the electric field in general is homogeneous and the electrostatic effect that remains is dipole coalescence.[8] The droplets are brought into close contact due to turbulent and laminar shear forces in the full scale CEC. As there is no turbulence in the lab scale CEC it is the laminar shear force that brings the drops in contact.

Drop break up may occur if the electric field exceed the critical conditions (Equation 5). Turbulent shear may also break up large droplets already formed by coalescence. The maximum droplet diameter surviving the turbulence can be estimated using the expression by Hinze.[28] Therefore, sharp bends and valves introducing shear should be avoided downstream of both the full size and the lab scale CECs. The Flow is also laminar (Re=200) in the 1/4" pipes downstream of the lab scale CEC and turbulent break up should not be a problem.

The intention of building the separation rig with the compact electro coalescer was first of all to have the opportunity for testing the behaviour of crude oils and demulsifiers under high electric fields at low costs. Secondly, the equipment provides the opportunity to check the scale up effect of E-critical measurements and bottle tests. Furthermore, it is possible with this equipment to study both the effect of voltage and demulsifier chemicals on the separation of water from crude oil. Further studies will look into the potential for using the CEC™ technology for desalting the crude oils by first emulsifying the crude oil with fresh water and then use the CEC to break the emulsion.

CONCLUSIONS

A compact electro coalescer was constructed with the intention to simulate a slice of the CEC™. The power supply which produces the necessary voltage consist of four 220 V transformers in parallel giving approximately 1000 V and 150 VA. The power to the transformers is controlled by a simplified Magtech unit, similar to the Magtech Controllable Transformer, but without the control electronics.

One crude oil blend was used and two different demulsifiers (A and B) were tested. The crude oil with and without demulsifiers were emulsified with brine at a water cut of approximately 30 vol%. The system with the CEC on and 20 ppm demulsifier B managed to separate most free water (83% of total water cut) and was considered the best demulsifier for the crude oil blend if electrostatic coalescence is to be involved.

The equipment made will be used in further research on crude oils and demulsifiers at high electric fields as in the CEC™ technology. The equipment has the purpose of a low cost research facility for both basic research and as a test facility for specific systems.

ACKNOWLEDGEMENTS

We want to thank Mika Tienhaaraa at Aker Kværner Process Systems, Espen Haug at Magtech for the MCT, and the people at the oil companies that delivered the oil and demulsifiers.

REFERENCES

1. Sjöblom, J., *Encyclopedic Handbook of Emulsion Technology*. Basel, 2001.
2. Sjöblom, J., *Emulsions and emulsion stability*. Taylor & Francis: Boca Raton, Fla., 2006; p 668 s.
3. Skodvin, T.; Sjöblom, J.; Saeten, J. O.; Urdahl, O.; Gestblom, B. *J. Colloid Interface. Sci.* **1994,** 166, 43-50.
4. Speight, J. G., *The chemistry and technology of petroleum*. Marcel Dekker: Boca Raton, Fla., 2007; p 945 s.
5. Mohammed, R. A.; Bailey, A. I.; Luckham, P. F.; Taylor, S. E. *Colloids and Surfaces a-Physicochemical and Engineering Aspects* **1993,** 80, (2-3), 223-235.
6. Sams, G. W.; Zaouk, M. *Energy & Fuels* **2000,** 14, (1), 31-37.
7. Melheim, J. A.; Chiesa, M. *Chemical Engineering Science* **2006,** 61, (14), 4540-4549.
8. Lundgaard, L. E.; Berg, G.; Pedersen, A.; Nilsen, P. J. *Proceedings of 14th international conference on dielectric liquids* **2002**, 215–219.
9. Eow, J. S.; Ghadiri, M.; Sharif, A. O.; Williams, T. J. *Chemical Engineering Journal* **2001,** 84, (3), 173-192.
10. Zhang, X. G.; Basaran, O. A.; Wham, R. M. *Aiche Journal* **1995,** 41, (7), 1629-1639.
11. Urdahl, O.; Williams, T. J.; Bailey, A. G.; Thew, M. T. *Chemical Engineering Research & Design* **1996,** 74, (A2), 158-165.
12. Urdahl, O.; Nordstad, K.; Berry, P.; Wayth, N.; Williams, T.; Bailey, A.; Thew, M. *Spe Production & Facilities* **2001,** 16, (1), 4-8.
13. Berg, G.; Lundgaard, L. E.; Becidan, M.; Sigmond, R. S. *Proceedings of 14th international conference on dielectric liquids* **2002**, 220–224.
14. Atten, P. *Journal of Electrostatics* **1993,** 30, 259-269.
15. Kim, B. Y.; Moon, J. H.; Sung, T. H.; Yang, S. M.; Kim, J. D. *Separation Science and Technology* **2002,** 37, (6), 1307-1320.
16. Yunusov, A. A.; Babalyan, G. A.; Akhmadiev, G. M. *Chemistry and Technology of Fuels and Oils* **1983,** 19, (7-8), 351-353.
17. Xu, X. R.; Yang, J. Y.; Jiang, Y.; Gao, J. S. *Petroleum Science and Technology* **2006,** 24, (11), 1307-1321.
18. Liu, G. L.; Xu, X. R.; Gao, J. S. *Energy & Fuels* **2003,** 17, (3), 543-548.
19. Mohammed, R. A.; Bailey, A. I.; Luckham, P. F.; Taylor, S. E. *Colloids and Surfaces a-Physicochemical and Engineering Aspects* **1993,** 80, (2-3), 237-242.
20. Sjöblom, J.; Aske, N.; Auflem, I. H.; Brandal, Ø.; Havre, T. E.; Sæther, Ø.; Westvik, A.; Johnsen, E. E.; Kallevik, H. *Advances in Colloid and Interface Science* **2003,** 100-102, 399-473.

21. Acevedo, S.; Borges, B.; Quintero, F.; Piscitelly, V.; Gutierrez, L. B. *Energy & Fuels* **2005,** 19, 1948-1953.
22. Ali, M. F.; Alquam, M. H. *Fuel* **1999,** 79, 1309-1316.
23. Mohammed, R. A.; Bailey, A. I.; Luckham, P. F.; Taylor, S. E. *Colloids and Surfaces a-Physicochemical and Engineering Aspects* **1994,** 83, (3), 261-271.
24. Chen, T. Y.; Mohammed, R. A.; Bailey, A. I.; Luckham, P. F.; Taylor, S. E. *Colloids and Surfaces a-Physicochemical and Engineering Aspects* **1994,** 83, (3), 273-284.
25. Aske, N. Characterisation of crude oil components, asphaltene aggregation and emulsion stability by means of near infrared spectroscopy and multivariate analysis. Department of Chemical Engineering, Norwegian University of Science and Technology, Trondheim, 2002.
26. Fossen, M.; Arntzen, R.; Hemmingsen, P. A.; Sjoblom, J.; Jakobsson, J. *Journal of Dispersion Science and Technology* **2006,** 27, (4), 453-461.
27. Haugs, E., Magtech, Personal communication. In 2007.
28. Hinze, J. O. *A.I.C.H.E. Journal* **1955,** 1, (3), 289-295.